Simulation of Enhanced Heavy Oil Recovery: History Match of Waterflooding and Polymer injection at Adverse Mobility Ratio

Master Thesis in Petroleum Technology – Reservoir Physics

Marwan AlSawafi

Department of Physics and Technology

Centre for Integrated Petroleum Research

University of Bergen

June 2015

Acknowledgment

First of all, I wish to express my sincere gratitude and appreciation to my supervisor, Professor Arne Skauge, for the immeasurable amount of support and guidance throughout my studying time. I wish also express my thanks to my co-supervisor Øystein Pettersen for his technical support and assistance.

Further, I would like to thank the Centre for Integrated Petroleum Research for providing me a good and supportive working environment. Special thanks goes to Iselin Salmo for her technical support and guidance in my simulation work. Also, I am very thankful and grateful to all my fellow students and colleagues at CIPR for their continuous and endless kindness and assistance. Thank you all for making my stay at CIPR fun and enjoyable.

Also, I would like to thank Petroleum Development Oman for providing me this opportunity to complete my master study at University of Bergen. Special thanks to Hamed Al-Hadhrami for his support and encouragement.

Finally, I would like to thank my family and my friends for their endless motivations and encouragement. Thank you for all your kind and supportive words, I really appreciate them. Thank you for being with me and keeping my spirit up all times.

Bergen, June 2015
Marwan AlSawafi

Abstract

Waterflooding and polymer flooding total recovery in the unstable immiscible displacement is very attractive and its applications are interesting in recent years. However, the simulation models of unstable immiscible flooding are not well understood and need more investigations and studies. The conventional method to simulate polymer flooding is to history match the waterflooding and uses relative permeability in addition to the bulk polymer rheology to predict the polymer flooding performance. In fact this straight forward method shows poor prediction abilities when the prediction results are compared to the experimental results

The main objective of this thesis is to history match six experiments using Buckle-Leverette type displacement model. All experiments consist of unstable waterflooding and polymer flooding at adverse mobility ratio. Also, relative permeabilities for both waterflooding and polymer flooding are to be obtained.

A sensitivity analysis was conducted to the models before starting history match. Numerical dispersion and physical dispersion were tested at the beginning to remove any numerical dispersion effect. After that, all polymer parameters that were used in the models were tested. Polymer viscosity, polymer concentration, polymer molecular weight, polymer adsorption, reversible and irreversible adsorption, inaccessible pore volume and the relative permeability were tested to investigate their degree of sensitivity in the history match.

There were some program restrictions in which two experiments could not be simulated using STARS. The restrictions were regarding the differential pressure profile, which showed unreal responses to the sensitivity analysis.

In the first part of this thesis, a history match was obtained for waterflooding using CMOST. Corey correlation for relative permeability was used to history match the cumulative oil production and the differential pressure. The history match was very good

for all experiments in cumulative oil profile and not very well fitted in the differential pressure profile.

In the second part of this thesis, a history match was obtained for polymer flooding. LET correlation for relative permeability was used to history match the cumulative oil production and the differential pressure. Also, other polymer parameters were used such as polymer adsorption, dispersion, inaccessible pore volume and resistance factor. A very good history match was obtained for all experiments.

It was found that the relative permeability was the main factor that affect the history match in both waterflooding and polymer flooding. Although, the polymer parameters had significant effects, but there had some constraints and cannot be used freely, and therefore, only the relative permeability had the most significant role in obtaining the history match. Water end point relative permeability trend was determined for both waterflooding and polymer flooding.

Nomenclature

Variables:

A	Adsorption	[kg/kg]
A	Area [m2]	[m^2]
c	Concentration	[kg/m3]
C	Concentration	[kg/m3]
D	Dispersion/diffusion coefficient	[cm^2/day]
D_p	Frontal advance loss	[-]
dp	Differential pressure	[Pa]
$\frac{dp}{dx}$	Pressure drop over distance x	[Pa/m]
E_R	recovery factor	[-]
f	fractional flow	[-]
G	Gravity	[m/s^2]
I	Irreducible water saturation	[-]
J	Residual oil saturation	[-]
k	Absolute permeability	[m^2]
$k_{e,i}$	Effective permeability of phase i	[m^2]
$k_{r,i}$	Relative permeability of phase I	[-]
L	Length	[m]
M	Mobility ratio	[-]
n	Corey exponent	[-]
N	Oil reserves	[m^3]
N_p	Cumulative oil production	[m^3]
P	Pressure	[Pa]
Q, q	Flow rate	[m^3/s]
R, r	Radius	[m]
S	Saturation	[-]
t	Time	[s]
u	Darcy velocity	[m^3/s]
v	Superficial velocity	[m/s]

V	Volume	[m^3]
x	Distance	[m]
Δ	Difference	[-]
γ	Shear rate	[s^{-1}]
λ	Mobility	[m^2/Pa*s]
μ	Viscosity	[Pa*s]
ρ	Density	[kg/m3]
σ	Interfacial tension	[N/m]
τ	Shear stress	[Pa]
ϕ	Porosity	[-]

Subscripts:

*	Normalized
*	Practical
o	End-point
a	Advanced
A	Area
abs	Absolute
b	Bulk
c	Connate
c	Contact
cr	Critical
D, d	Dimensionless
D	Microscopic
eff	Effective
i	Component (phase)
i	Imbibition
i	Initial
i	Irreducible
ineff	Ineffective
n	maximum
n	maximum
n	Component (phase)
o	Oil
p	Pore
P	Produced
Pol	Polymer
r	Relative
r	Residual
R	Recovery
s	Solid
t	trapped

v	Vertical
vol	Volumetric
w	Water
w	Waterflooding

Acronyms and Abbreviations:

1D	One dimensional
2D	Two dimensional
3D	Three dimensional
BHP	Bottom hole pressure
BT	Breakthrough
CIPR	Centre for Integrated Petroleum Research
CMG	Computer Modelling Group Ltd.
EOR	Enhanced oil recovery
FW	Fractional-wet
IOR	Improved oil recovery
IVP	Inaccessible pore volume
HPAM	Hydrolyzed polyacrylamide
OOIP	Original oil in place
OW	Oil wet
PAM	Polyacrylamide
PSM	Pore scale modelling
PV	Pore volume
WC	Water-cut
WW	Water-wet

Table of Contents

List of Figures

List of Tables

1. Introduction

Crude oil is a very important part of the international energy market, which is expected to observe a continued consumption growth (especially in emerging market) [1]. All sources of energy such as nuclear power and renewables in power generation grew at below-average rates, but the oil is still the world's leading fuel with 32.9% of the global energy consumption [2]. In addition, according to United States Energy Information Administration, the world crude oil consumption is increasing as it is shown in Figure 1.

In the early 2015, the IEA Oil Market Report predicted the average demand for this year of more than 93 million barrels of oil and liquid fuels per day worldwide. In the next five years, China will be large consuming oil country in which almost half of the global oil demand will come from it, and this prediction is expected to continue to 2040. The most sector that demands oil is the transportation sector as it is growing strongly in China and India [3].

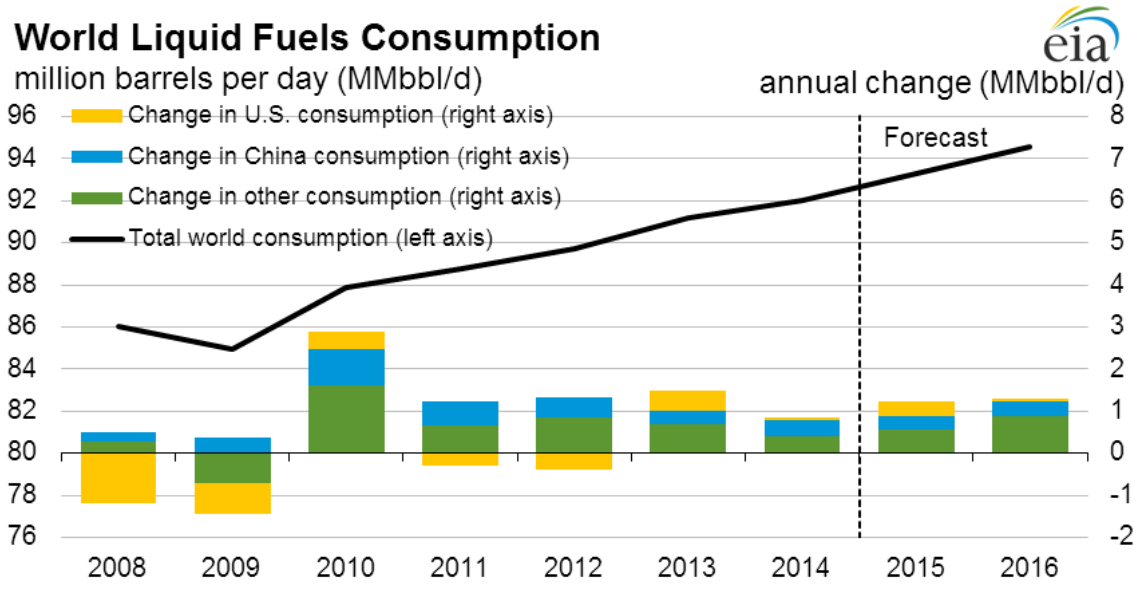

Figure 1.1: World Crude Oil Consumption *[4]*.

Therefore, it is clear that the oil is very important since it is the dominant source of energy globally. Typically, there are three methods to produce oil from the reservoirs, which are;

primary recovery method, secondary recovery method and tertiary recovery method; and there are some factors to select any of these stages such as reservoir production stage fluid and formation properties, reservoir geology and others.

The first stage is the primary recovery and in this stage the hydrocarbons are produced using the natural energy sources such as water drive which comes from the water aquifer (if it is available), gas drive which comes from the gas cap (if it is available) and gravity drainage, which displaced the hydrocarbons from the reservoir into the wellbore and up to the surfaces. As the differential pressure between the reservoir and the wellbore is large, higher recovery factor is obtained from this reservoir with primary recovery. However, the reservoir pressure will decline after a while and the oil will not be able to come to the surface because of low differential pressure, therefore an artificial lift system should be implemented such as gas-lift, rod pump and electrical submersible pump (ESP).

As a result of the pressure decline by the primary recovery, and to maintain the pressure and sweep out more oil, the secondary shloud be implemented. Waterflooding is the main standard practice in many reservoir formations [5]. Waterflooding will be discussed in more details in chapter 2.

Tertiary or Enhanced Oil Recovery (EOR) can be defined as oil recovery by injection of any unconventional materials not normally present in the reservoir. Also, there is a recovery type called Improved Oil Recovery (IOR) which can be defined as any process that improved the oil recovery, and because of unclear definitions of EOR and IOR, usually IOR has been used interchangeably or even in place of EOR [6].

In general, Enhanced oil recovery methods can be grouped in four main methods; thermal methods, chemical methods, miscible or solvent injection and microbial methods.
Thermal methods can be defined as the process of increased reservoir temperature to reduce the oil viscosity and therefore, increases oil mobility. The main two types of thermal EOR are steam flooding and in-situ combustion. Chemical EOR is the type of EOR in which some chemicals are injected to increase the oil recovery. The main chemicals which are

used in this type of EOR are polymer which will be discussed in more details in chapter 2, surfactants and alkaline solutions. The principle of Miscible EOR is to reduce the interfacial tension between the displacing fluids and displaced fluids to almost zero. Finally Microbial EOR, which is basically the use of some microbes to produce biosurfactants, biopolymers, acids, solvents and gases to improve the efficiency of the oil recovery [7].

Figure 1.2 shows all types of oil recovery from primary to tertiary.

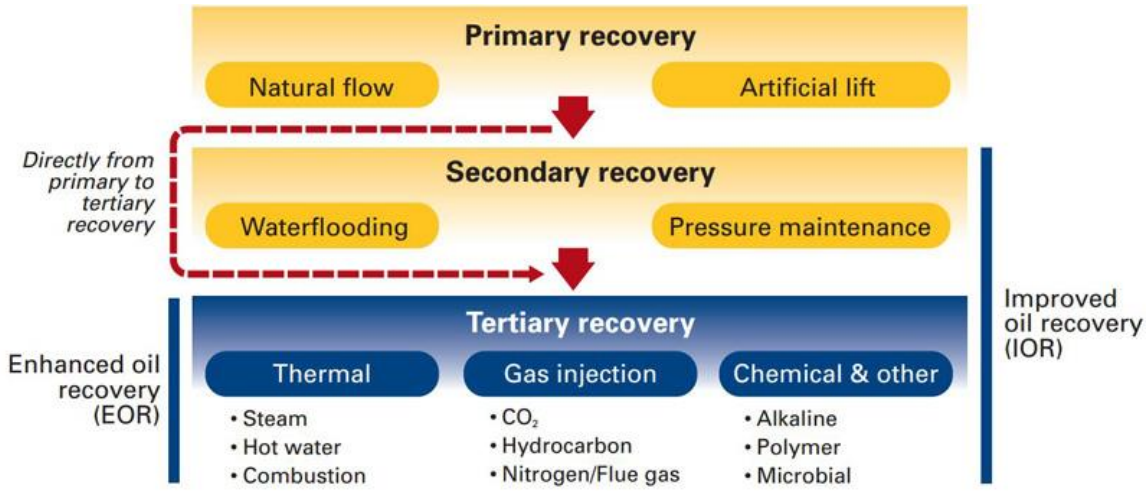

Figure 1.2: Oil recovery methods *[8]*

Figure 3 shows the concept of the three types of oil recovery which is basically to increase oil recovery as much as possible.

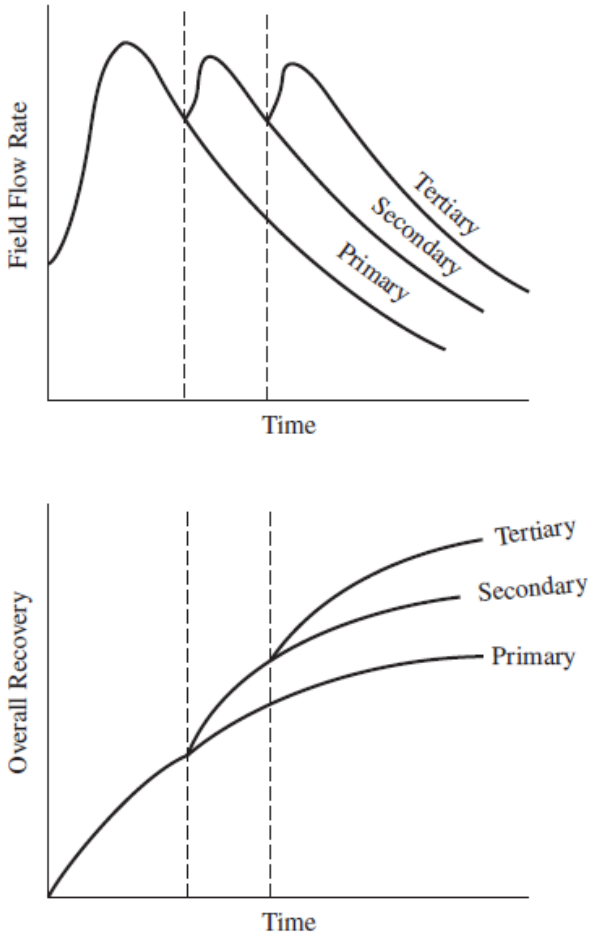

Figure 1.3: EOR Oil Recovery [8]

2. Water Flooding

As a result of the pressure decline by the primary recovery, and to maintain the pressure and sweep out more oil, the secondary method should be implemented. Waterflooding is the main standard practice in many reservoir formations. Waterflood can be defined as the process of producing the mobile hydrocarbon phase from the subsurface by using pump wells that pump water into the reservoir to push the hydrocarbon toward the production wells. Waterflood has been considered as secondary recovery in petroleum industry in the late 1800s [5].

The total efficiency or the total recovery factor of waterflooding or any secondary recovery methods or tertiary can be determined from the following equation [8]:

$$RF = {}^{N_p}/_{N} = E_D\, E_A\, E_V \qquad \text{Equation 2.1}$$

Where,

RF = overall recovery factor

N = initial oil in place at the start of the flood,

N_P = cumulative oil produced,

E_D = displacement efficiency

E_A = areal sweep efficiency

E_V = vertical sweep efficiency

Displacement efficiency is the ratio between the oil displaced volume to the injected pore volume, while the areal sweep efficiency is the fractional area that has been swept by the displacing fluid. The main factors that affect the areal sweep efficiency are fluid mobilities, pattern type, areal heterogeneity and total volume of fluid injected. The vertical sweep efficiency "is the fraction of the vertical section of the pay zone that is contacted by injected fluids" and the main factors affecting Ev are vertical heterogeneity, degree of gravity segregation, fluid mobilities and total injected volume [8].

The figure below illustrates the difference between the areal and vertical sweep efficiencies.

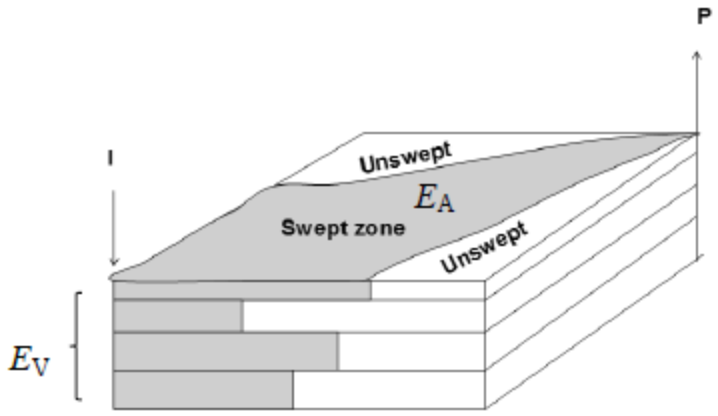

Figure 2.1: Areal and Vertical Sweep Efficiencies *[9]*

In the next sections, some of the important parameters that affect waterflood efficiency will be highlighted.

2.1.Porosity

Porosity is defined as the rock void space of the total volume, unoccupied by the grains and mineral cement [10]. Porosity is a dimensionless parameter, and it has a direct relationship to the total fluids volume in the reservoir since all fluids are occupied in the pore space.

There are two types of porosity in the hydrocarbon reservoirs; effective porosity ϕ_{eff} and ineffective porosity $\phi_{ineff.}$ Effective porosity is volume of interconnected pores that allow fluids to flow through them and ineffective porosity is the volume of pores that are not connected and the fluids occupied by those pores cannot flow. Absolute porosity is the total porosity:

$$\emptyset_{abs} = \emptyset_{eff} + \emptyset_{ineff} \qquad \text{Equation 2.2}$$

Where, ϕ_{abs} is the absolute porosity, ϕ_{eff} is the effective porosity and ϕ_{ineff} is the ineffective porosity.

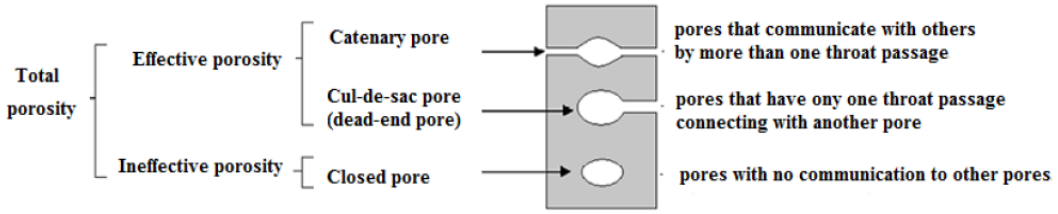

Figure 2.2: illustration of porosity types [11].

2.2.Fluid Saturation

Fluid saturation can be defined as the fluid fraction in the pore volume [12]. Mathematically, fluid saturation is:

$$S_i = \frac{V_i}{V_p}, \qquad i = w, o, g \qquad \text{Equation 2.3}$$

Where, S_i is the fluid saturation of phase *i*. V_i is the fluid volume of phase *i* and V_p is the pore volume.

The total fluids saturation in the hydrocarbon reservoirs is always equals to 1:

$$S_w + S_o + S_g = 1 \qquad \text{Equation 2.4}$$

2.3.Permeability

Permeability is one of the most important property in hydrocarbon reservoirs. It is a measure of the formation ability to transmit fluids [8]. Rock permeability, k, controls the fluid flow direction and movement in the formation pores. In 1856 Henry Darcy, developed a mathematical formula that describes the fluids movements through a porous media. For a horizontal linear flow of an incompressible fluid through a core sample of length L, and a cross-section area A, [8]:

$$q = -\frac{k\ A\ dp}{\mu\ dL} \qquad \text{Equation 2.5}$$

Where, q= flow rate [cm^3/sec]

A= cross-section area, [cm^2]

k= Permeability, [Darcy]

μ= fluid viscosity, [cp]

dp/dL= pressure drop per unit length, [atm/cm]

2.3.1. Effective and Relative Permeability

Normally, in the hydrocarbon reservoirs, the porous medium is saturated with more than one phase, therefore, a new definition of the phases permeability is given. Effective permeability is the relative measure of a single fluid conductance in the porous medium when the medium is saturated with more than one fluid [8]. Therefore, there are three types of effective permeability; effective water permeability, effective oil permeability and effective gas permeability.

Effective permeability can be mathematically defined by Darcy's Law. For example, oil effective permeability is [8]:

$$q_o = \frac{k_o\ A\ (P_1 - P_2)}{\mu_o\ L} \qquad \text{Equation 2.6}$$

where, q_o = oil flow rate, [cc/sec]

μ_o = oil viscosity, [cp]

k_o = oil effective permeability, [Darcys]

Effective permeability is usually measured directly in the laboratory on small core samples. However, the data then, are collected for different phases and reported as relative permeability. Relative permeability is a dimensionless property, and it is defined as the

ratio of the effective permeability of a given fluid to the absolute permeability [8]. For oil, water and gas, relative permeability is:

$$k_{ri} = \frac{k_i}{k}, \quad i = o, w, g \qquad \text{Equation 2.7}$$

where, k_{ri} is the relative permeability of the phase i, k_i is the effective permeability of the phase i and k is the absolute permeability.

Relative permeability is a function of the reservoir fluid saturation and the wetting characteristics of the formation. When wetting and non-wetting fluids flow together in the porous medium, each phase follows different path depending on the fluid saturation [8]. The figure below shows a typical two-phase relative permeability curve for water/oil system, where water is the wetting phase.

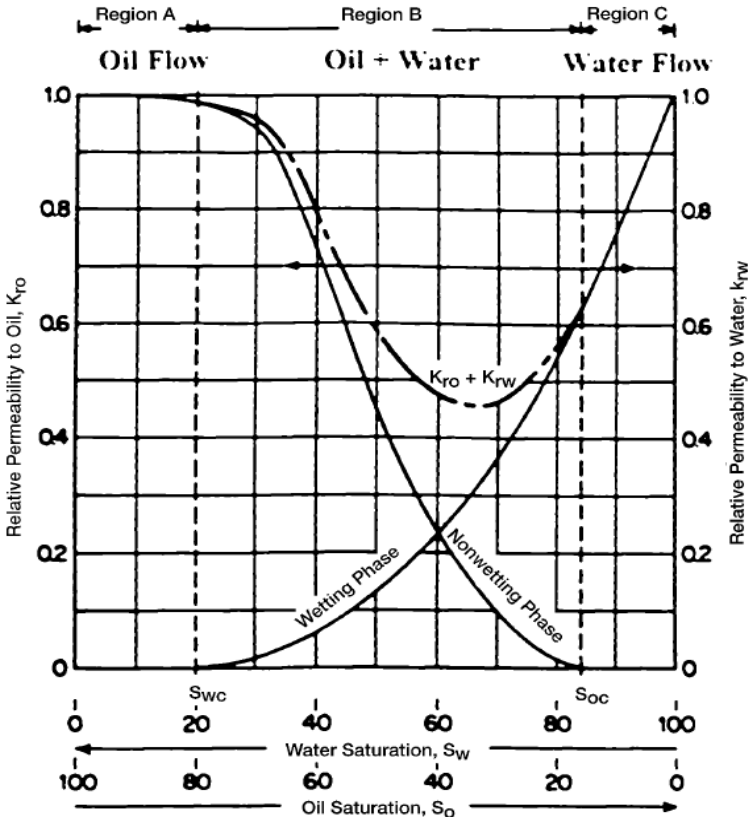

Figure 2.3: Typical two-phase relative permeability curves *[8]*.

Several studies have conducted to study the factors that affect two-phase relative permeability. Leverett [13] and Snadberg et al [14] have investigated the effect of flow rate and viscosity on the two phase relative permeability, and their conclusion was that relative permeability is only function of saturation and wettability and it is independent on flow rate and viscosity ratio. However, Odeh [15] was the first one who reported that relative permeability is also depends on viscosity ratio.

Others studies were conducted to investigate the temperature dependence on relative permeability. Edmondson [16] and Poston [17] have showed that temperature affects the residual oil saturation, as temperature increases residual oil saturation decreases. However, several studies reported that temperature is independent on relative permeability [18] [19]. Lo and Mungan [20] , Kumar and Inouye [21] and Doorwar and Mohanty [22] believed that the effect of temperature on relative permeability is due to the change in the viscosity ratio because of the temperature change. Akin et al [23], Wang et al [24] and Mosavat el at [25] have studied the effect of viscosity ratio on the relative permeability and they showed a clear dependence of viscosity ratio on the relative permeability.

From the studies above, it is clear that the viscosity ratio is an important factor on relative permeability, and since in this thesis, the experiments were conducted with high viscosity ratio, the main factor to simulate these experiments is the relative permeability.

2.4.Residual Oil Saturation

During waterflooding, there is immobile trapped oil remain in the pore space called residual oil saturation and the capillary forces acting in the pore space are responsible for this residual oil saturating [26]. There are several models proposed which explained why there is trapped oil after the waterflooding. The two main models, which describe that, are the pore doublet model and the snap-off model [9].

In the doublet model, when there are two paths or two channels for the flow, the wetting phase will flow quicker through the narrow channel because of the capillary difference and the non-wetting phase will be trapped [9]. The figure below illustrates the doublet model

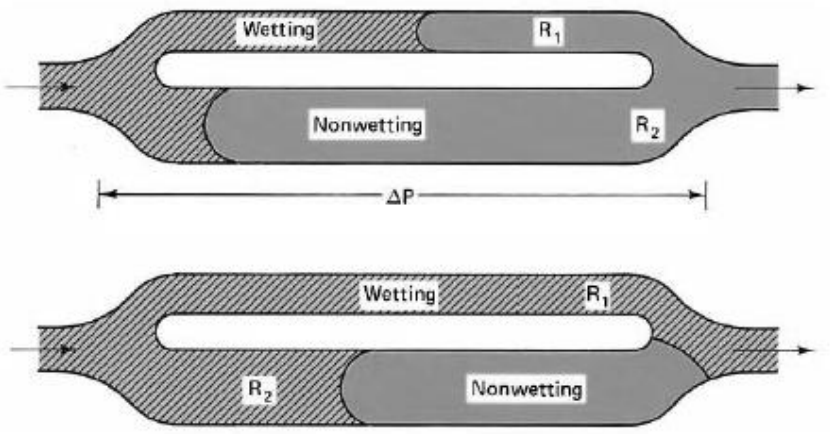

Figure 2.4: Trapping in a pore doublet model *[9]*.

In the snap-off model, the oil phase snaps off in the pore throat because of the capillary differences and the oil will be trapped in the pore body as it is shown in the figure below [9].

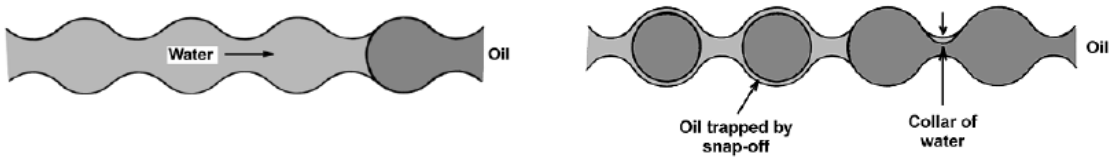

Figure 2.5: Trapping in a Snap-off model *[9]*.

2.5.Mobility

In Waterflooding where water is displacing oil, the mobility of each phase (water and oil) is the basic mechanics that describes the immiscible flooding and help to understand the stability of the flood. The fluid mobility can be defined as the following [27]:

$$\lambda = \frac{kk_r}{\mu} \qquad \text{Equation 2.8}$$

Where, λ is fluid mobility, k is the absolute permeability, k_r is the fluid effective permeability and μ is the fluid viscosity.

Mobility ratio is the mobility of the displacing fluid to the mobility of the displaced mobility. [8]. For water and oil system, mobility ratio can be writing as following:

$$M = \frac{k_{rw}\,\mu_o}{k_{ro}\,\mu_w} \qquad \text{Equation 2.9}$$

Where, M is the mobility ratio, k_{rw} and k_{ro} are the water and oil relative permeabilities respectively and μ_w and μ_o are the water and oil viscosities respectively

By knowing the fluids mobilities and the mobility ratio, the fluid flow and the fluid front can be understood. The figure below illustrates the waterflooding process in term of fluids mobilities.

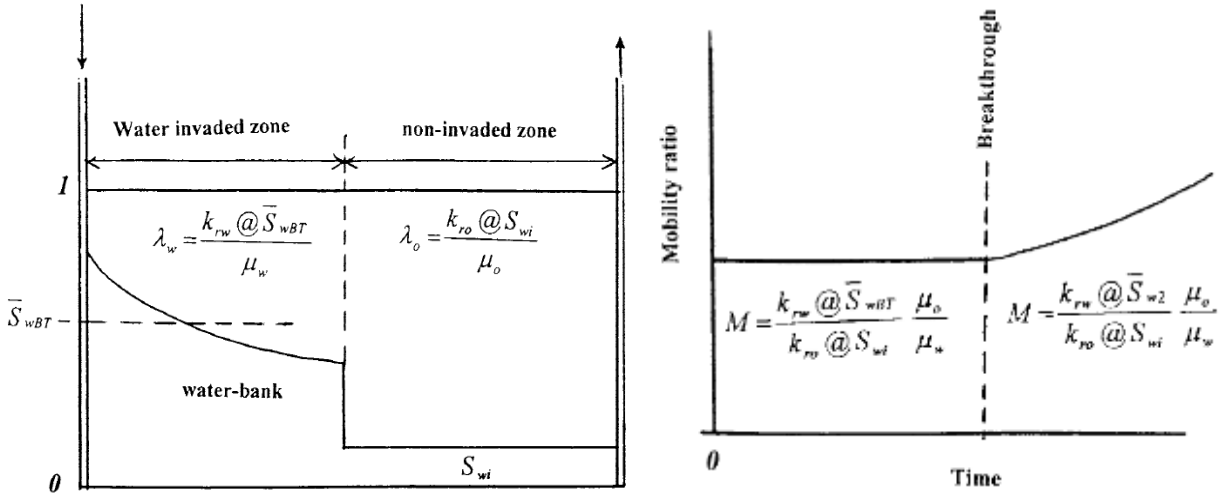

Figure 2.6: Oil and water mobilities to breakthrough, modified from *[8]*

Mobility ratio has a direct relationship in flooding performance and direct impact on water fraction flow, which describes the immiscible flooding, and determines its efficiency and stability.

Fraction flow equation first was developed by Buckley and Leverett [28] in 1941 by combined fraction of water production compared to the total production, Darcy's law and continuity equation [6] [9]. The final water fraction flow equation in term of the mobility neglecting capillary effect and gravitational effect is:

$$f_w = \frac{1}{1 + {}^{1}/_{M}} \qquad \text{Equation 2.10}$$

Where, f_w is the water fraction flow and M is the mobility ratio.

The assumptions that are made to develop the water fraction flow are [6] [9]:

- Immiscible displacement
- Two phases and incompressible, oil and water
- Steady-state flow in a homogeneous system

The figure below shows a typical fraction flow curve for water/oil system. Water breakthrough time, saturation and fraction flow, average water saturation and other parameters can be determined from this curve. It also shows the mobility ratio effect on the fraction flow curve.

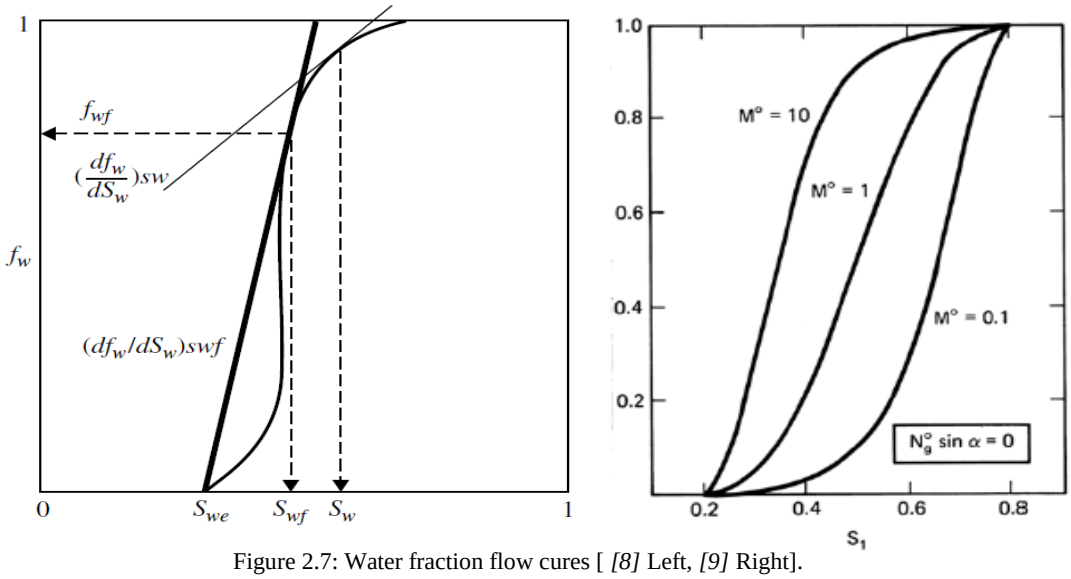

Figure 2.7: Water fraction flow cures [*[8]* Left, *[9]* Right].

The mobility ratio has a direct impact on the waterflooding efficiency since it has a direct influence on the fractional flow curve. The figure below illustrates the mobility ratio impact on the microscopic displacement efficiency.

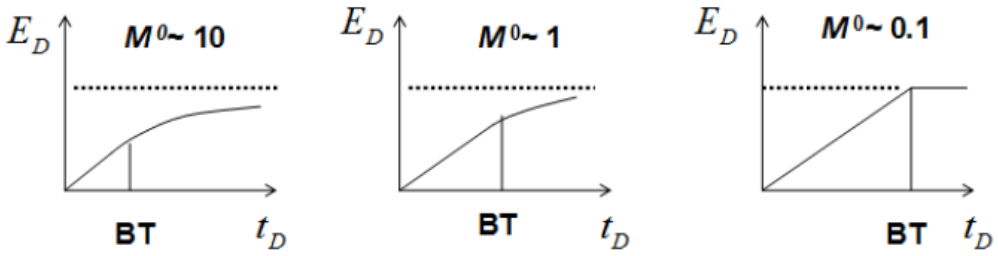

Figure 2.8: Mobility ratio and microscopic displacement efficiency relationship *[9]*.

2.6. Unstable Immiscible Displacement

The main reason for the unstable displacement for both miscible and immiscible flooding is the adverse mobility as it shown in figure 2.11 and 2.12. For mobility ratio >1, the saturation wave which is saturation change in time and position, becomes more diffuse and hence, is gives less recovery because there is an early breakthrough. On the other hand, the mobility ratio <1, the saturation wave becomes less diffuse and shocks. This displacement called piston displacement. [9].

The main unstable displacement phenomenon in the oil industry is the viscous fingering and it has been a challenge for more than a half-century. For waterflooding, the main reason for viscous fingering is the large adverse mobility contrast. However, for both miscible and immiscible, the adverse mobility contrast is the reason for viscous fingering [29]. As mobility ratio increases the viscous fingering increases [30]. The figure below shows the mobility ratio influence on the viscous fingering.

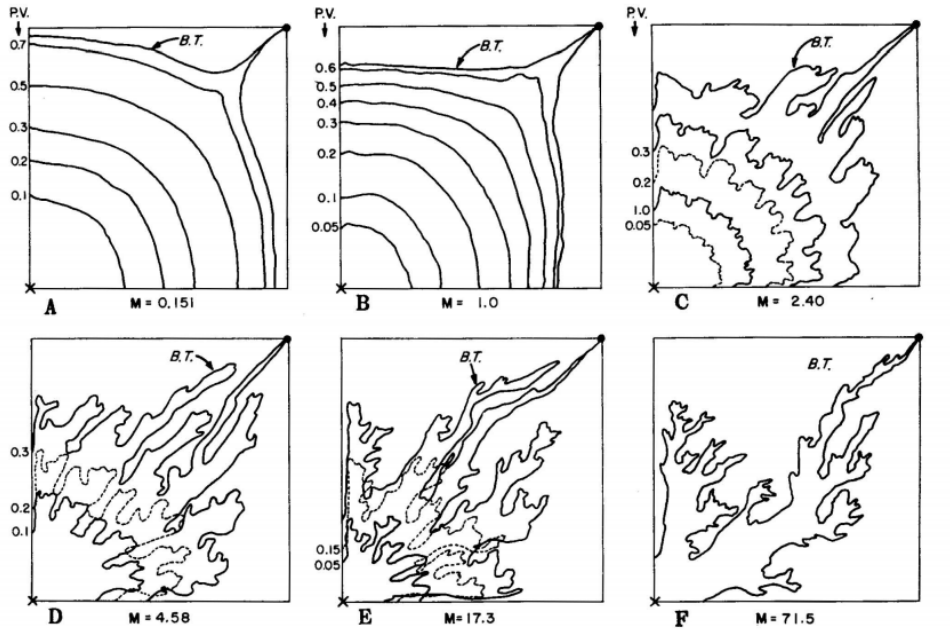

Figure 2.9: Mobility ratio influence on the viscous fingering and breakthrough *[30]*.

In 1958 Saffman and Tylor [31] explained the viscous fingering or instability development in water/oil system where, water is displacing oil. The experiment was conducted in Hele-Shaw cells (2-dimensionless channels between parallel glass plates and they were separated by a small gap). They concluded that:

- The dimensionless width of viscous fingering is equal to the width of finger divided by the width of channel. This dimensionless width is decreasing as the capillary number increases.

$$\text{capillary number} = \frac{\mu\, U}{\sigma} \qquad \text{Equation 2.11}$$

  Where, μ is the oil viscosity, U is the velocity of the instability and σ is the interfacial tension.

- The oil viscosities and viscosities for different channel width, the dimensionless width of viscous fingering falls on the same curve, which decreases to 0.5 as the capillary number increases [31].

However, this approach of understanding viscous fingering makes some difficulties in the porous media because of the absence of a clear interface between displacing and displaced fluids [32].

The initiation of viscous fingering is usually associated with the reservoir heterogeneities especially in permeability heterogeneities. The viscous fingering initiation can easily be visualized in the porous media, as the pores structures are microscopically random. It can be observed even with Saffman-Tylor Hele-Shaw model which is considered to be homogenous in permeability [33]. The main factor that governs with the fingers initial number, location and the relative growth rates is the permeability distribution at the injection area. Viscous fingering initiation and propagation have been studied and examined by mathematical perturbation theory and frontal perturbation methods [34], [35], [36], [37], [38].

At the beginning of the unstable flooding, the fingers start to form with different lengths based on the heterogeneity of the core. Normally, and because of the suppression, there will be a small initial space of fingers. The change in finger lengths become large with unstable fingers propagation as the pore volume injected increase. Also, the width and length of the fingers will increase when the small suppressed fingers and the large fingers coalesced [39]. The figure below illustrates the suppression and coalescence of viscous fingering.

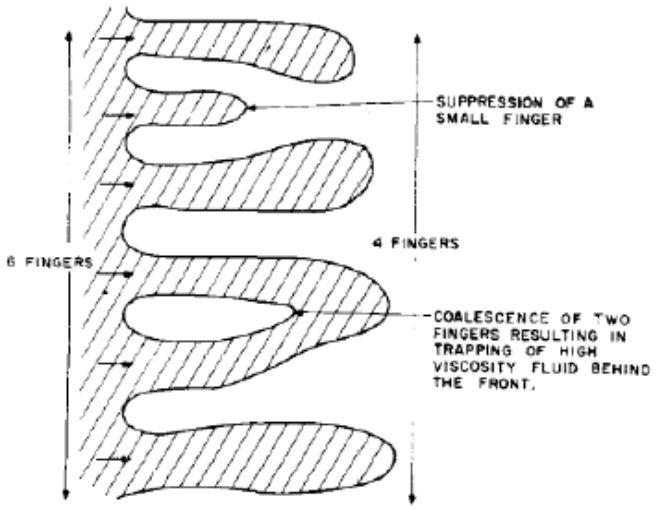

Figure 2.10: Suppression and coalescence of viscous fingering in a linear flowing system *[39]*

3. Polymer Flooding

3.1. Polymer Types

Polymer is used as enhanced oil recovery method to increase the oil recovery factor in the heterogeneous reservoirs. This heterogeneity is related to the high mobility ratio between oil and water, which causes poor sweep efficiency, by viscous fingering as mentioned before, and heterogeneity in the permeability. Polymer flooding is a solution to these problems because it reduces the mobility ratio by adding polymer to the water in the waterflood which increases the water viscosity by several magnitudes. Also, it decreases the water permeability. Therefore, polymer can improve the sweep efficiency and hence, improves the oil recovery. On the other hand, polymer flooding does not change the residual oil saturation in the reservoir. It just improves the sweep efficiency by producing more mobile oil which cannot be produced by conventional waterflooding [6]. In other words, Polymer flood is more to accelerate than to enhance the oil recovery [9]. Therefore, polymer is an applicable option for EOR when there is high mobility ratio and high level of heterogeneity in the reservoir because of economic reasons (polymer is expensive) [6].

In oil industry there are two main types of polymer which are normally used in polymer flooding. First one is a synthetic polymer, polyacrylamide especially in its hydrolysed form which is called HPAM. The other polymer type is a biopolymer called xanthan. The reason why only those two types of polymers are used in oil industry is because that both HPAM and xanthan have many others applications in other industries, and therefore, there is enough information about those two polymers. [5].

Polyacrylamide or in its hydrolysed form HPAM is used most frequently than xanthan in oil industry. It consists of synthetic straight-chain of acrylamide monomers, some of them are hydrolised as shown in the figure below. HPAM molecule is called random coil because of its flexible chain structure [5]. The size of HPAM is about 0.5 μm and its molecular weight is about 5 million a.m.u [9]. The degree of HPAM hydrolysis is very important and very sensitive property since it can affect the physical properties of the polymer such as adsorption, salinity/hardness, thermal stability, shear stability and water solubility. The fact that HPAM has a flexible structure makes HPAM more sensitive to the environment

condition in the reservoir. Therefore, a good knowledge of HMAP should be obtained and a lot of experimental investigations should be conducted before it is used in the large scale [5].

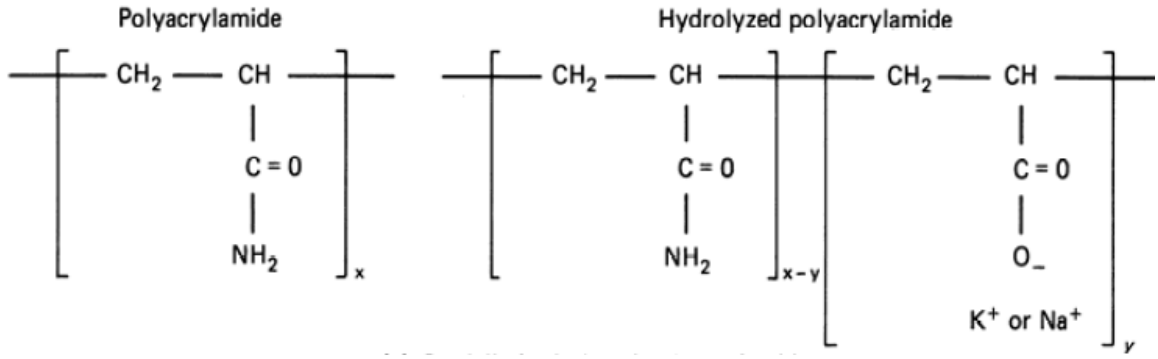

Figure 3.1: Partially hydrolyzed polyacrylamide *[6]*

Xanthan is a biopolymer produced by the micro-organism Xanthomonas camperstris. The structure of xanthan is shown in the figure below. Its structure consists of a cellulose-like chain of glucose monomers with β (1-4) glycosides linkages. Unlike HPAM, xanthan has been considered as a rigid rod structure. In 1977 ,X-ray diffraction steadies by Moorhouse et al. [40], suggest that xanthan has a helical structure in which the side groups fold down along the helix creating a stiff, rod-like macromolecular. The xanthan size length was estimated by different workers (Whitcombe and Macosko [41], Chauveteau [42], Seright and henrici [43]) to be in the range of 0.6 to 1.5 µm. The molecular weight of xanthan is about 2 million a.m.u [9]. Because of xanthan rigid rod-like structure, it shows less sensitivity to temperature, PH and ionic strength of solution (salinity/hardness) compared to HPAM.

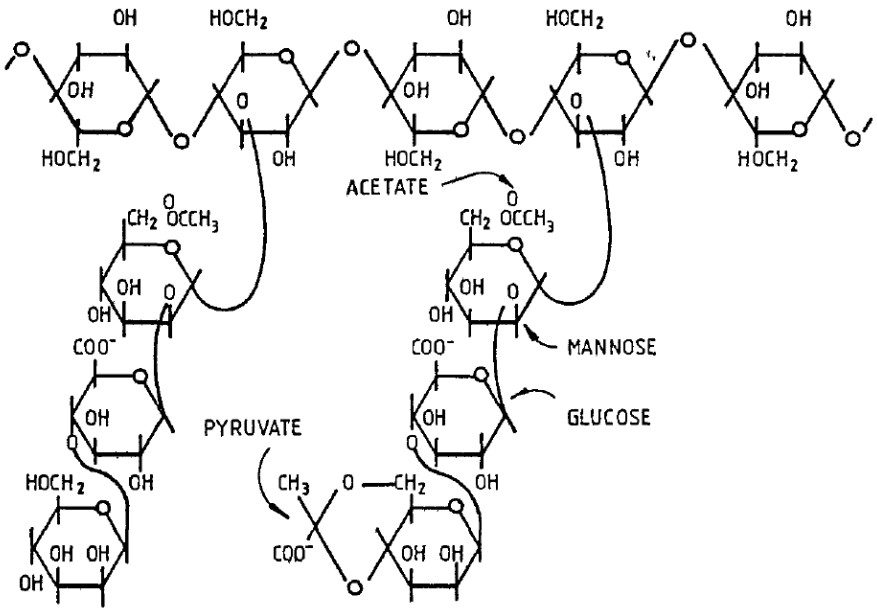

Figure 3.2: Xanthan biopolymer structure *[44]*

3.2.Polymer Rheology

Rheology is known as the study of the non-Newtonian flow behavior and it is a large study area [45], [46], [47]. The most important property in polymer rheology is viscosity because the main reason to use polymer in EOR is its ability to increase the water viscosity.

In general, a fluid viscosity refers to how thick the fluid is [5]. In more specific way, the fluid viscosity can be defined as the resistance of the fluid to the shear. The shear stress (τ) between two thin sheets of fluids is given by [5]:

$$\tau = \frac{F\ (Force)}{A\ (Area)} \qquad \text{Equation 3.1}$$

It was found experimentally, the velocity gradient of the fluid in small distance between the sheets is linear for many fluids. This is shown in the figure below. And it was found experimentally that [5]:

$$F \propto \frac{AV}{r} \qquad \text{Equation 3.2}$$

Where, *r* is the distance between the surfaces in the figure below and *V* is the velocity of the upper surface. Combined Equation 3.1 and 3.2 [5]:

$$\tau \propto \left(\frac{dV}{dr}\right) \qquad \text{Equation 3.3}$$

Where, (*dV/dr*) is the rate of deformation of the fluid which is the shear rate.

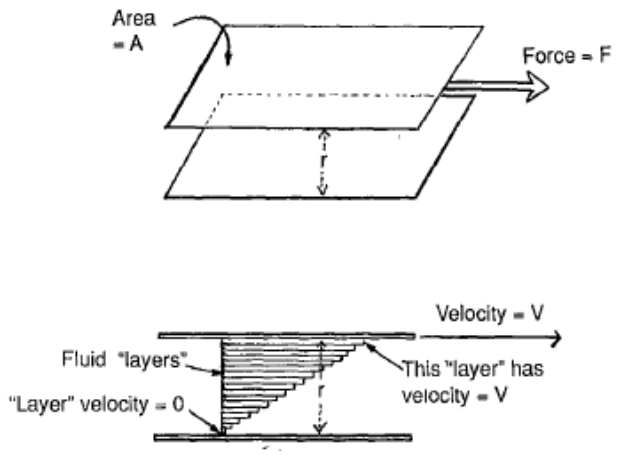

Figure 3.3: Illustration of fluid motion in simple shear flow *[5]*

For Newtonian fluid the relationship between shear stress and the rate of deformation (shear rate) is described by the following equation [5]:

$$\tau = -\mu\left(\frac{dV}{dr}\right) = \mu\dot{\gamma} \qquad \text{Equation 3.4}$$

Where, μ is the constant viscosity and $\dot{\gamma}$ is the shear rate. However, this equation describes the flow behavior of the Newtonian fluid only. Polymer is considered as non-Newtonian fluid and it has different flow behaviors. The figure below shows different types of fluids behaviors.

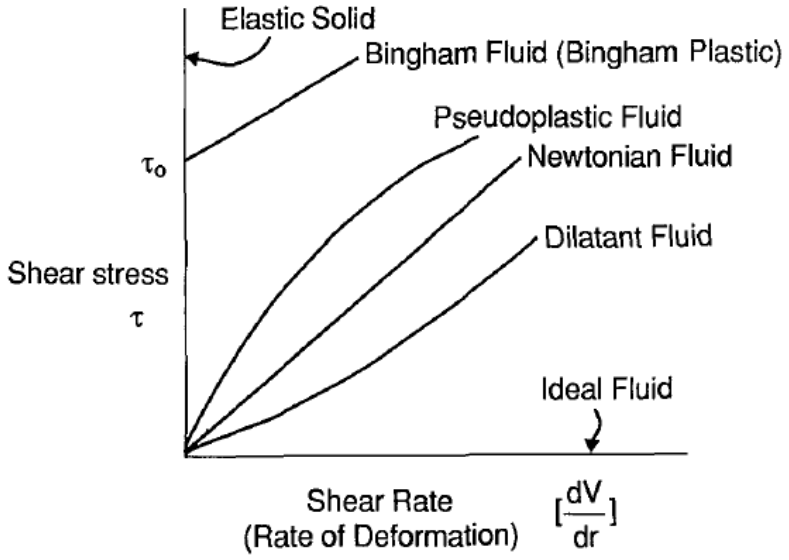

Figure 3.4: different types of shear stress/shear rate behaviors *[5]*

As mentioned above, Newtonian fluids show a linear relationship between the shear stress and shear rate, which means that the viscosity is constant at different shear rates. On the other hand, the viscosity of Dilatant fluids and pseudoplastic fluids is not constant and it changes as the shear rate changes. The viscosity of Dilatant fluids increases as the shear rate increases and this type of fluids called shear thickening fluids. While the viscosity of pseudoplastic fluids is decreasing as the shear rate increases and this type of fluids called shear thinning fluids. The vast majority of polymer solutions are shear thinning [5].

The most common way to describe polymer viscosity behavior is to plot viscosity against shear rate [5].

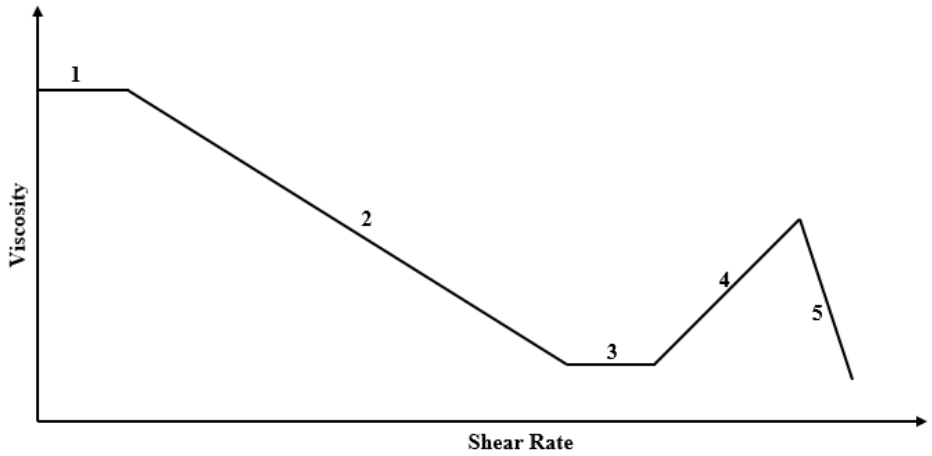

Figure 3.5: Illustration of polymer viscosity/Shear rate relationship.

- Region 1: The polymer shows a Newtonian behavior at low shear rate.
- Region 2: The polymer shows a shear thinning behavior after exceeding the critical shear rate $\dot{\gamma}_c$.
- Region 3: At high shear rate, the polymer shows a Newtonian behavior and the polymer viscosity value is just above the solvent viscosity.
- Region 4: Some types of polymers show a shear thickening behavior which means that the polymer viscosity increases at very high shear rate.
- Region 5: At extremely high shear rate the polymer viscosity decreases rapidly. Mainly because of mechanical degradation (will be discussed later).

Both HPAM and xanthan show the same behavior in regions 1,2 and 3. However, only HPAM shows an elastic behavior at high shear rate (flow rate) [5]. This polymer rheology behavior also can be observed in-situ in pores media [48].

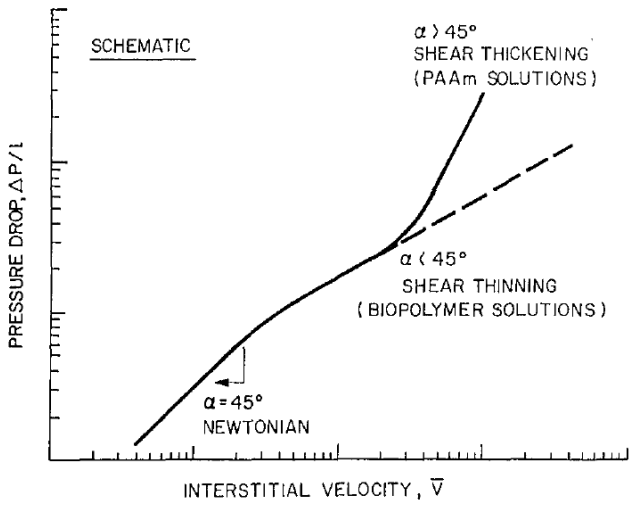

Figure 3.6: Schematic diagram of in-situ rheology behavior of polymer solutions *[48]*

3.3. Polymer Retention

When polymer is injected in the pores media with water solution, there will be an interaction between the polymer and the porous medium. As result of this interaction, some polymer will be retained by the porous medium. This retention in polymer will affect the efficiency of the polymer because of the reduction in polymer concentration, and as a result, reduction in water viscosity. Also, polymer retention causes reduction in rock permeability and sometime will block the formation pores [5]. Sorbie [5] has observed that the level of polymer retention is a main factor that affects the economical viability of a polymer flood.

The field measured values of polymer retention range from 7 to 150 μg of polymer / cm^3 of bulk volume [9]. There are three main polymer retention mechanisms in porous media, which are polymer adsorption, mechanical entrapment and hydrodynamic retention. Polymer adsorption happens because of the interaction between the polymer molecules and the rock surface mainly by physical adsorption (van der Waal's and hydrogen bonding). As the surface area of the porous medium is large, the level of polymer adsorption will be large. Retention by mechanical entrapment happens when there are high polymer molecules flowing through narrow channels in the porous medium. The high polymer molecules will be trapped in that channel. The hydrodynamic retention happens when the polymer molecules are trapped temporarily in stagnant flow regions by hydrodynamic drag

forces. Then, when the flow stops, these polymer molecules will be back in the main channels. However, this physical picture of the hydrodynamic retention is to clear yet and there may be other explanations of this type of retention [5]. The figure below illustrates the three types of polymer retentions.

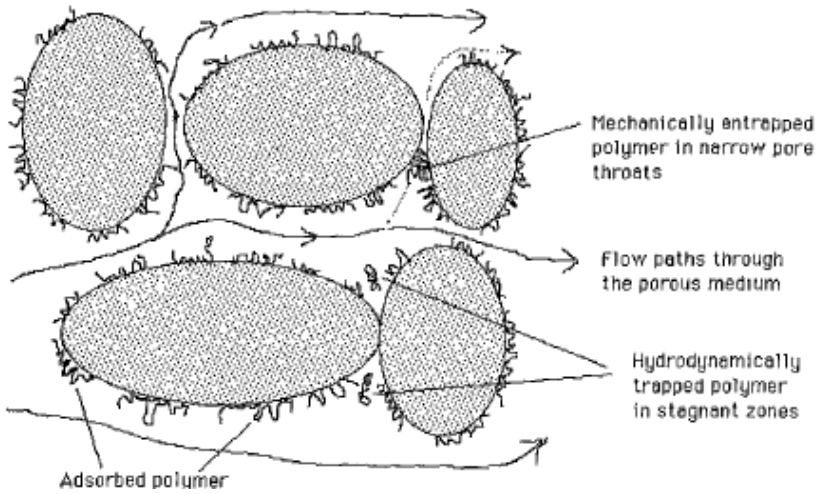

Figure 3.7: Illustration of polymer retention mechanisms in porous medium *[5]*

Both mechanical entrapment and hydrodynamic retention can be neglected in polymer flooding because of their small contribution in field-scale polymer flooding. Therefore, polymer adsorption is the main mechanism that affects the polymer flooding and it should be studied more [5].

There are many factors that affect the polymer adsorption in porous medium [5]:

- Polymer type such as specific properties of polymer molecules (HPAM, xanthan, molecular weight, charge density and hydrodynamic size.
- The solvent conditions such as PH, temperature and hardness/salinity.
- The surface chemistry of the rocks and the surface area.

Polymer adsorption can be represented by a Langmuir-type isotherm [6]:

$$C_s = \frac{a\, C_p}{1 + b\, C_p} \qquad \text{Equation 3.5}$$

Where C_s is the polymer adsorption, C_p is the polymer concentration and, a and b are tuning constants. The common unit for polymer adsorption is mass of polymer per mass of rock [6]. The figure below shows the Langmuir-type isotherm adsorption and the effects of the constants a and b.

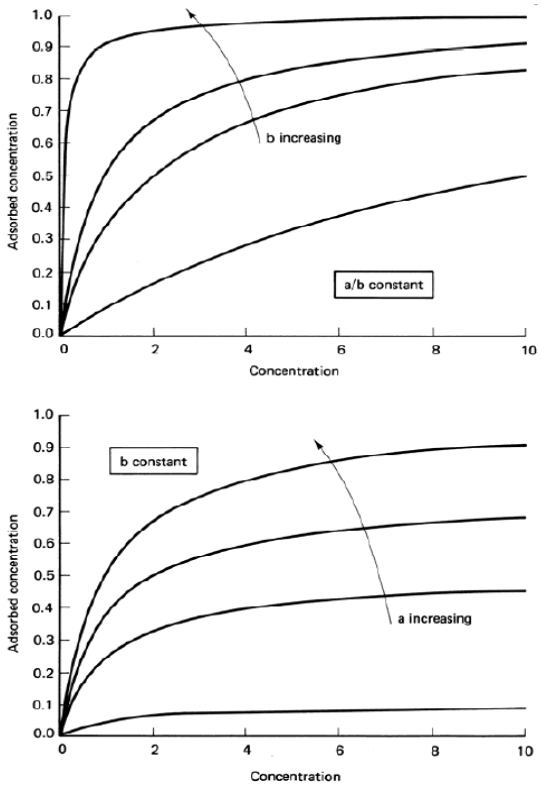

Figure 3.8: Langmuir-type isotherm adsorption curve *[6]*

3.4. Inaccessible Pore Volume

It was observed experimentally in polymer flooding, when there is no polymer retention or when the polymer adsorption is fully satisfied, the polymer molecules are transported faster in the porous medium then the inter tracer dose [42], [48], [49]. Dawson and Lantz, 1972 [48], first reported this phenomenon and called it inaccessible pore volume (IPV). They suggest that the porous media is made of very large range of pore sizes from very small to very large compared to the polymer macromolecule dimensions. Therefore, the polymer, which has large molecules, will not flow through the small size pores and tend to flow in

the large pore size [48]. Therefore, the polymer rends to move faster than the tracer species, typically 20% faster [5].

IPV values are in the range of 1 to 30%. IVP has the opposite effect to polymer retention since IPV enhanced the polymer velocity and retention reduces the polymer velocity [6] [9]. IPV depends on pore size distribution, porosity, permeability and polymer molecular weight. IPV can be very significant as polymer molecular weight increases and permeability to porosity ratio decreases [9].

3.5. Polymer Degradation

Polymer degradation definition is referred to any process that breakdown the polymer molecular structure during any polymer flooding [5]. There are three main types of polymer degradation which are chemical degradation, mechanical degradation and biological degradation [5].

Chemical degradation is any chemical process that breakdown the polymer molecular structure both in a short-term period and in a long-term period. There are chemical factors that affect the polymer stability such as temperature, salinity/hardness, PH, oxidation and hydrolysis. Most polymers are thermal stabile at reservoir temperature since the temperature where polymers will thermally cracks is very high and normal reservoirs temperature is often below that thermal crack temperature. It has been observed experimentally that polymers are stabile at very high and very low PH, especially at high temperature. Hydrolysis is a long-term factor that affects the polymer stability. Hydrolysis will destroy the hydrolyzed extent in HPAM slowly, as a result, the sensitivity to hardness will increase and the viscosity will decrease. The effect of hydrolysis for xanthan is even more serious because the backbone of xanthan is rigid. Oxidation is the most serious chemical process that affects the polymer stability, therefore, oxygen scavengers and antioxidants are added to the polymer to prevent the chemical reactions that happens because of oxygen presence [5] [9].

Mechanical degradation means that the fluid flow rate is high enough that polymer molecules breakdown because of the high stress. Because of this mechanical degradation, there will be irreversible viscosity and resistance factor reduction [50]. It has been observed that the biopolymer xanthan is very stable regarding the mechanical degradation. This is because of its rigid molecular structure. On the other hand, PAM is considered to be very sensitive to shear degradation because of its flexible molecular structure [5]. The figures below show the mechanical stability for both xanthan and PAM.

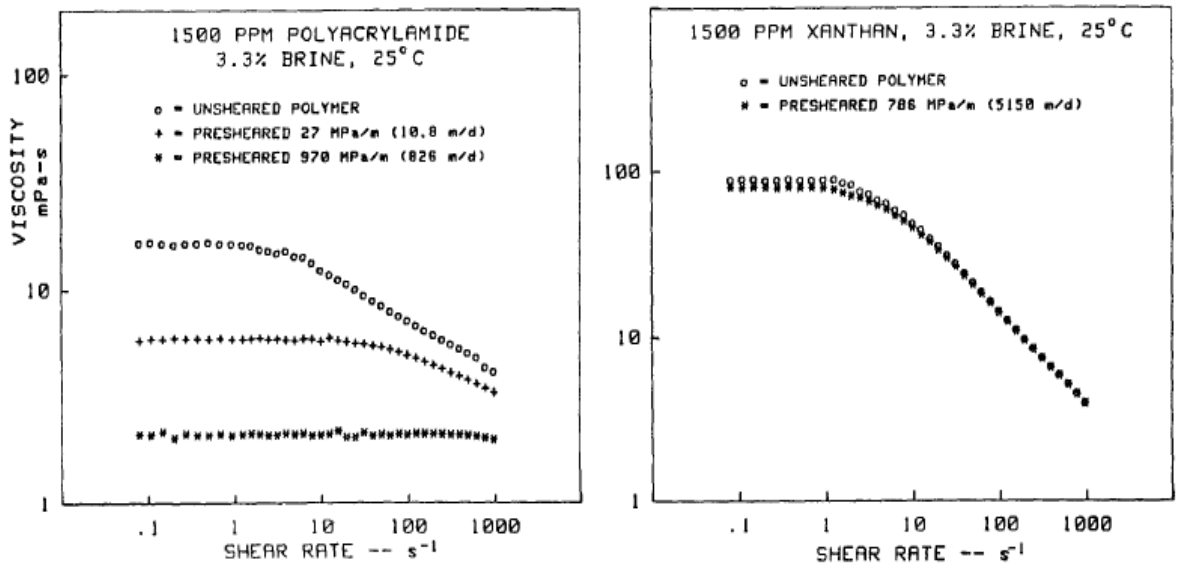

Figure 3.9: Xanthan and PAM mechanical degradation, modified, *[51]*

Biological degradation is the microbial breakdown of the polymer molecular structure, normally this happens because of the bacteria in the brine [5] [6]. Biological degradation can happen both in the surface before polymer injection or in the reservoir if it is sufficiently cool. Normally, biocides are added in the polymer to prevent Microbes' attack [5]. There are many factors that affect the biological degradation such as type of bacteria in the brine, brine salinity, reservoir pressure and temperature and the chemicals present in the reservoir [6].

3.6. Resistance factor

Resistance factor can be defined as the polymer solution resisted to the flow compared to water flow. Resistance factor is due to permeability reduction and viscosity enhancement because of polymer injection. Mathematically, Resistance factor is the ratio of water mobility to polymer solution mobility [9]:

$$R_F = \frac{\lambda_w}{\lambda_p} \qquad \text{Equation 3.6}$$

Where, R_F is the resistance factor and λ_w and λ_w are water and polymer mobilities respectively.

Resistance factor is an induction of the total mobility reduction because of the polymer molecules. Thus, to describe the permeability reduction alone using resistance factor, the following equation can be used [6] [9]:

$$R_K = \frac{k_w}{k_p} = \frac{\mu_w}{\mu_p} R_F \qquad \text{Equation 3.7}$$

Where, R_K is the permeability reduction factor, k_w and k_p are the water and polymer effective permeability, respectively and μ_w and μ_p are water and polymer viscosities, respectively.

There is another factor related to resistance factor which is the residual resistance factor. It can be defined as the mobility of the brine solution before and after polymer injection [9]:

$$R_{RF} = \frac{\lambda_w}{\lambda_{wa}} = \frac{k_w}{k_{wa}} \approx \frac{k_w}{k_p} \qquad \text{Equation 3.8}$$

Where, R_{RF} is the residual resistance factor, λ_w and λ_{wa} are water mobility before and after polymer injection, k_w and k_{wa} are brine effective permeability before and after polymer injection and k_p is polymer effective permeability.

R_{RF} is an induction for present of permeability reduction effect during polymer injection. In many cases, R_{RF} and R_K are normally equal, but R_F is much greater that R_K because it contains both viscosity enhancement effect and permeability reduction effect [6].

Permeability reduction factor is sensitive to polymer type, molecular weight, degree of hydrolysis, shear rate and pore structure. In addition, it has been found, that polymer which has undergone to a small amount of mechanical degradation, has lost some of its permeability reduction effect [6].

The figure below shows the resistance factor and the residual resistance factor with respect to screen factor.

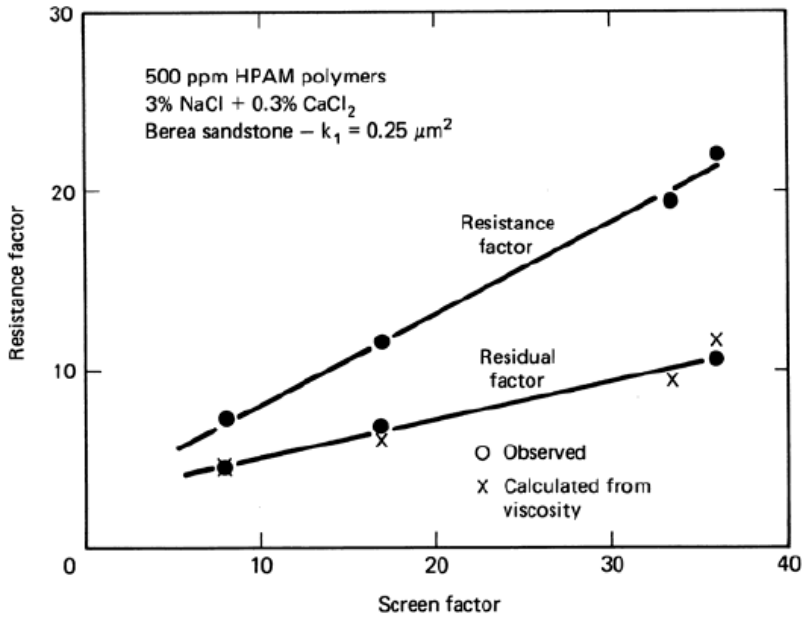

Figure 3.10: Resistance and residual desistance factors verse screen factor *[52]*

4. Simulation Models

Six 2-D unstable waterflood and polymer flood experiments will be simulated and history matched in this thesis. The experiments petrophysical and fluids properties are shown in table 1 below. The oil viscosity range for all experiments is between 7000 cp to 5.1 cp. Also, the experiments were imagined by an X-ray scanner machine at CIPR [53].

The experiments set up in the X-ray scanner is shown in the figure 4.1. The water and polymer injected vertically because of the X-ray scanner machine set up, but the displacement was always gravity stable because the oil and water densities are identical during experiments lifetime [54].

The experiments results are shown in the figure below. Oil recovery and differential pressure are shown in the figure for both waterflooding and polymer flooding.

The X-ray scanner images for both waterflooding and polymer flooding are shown in Appendix[]. Viscous fingering and the unstable displacement are clear in the images.

Table 4.1: Petrophysical and fluids properties of the simulated experiments, modified, *[55]*, *[54]*, *[56]*

Experiment	E7000	E2000	Exp1	Exp2	Exp3	Exp4
Slab dimension [cm]	29.7x29.9x2.05	30x29.8x2.55	30x30x2.9	14.8x14.9x2.1	14.9x15x2.1	15.1x14.9x2.1
Porosity	24%	24.8%	24.2%	22%	22.3%	21.6%
Pore Volume [ml]	440	546	663	102	104	104
S_{wi}	7%	13%	14.6%	10.2%	10.3%	8%
kw(S_w=1) [Darcy]	2.8	2.3	1.76	1.92	2.77	2.44
Oil Viscosity [mPas]	7000	2000	616	412	66	5.1
Polymer Viscosity [mPas]	58	58	28	18.2	10.8	6.4
Polymer Concentration [ppm]	1650	1650	1250	1000	600	400
Injection rate [ml/min]	0.05	0.05	0.05	0.05	0.05	0.05
PV water injected	5.1	2.3	1.1	1	1	1
PV polymer injected	3.18	1.5	1.47	4.74	3.06	2.57

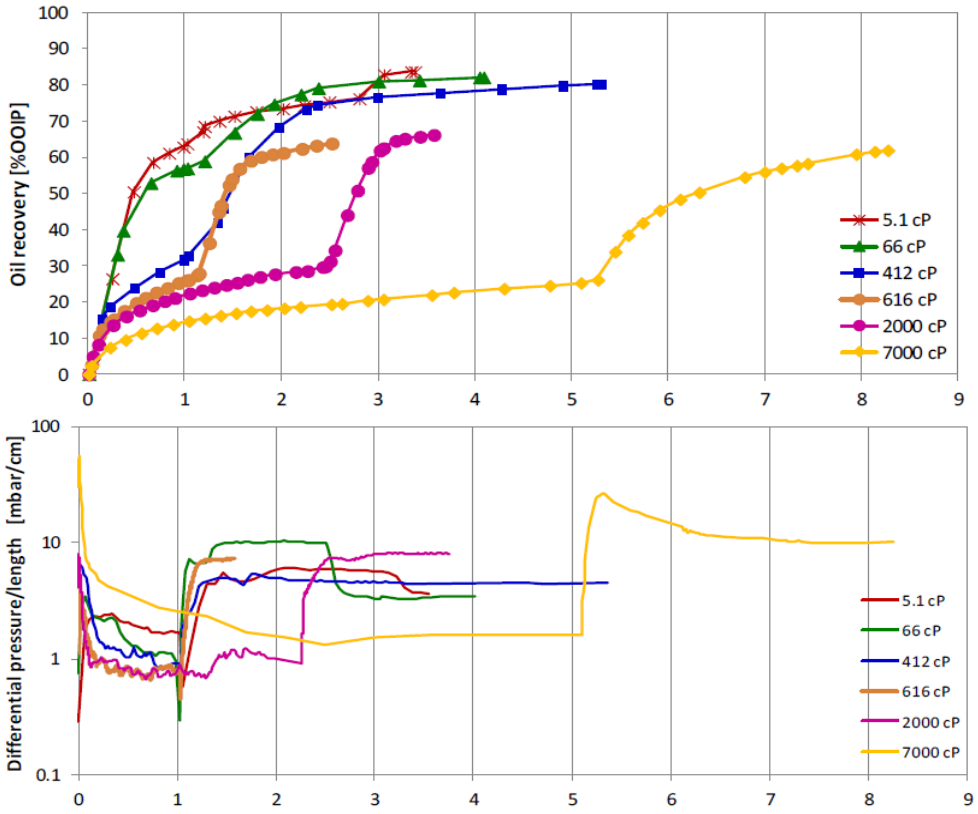

Figure 4.1: Oil recovery and differential pressure results for the six experiments *[55]*

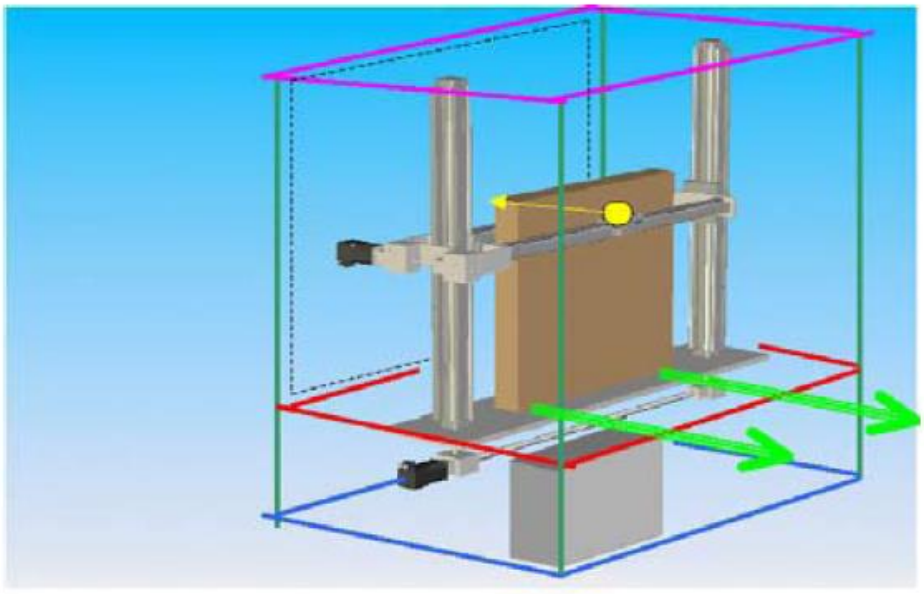

Figure 4.2: Schematic set up of the slab in the 2-D X-ray Scanner *[53]*

Two reservoir simulators were used in this thesis; STARS and CMOST. For the first part of this thesis, waterflooding was simulated using CMOST to find the best history matching of the experiments. Then manual history matching was found using STARS simulator. In the next sections, a short description will be given for STARS and CMOST.

4.1. STARS Simulator

"STARS is a three-phase multi-component thermal and steam additive simulator" [57]. STARS software is developed by CMG (Computer Modelling Group LTD.). It has many simulation options such as waterflooding, chemical flooding, thermal application and other options.

4.2. CMOST Simulator

CMOST is a CMG software that works with others CMG applications. CMOST with help of other SMG softwares can perform sensitivity analyses, history matches, optimizations, and uncertainty assessments. [58]. In this thesis, history matching option will be used for the first part (Waterflooding).

CMOST is used for waterflooding history matching only because CMOST uses only Corey correlation for relative permeability. However, for polymer flooding history matching, more flexible permeability correlations should be used since it is more complex to conduct a history matching for polymer flooding. More details will be highlighted regarding this issue.

5. Sensitivity Analysis

In this chapter, a sensitivity analysis will be conducted to some parameters that influence the history matching. The E7000# experiment model will be the base file of the sensitivity analysis. First, grids regulation will be tested to minimize the numerical dispersion. Then, the physical dispersion will be tested to find its sensitivity to the history match. After that, polymer concentration, polymer molecular mass, polymer adsorption, polymer viscosity and the relative permeability curves of the polymer flooding will be examined and find how sensitive these parameters to the history match are.

5.1. Numerical Dispersion

Numerical dispersion is an issue related to the large time step and/or less grid blocks number (less grid resolution) that leads to smeared spatial gradients of saturation or concentration. STARS grid model was created to represent the real experiments. The flow direction is vertical, therefore, more grid resolution should be defined in the vertical direction to minimize or even remove the numerical dispersion Four different grid lengths will be tested; 10 cm, 5 cm, 1 cm and 0.1 cm as Δk as it is shown in figure 5.1.

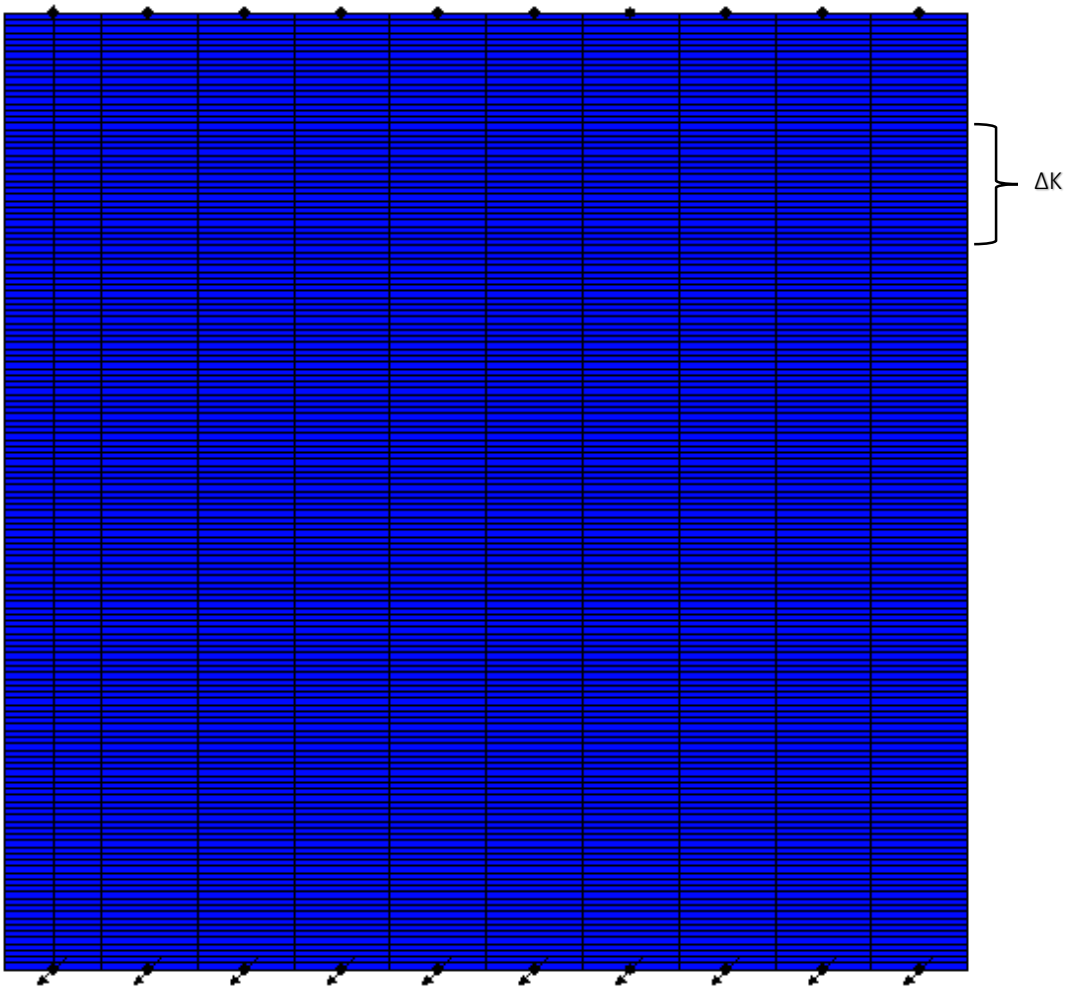

Figure 5.1: STARS grid model

The numerical dispersion will be tested by using the concentration profile of a grid block located in the middle of the model. Also, the time step is minimize to its lowest possible value in STARS. The figure below shows the numerical dispersion effect of different grid lengths on the polymer concentration profile.

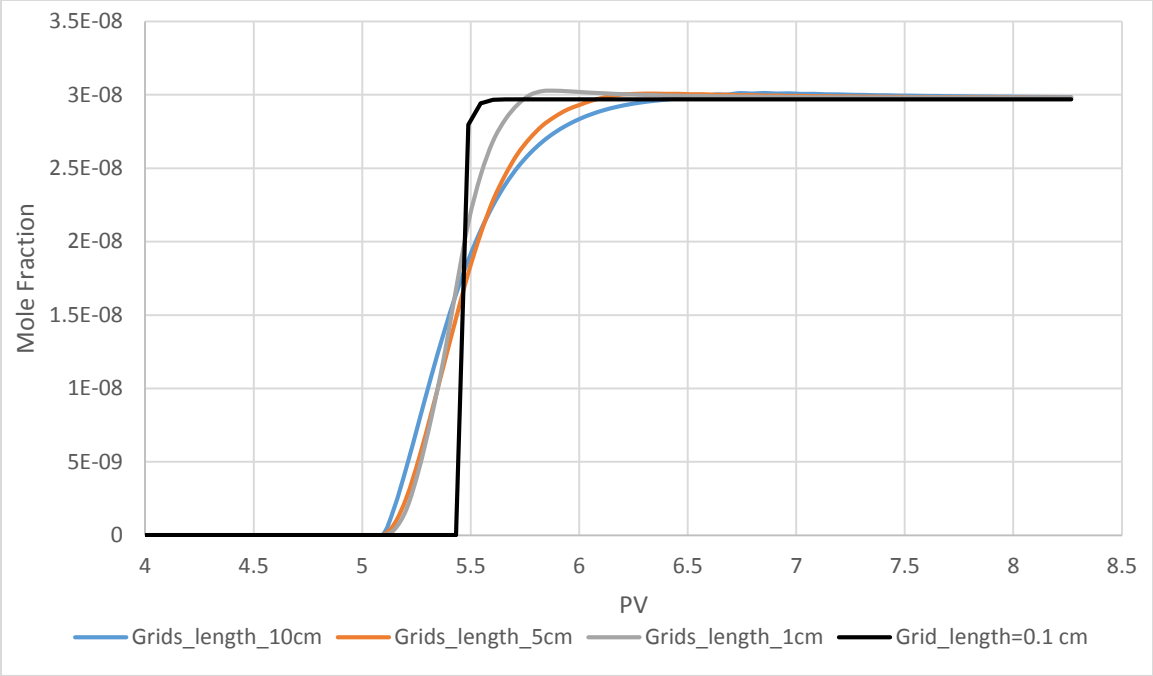

Figure 5.2: Numerical dispersion effect on polymer concentration profile

It is clear from the figure above that the numerical effect is reduced as the grid length is decreasing. A large numerical dispersion effect was observed with grid length of 10 cm, 5 cm and 1 cm, and there is almost no numerical dispersion for grid length of 1 cm and 0.1 cm. Therefore, it is clear that 0.1 cm grid length is a good length that minimizes the numerical dispersion effect.

5.2.Physical Dispersion

Physical dispersion can be defined at the broadening and spreading of concentration fronts and its unit is cm^2/day in a lab scale. A wide range of physical dispersion values will be tested; 1E-3 cm^2/day, 1E-2 cm^2/day, 0.01 cm^2/day, 0.1 cm^2/day, 1 and 10 cm^2/day. The figure below shows the sensitivity analysis results of the physical dispersion on the concentration profile of one grid block located in the middle of the model.

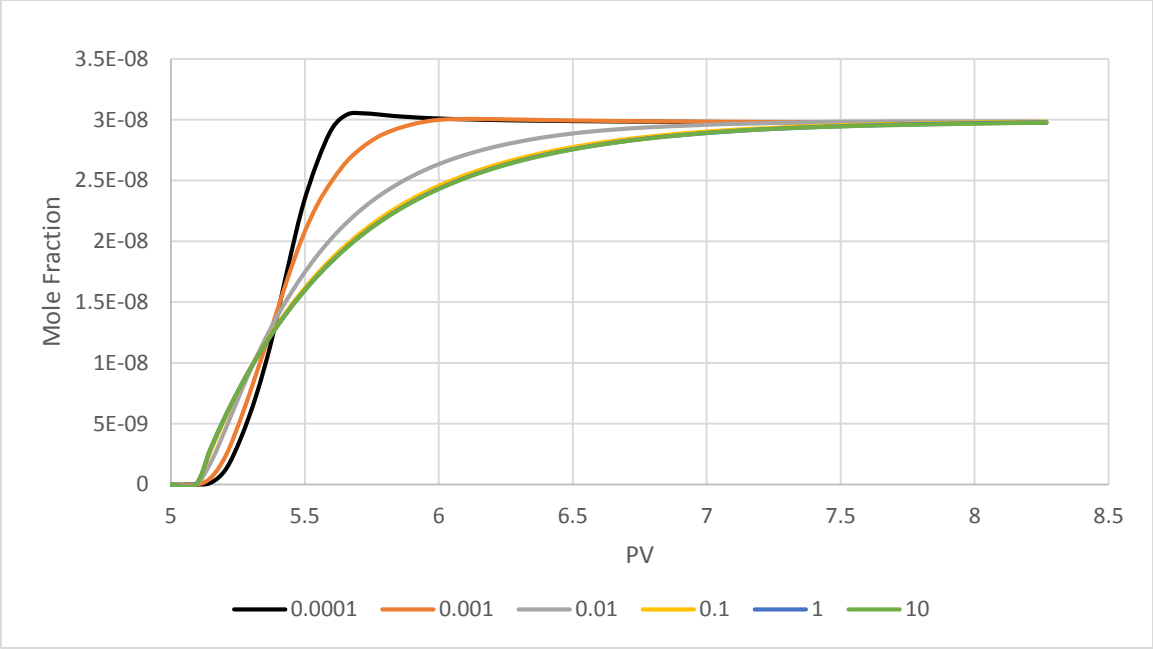

Figure 5.3: Physical dispersion sensitivity analysis on polymer concentration profile

It is clear from the figure above that a high physical dispersion value corresponds to a late response to the polymer flooding. For 0.1 cm^2/min, 1 cm^2/min and 10 cm^2/min it is required to inject two PV of polymer to reach the desired polymer concentration while for the other physical dispersion values, it is required less than one PV of polymer to reach the desired polymer concentration. Therefore, the physical dispersion is a good history matching parameter that can give earlier or late polymer response.

5.3.Molecular Mass

Since many fluid properties are specified by a per-mole basis, molecular mass is very important to define the proper properties in STARS. For example to convert the concentration in ppm to the mole fraction, the given equation should be used:

$$\text{Concentration in Mole Fraction} = \frac{m_p}{m_w} \times \frac{M_w}{M_p} \qquad \text{Equation 5.1}$$

Where m_p ,and m_w are the polymer and water mass respectively, and M_p and M_w are the polymer and water molecular mass respectively.

The adsorption value should be corrected to the molecular mass defined in STARS.

Three different values of polymer molecular mass were tested; 10,000 *g/mole*, 5000 *g/mole* and 1000 *g/mole*. The figure below shows the sensitivity of the molecular mass on cumulative oil production profile.

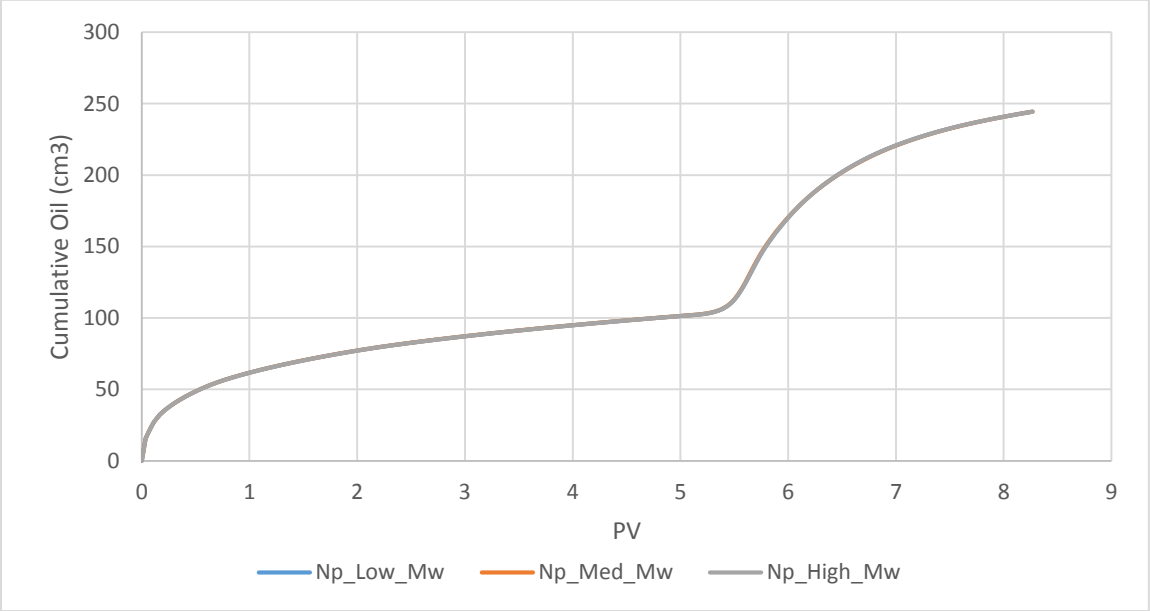

Figure 5.4: Molecular mass sensitivity analysis results on cumulative oil production profile

It is clear from the figure above that the molecular mass has no effect to the model. Therefore, polymer molecular mass can be any value, but it is better to define it as close as possible to the correct polymer molecular mass used in the experiment.

5.4. Viscosity

Viscosity is one of the most important property in polymer flooding. It has a direct effect on the polymer flood efficiency. Although, polymer viscosity will not be change in the history matching foe each experiment, but polymer viscosity profile and how the viscosity developed in the model will be viewed. In addition, different polymer viscosities will be examined to test polymer viscosity efficiency. Polymer viscosity is defined in STARS using the keyword SHEARTAB which is a table of Darcy velocity and viscosity. The desired polymer viscosity is therefore, will be based on the polymer flow rate that is defined

in the injection well. The figure below shows the different three viscosity tables that are defined in STARS.

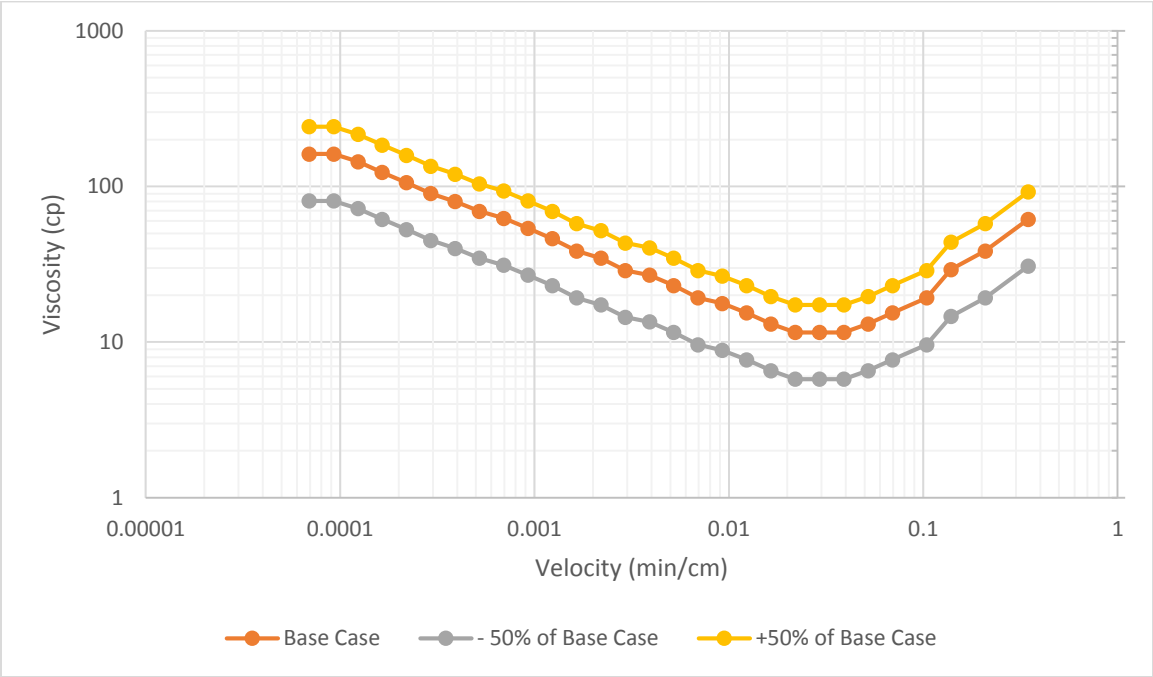

Figure 5.5: Darcy velocity versus polymer viscosity for E7000 experiment

And the figure below shows how the three polymer viscosities were developed in the model.

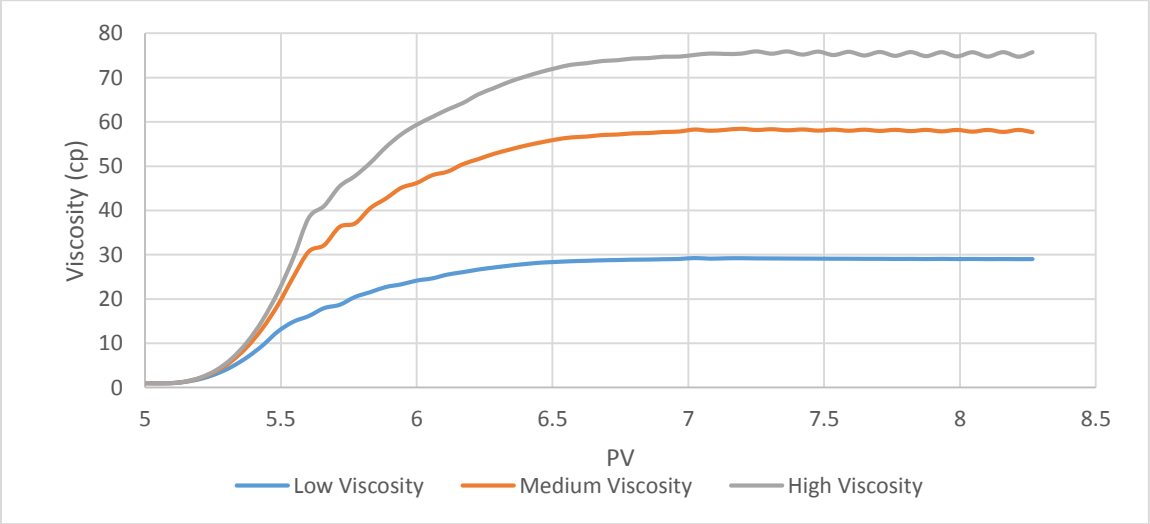

Figure 5.6: Viscosity profile for polymer flooding in E7000 experiment

It is clear from the figure above that it is required almost one PV to reach the desired polymer in a block that is located in the middle of the model.

The sensitivity analysis of polymer viscosity on the cumulative oil produced and differential pressure is shown in the figure below.

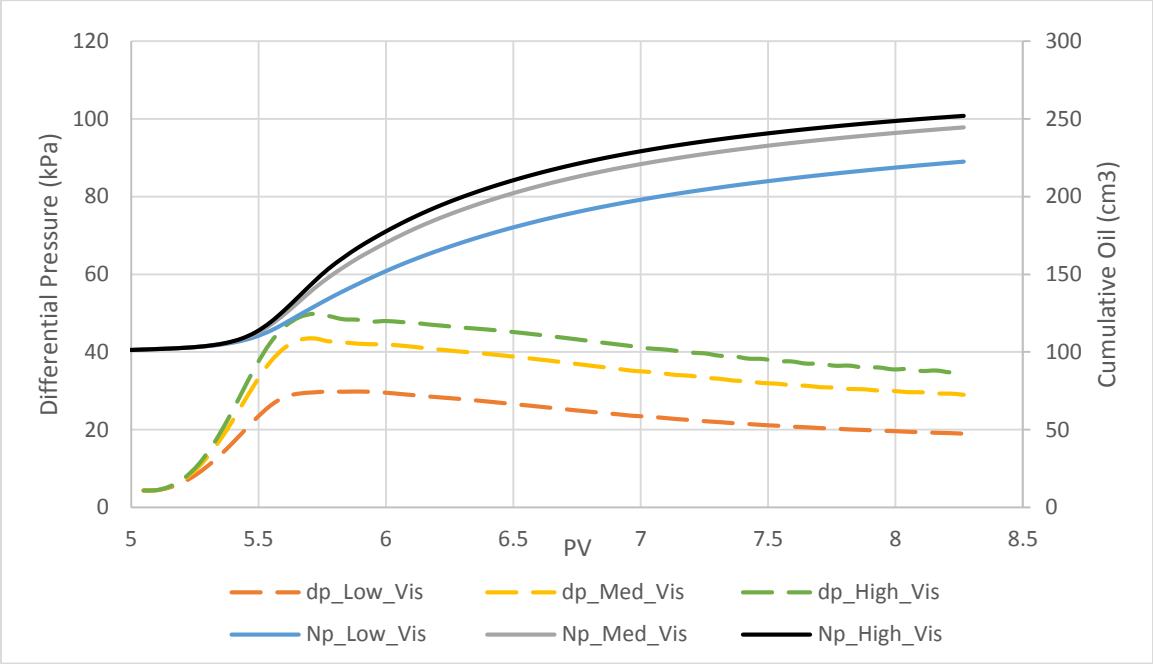

Figure 5.7: Viscosity sensitivity analysis results on cumulative oil production and differential pressure profiles

The figure above shows the polymer viscosity effect on the polymer flood efficiency. It is clear that the high polymer viscosity case (76 *cp*) which is 50% more than the polymer viscosity base case (58 *cp)* has no large effect on the flood efficiency, while the low polymer viscosity case (30 *cp*) which is 50% less than the base case has a large effect compared to the other two viscosities. The difference in oil recovery between the low polymer viscosity (30 *cp*) and the base case polymer viscosity (58 *cp*) is 5% less oil recovery, while the difference between the base case polymer viscosity (58 *cp*) and the high polymer viscosity (76 *cp*) is only 1.8% more oil recovery.

The effect of different polymer viscosities on the differential pressure profile is almost identical to the difference on the cumulative oil profile. The difference between the high

polymer viscosity case and base polymer viscosity case on differential pressure is slightly less than the difference between the low polymer viscosity case and the base polymer viscosity case.

5.5. Adsorption

Polymer adsorption is considered one of most important parameter for history matching since it can provide some flexibility to the polymer front. Polymer adsorption is defined in STARS using the keyword ADSTABLE in which polymer adsorption is defined at the corresponding polymer concentration. For this case, only two points are defined in the adsorption table, which are zero adsorption at zero concentration and maximum adsorption at the desired polymer concentration. The relationship between the polymer concentration and polymer adsorption in this test model was defined to be linear. Three different polymer adsorption values were tested.

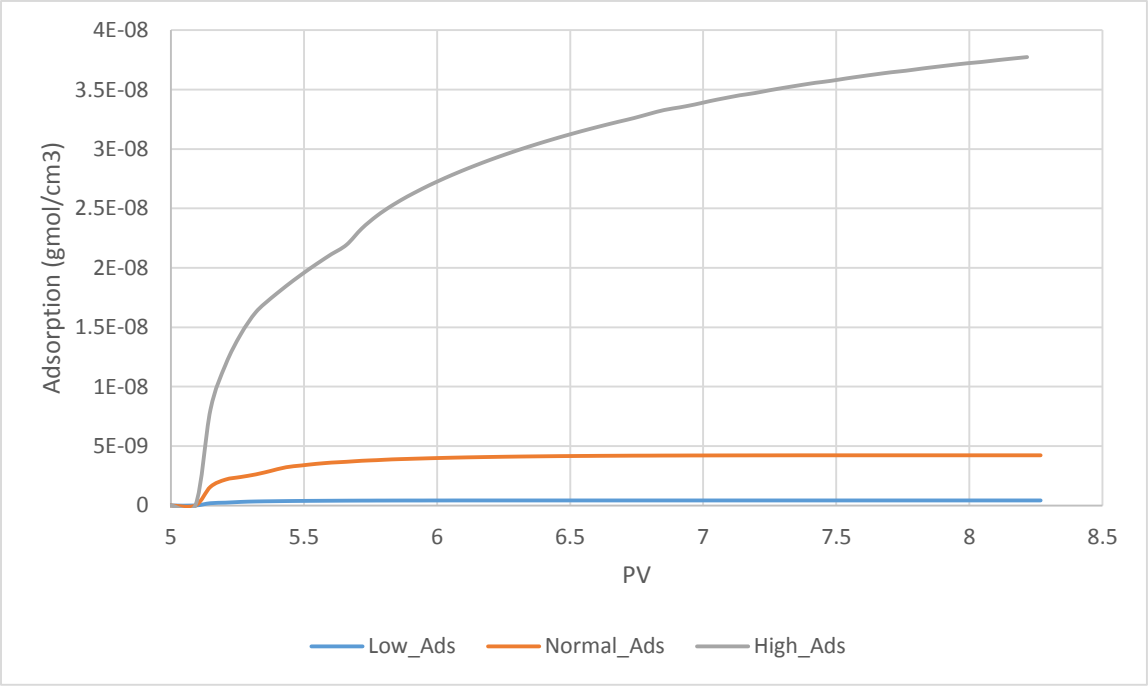

Figure 5.8: Polymer adsorption profile

The figure above shows the polymer adsorption profile in the injection well grids. It is clear that the high polymer adsorption case requires a lot of polymer PV injected to reach the adsorption defined in STARS. The figure below shows more details.

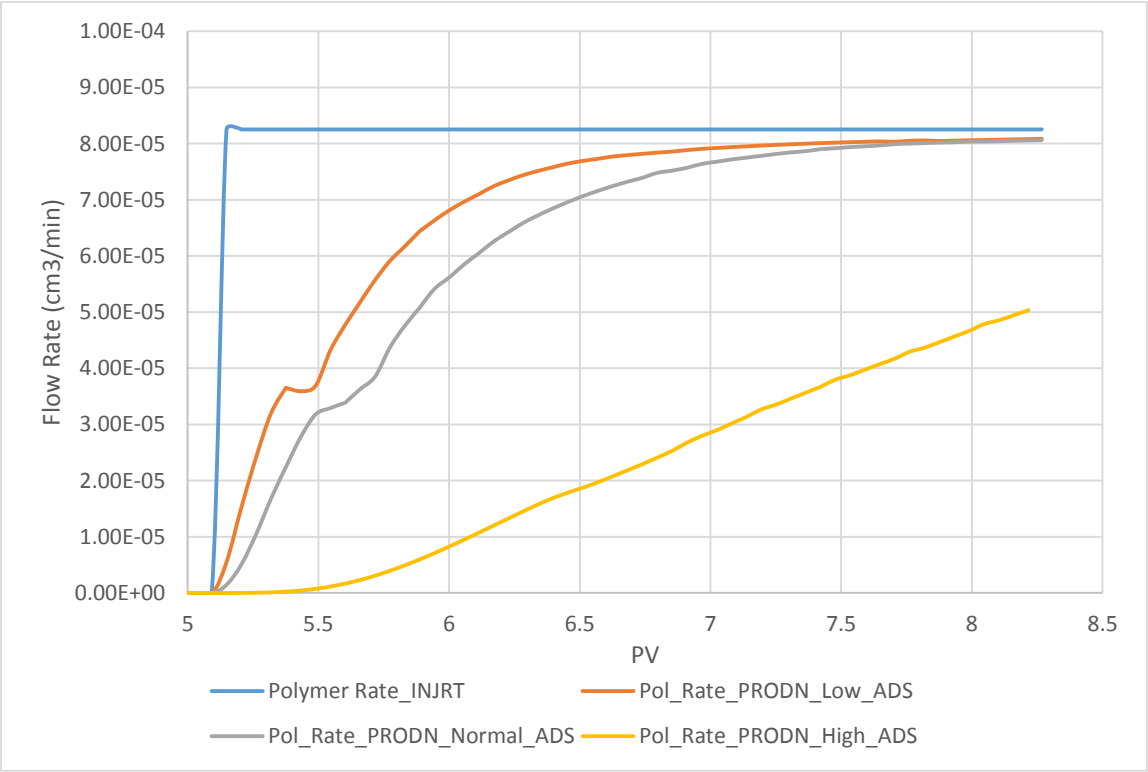

Figure 5.9: Polymer Adsorption Sensitivity Analysis Results

Figure 5.9 shows the polymer flow rate at the injection well and the polymer flow rate at the production well. This figure shows the effect of polymer adsorption on the produced polymer flow rate. The polymer flow rate in the high polymer adsorption case will not reach the flow rate injected because the polymer is adsorbed through the whole experiment time, while in the other cases, the polymer flow rate at the production well reaches the injected polymer flow rate because the maximum adsorption is reached before the end of the experiment. Therefore, it is very important to find the correct polymer adsorption for the used polymer concentration since adsorption has a direct effect to the flood efficiency. The higher polymer adsorption is defined the late polymer response will be observed because it will required higher polymer PV injected to reach the maximum adsorption.

5.5.1. Reversible and Irreversible Polymer Adsorption

STARS has an option to define the polymer adsorption reversibility through the keyword ADRT. The polymer adsorption is considered to be completely reversible if ADRT equals zero, and it is completely irreversible if ADRT value equals ADMAXT value. In polymer adsorption reversibility sensitivity analysis, it was tested when the polymer adsorption is completely reversible (ADRT=0), when the polymer adsorption is completely irreversible (ADRT=ADMAXT) and when the polymer adsorption is partially reversible (ADRT= 0.5 ADMAXT). Although in this thesis, polymer flooding is the last phase injected, and therefore, polymer adsorption reversibility effect cannot be observed, four pore volume of water was injected after polymer flooding to examine the polymer adsorption reversibility effect. The figure below shows the three states of polymer adsorption.

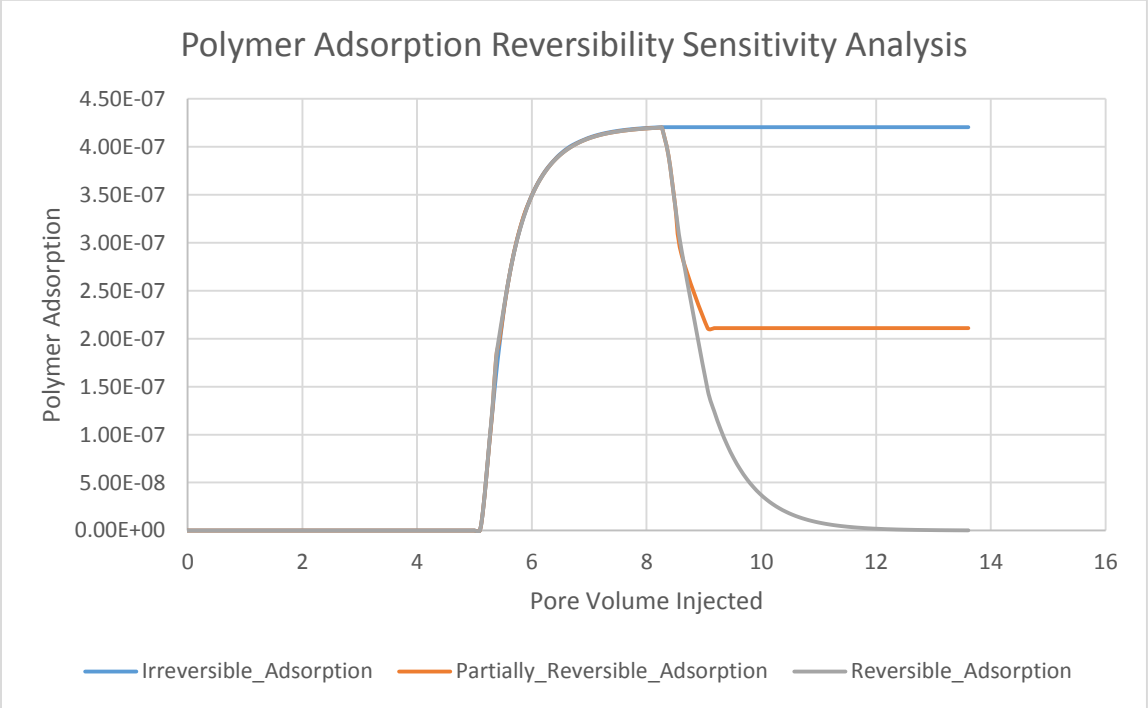

Figure 5.10: Polymer adsorption reversibility sensitivity analysis

From the figure above which shows the polymer adsorption reversibility effect, as it is expected, when the polymer adsorption is completely irreversible, the polymer adsorption stayed at the maximum level and it did not decrease when there is no polymer flooding. On the other hand, the polymer adsorption declined to zero when the adsorption is

completely reversible. For the case when the polymer adsorption is partially reversible, polymer adsorption declined to approximately half of the adsorption profile and then stayed constant.

5.6. Inaccessible Pore Volume

Inaccessible pore volume option in STARS can be specified by the keyword PORFT. PORFT determines the fraction of accessible pore volume in the model. If PORFT is 1, that means that all the pore volume is accessible and if it is 0.9, that means 10% of the pore volume is inaccessible. In this sensitivity analysis, fore value of PORFT were tested; 1, 0.9, 0.8 and 0.7. The maximum inaccessible pore volume that was tested is 30% since it was reported that 30% inaccessible pore volume is the extreme case [9].

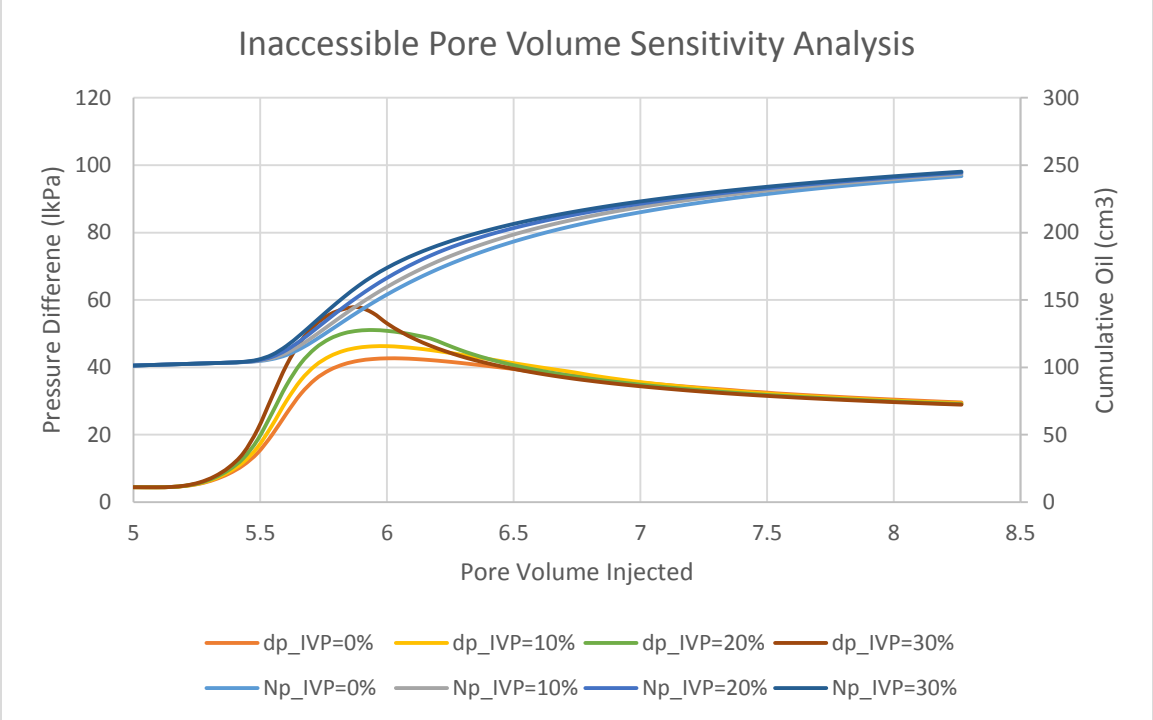

Figure 5.11: Inaccessible pore volume sensitivity analysis on cumulative oil production and differential pressure profiles

The figure above shows inaccessible pore volume effect on polymer flooding efficiency. It is clear that as the inaccessible pore volume increases the polymer velocity increases. This is clear in the pressure profile. There is a small change in cumulative oil profile and when

the inaccessible pore volume is greater, a quicker response is observed in cumulative oil profile.

5.7.Polymer Concentration

The polymer concentration has a direct relationship with polymer adsorption. Three polymer concentration were tested; 10,000 ppm [1.8E-7 in mole fraction], 5000 ppm [9.0E-8 in mole fraction] and 1000 ppm [1.8E-8]. The figure below shows the polymer concentration sensitivity analysis results.

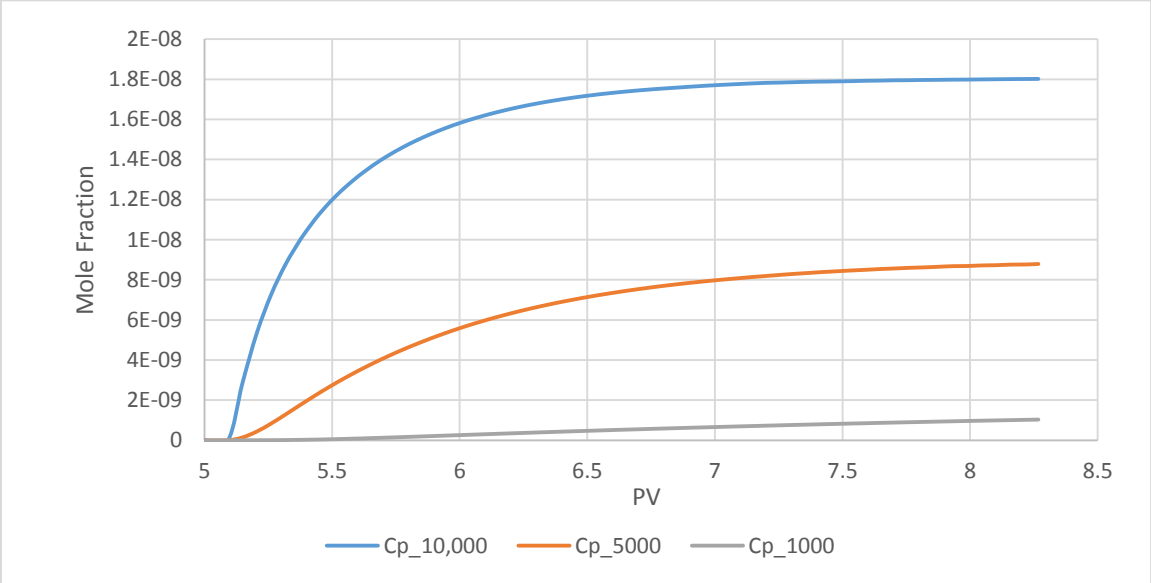

Figure 5.12: Polymer concentration profile for E7000 experiment

The figure above shows the polymer concentration profiles for the different three concentrations. It is clear that the high polymer concentration case reached the desired concentration faster than the other cases. This is obviously because of the polymer adsorption. Since the same polymer adsorption is defined for the all cases, the high polymer concentration case will reach the desired concentration faster because there is a higher amount of polymer that can be adsorbed and thus quicker maximum adsorption will be reached. This effect can be noticed from the figure below, which shows polymer adsorption profile.

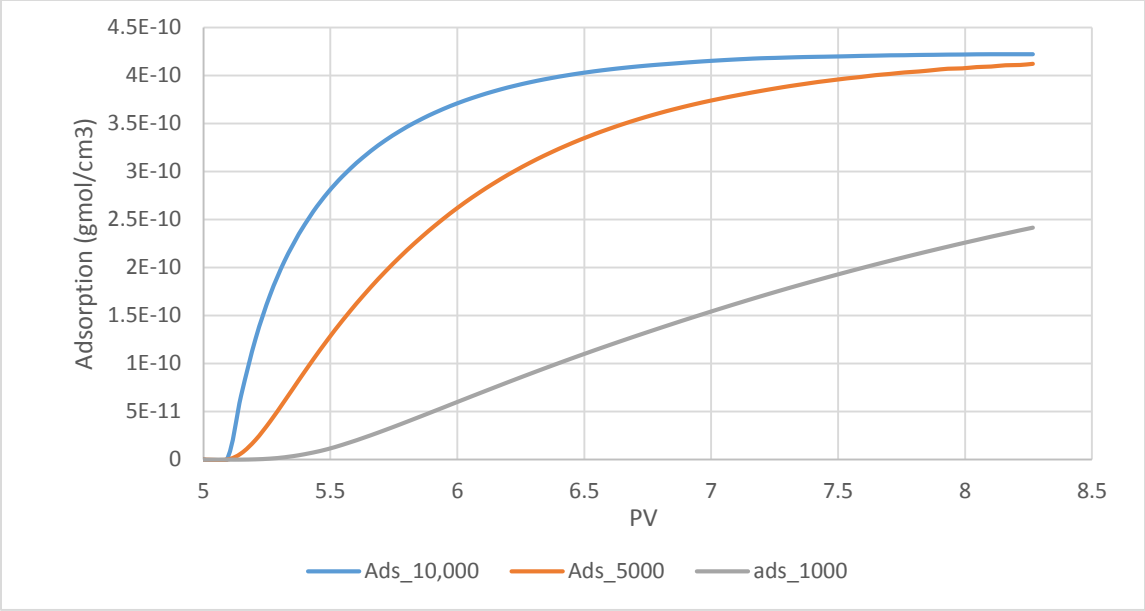

Figure 5.13: Polymer adsorption profile

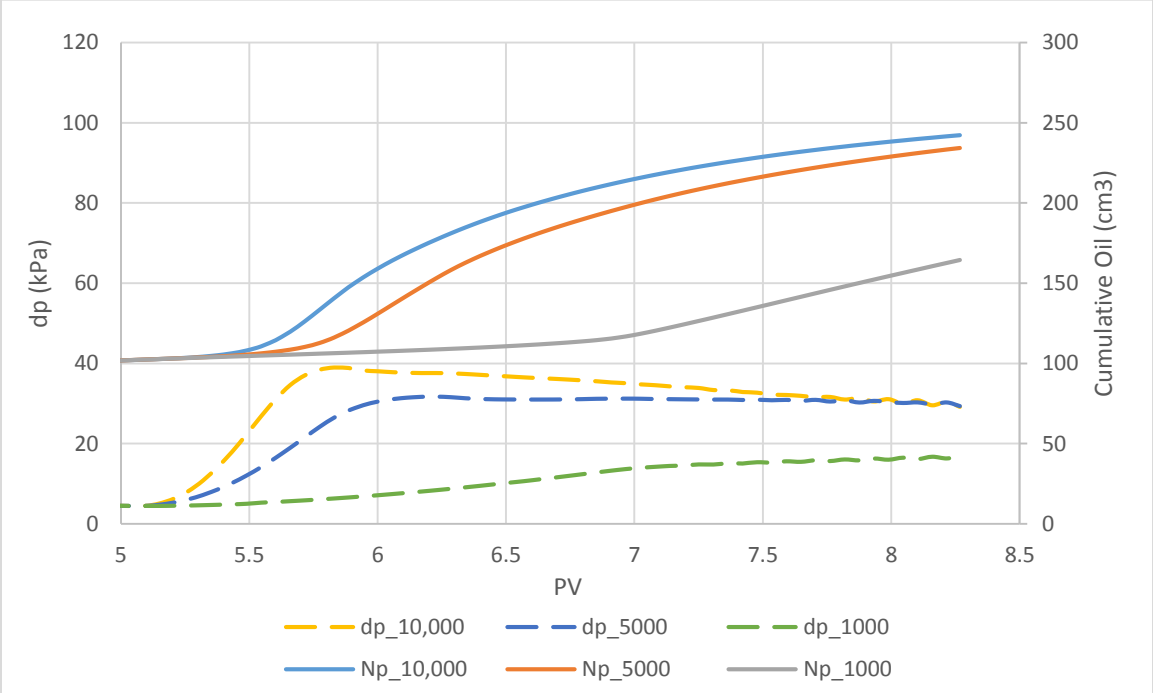

Figure 5.14: Polymer concentration sensitivity results on cumulative oil production and differential pressure profiles

Figure 5.14 shows the polymer concentration sensitivity analysis results on cumulative oil and differential pressure profiles. It is clear from this figure that the low polymer concentration has very unfavorable effect which can be related directly to the polymer

adsorption as it is discussed above. Also, it can be noticed that the high polymer concentration affects the polymer front. It gives a fast polymer response compared to the base case, but also this effect is directly related to the polymer adsorption. However, it is difficult to test polymer concentration without relating it to the polymer adsorption since the two properties are highly connected.

5.8.Relative Permeability

Relative permeability is the most important parameter for history matching and it is the main parameter that describes oil and water mobility in the simulation model. In this thesis, two relative permeability correlations will be used; Corey correlation [59] and LET correlation [60]. Corey correlation will be used in the first part which is waterflooding history matching, and LET will be used in the second part which is polymer flooding history matching.

Corey correlation for relative permeability will be used in this sensitivity analysis. First, water relative permeability will be tested by varying the water exponent. Then, oil relative permeability will be tested also by varying the oil exponent. The figures below show the oil and water relative permeabilities that were used in the sensitivity analysis. Note that water relative permeability is in logarithmic scale for better viewing of variations in small scale.

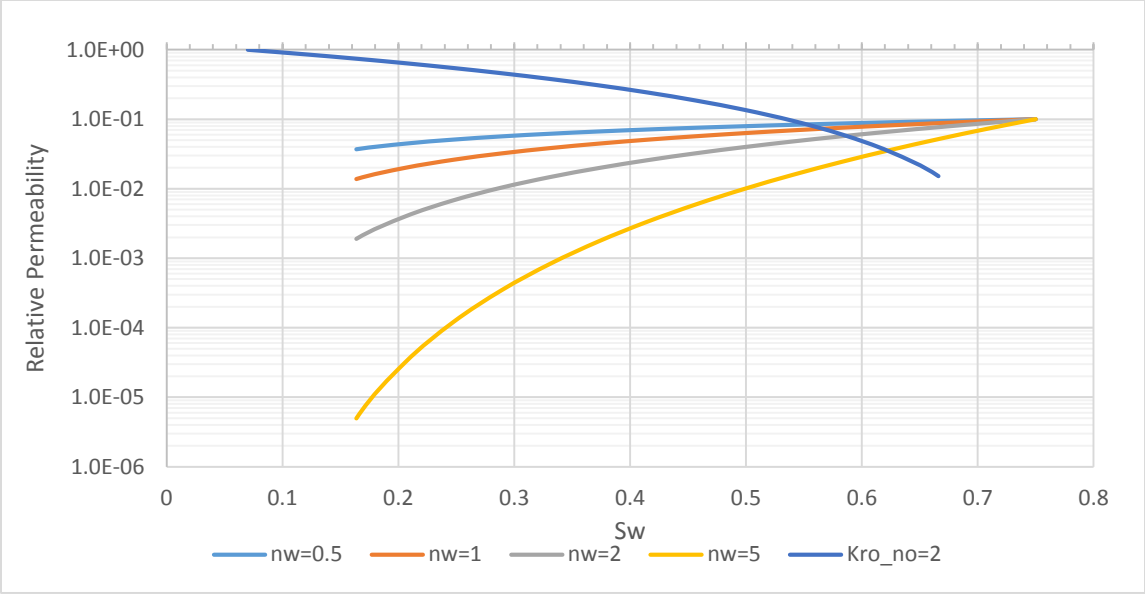

Figure 5.15: Water relative permeability with different water exponents

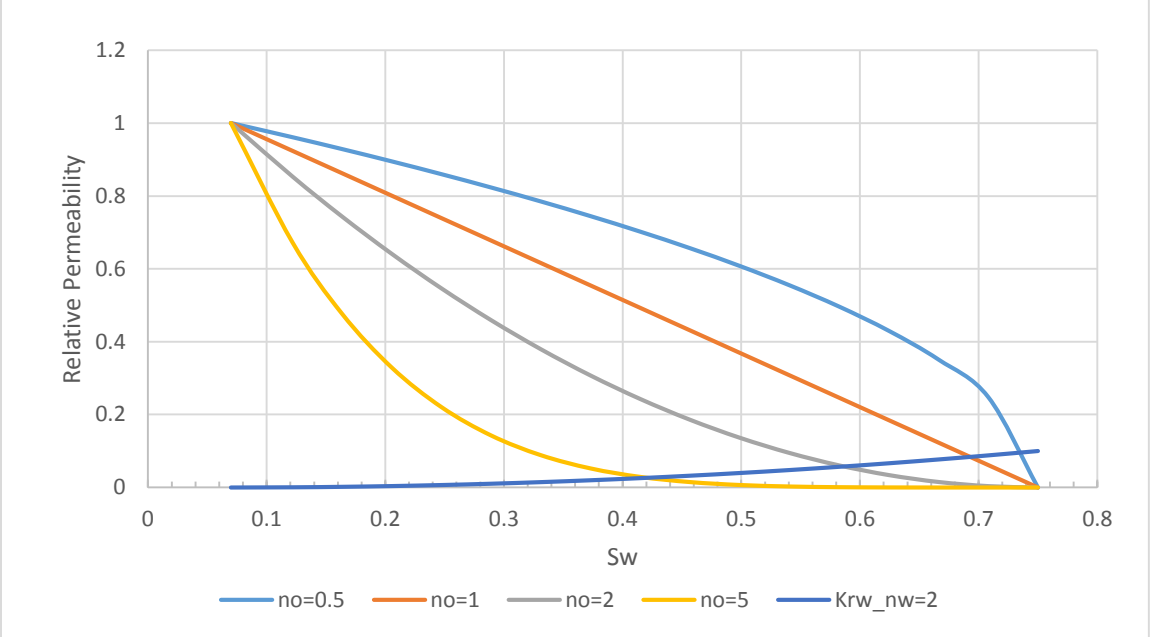

Figure 5.16: Oil relative permeability with different oil exponents

The figures below show the results of water and oil relative permeability sensitivity analysis on cumulative oil production and differential pressure profiles.

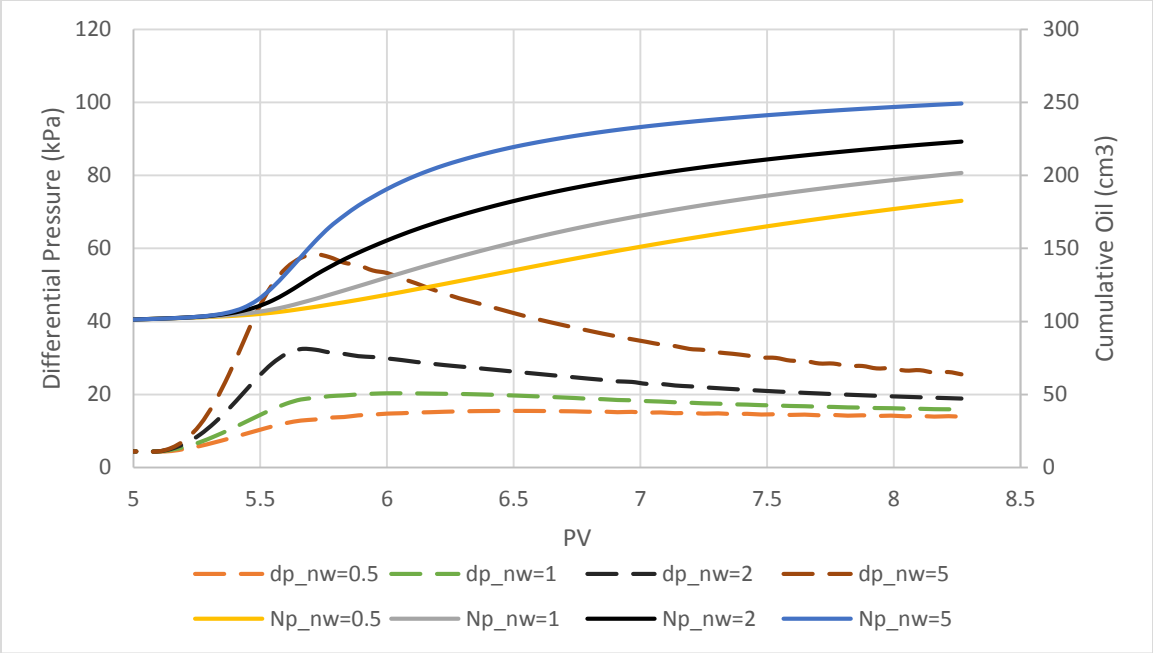

Figure 5.17: Water relative permeability sensitivity analysis results on cumulative oil production and differential pressure profiles

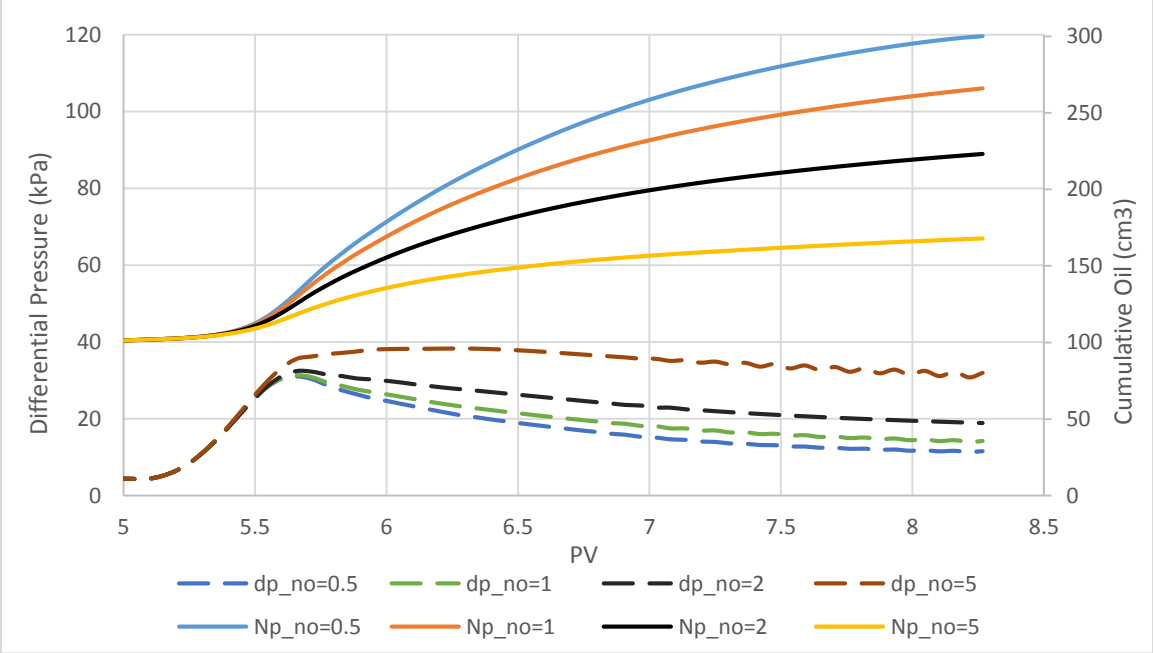

Figure 5.18: Oil relative permeability sensitivity analysis results on cumulative oil production and differential pressure profiles

From the figures above it is clear that water relative permeability governs the earlier response of the polymer flooding because it is very sensitive at low water saturation as it

is clear from figure 5.16, while oil relative permeability is not. On the other hand, oil relative permeability is sensitive at the end of the polymer flood.

The same behavior can be noticed for the differential pressure profiles. A quicker response in differential pressure profile is noticed when water relative permeability is varying while, there is a small change in the pressure profile only at the end of the polymer flood when oil relative permeability is varying. However, in this case, water relative permeability is sensitive and will help more in history matching since it gives more similar behavior to the experimental behavior.

Another parameter related to the relative permeability, which may have an influence to the polymer flooding, is the relative permeability set used in the transition zone. STARS uses the polymer relative permeability set based on the polymer concentration desired. It starts to use the relative permeability set defined for polymer flooding when the polymer concentration defined is reached, however it was noticed as mentioned above it requires sometimes more than one PV injected to reach the desired concentration. It depends on several parameter such as numerical dispersion, physical dispersion and adsorption. However, STARS uses an interpolated relative permeability set base on the relative permeability defined before the polymer flood and the relative permeability defined for the polymer flood. The following equations shows how stars interpolates the relative permeability set [49]:

$$\mathrm{k_{rw}} = \mathrm{k_{rwA}} \times (1 - \mathrm{wtr}) + \mathrm{k_{rwB}} \times \mathrm{wtr} \qquad \text{Equation 5.2}$$

$$\mathrm{k_{ro}} = \mathrm{k_{roA}} \times (1 - \mathrm{oil}) + \mathrm{k_{roB}} \times \mathrm{oil} \qquad \text{Equation 5.3}$$

$$\mathrm{wtr} = \mathrm{ratw}^{\mathrm{WCRV}} \qquad \text{Equation 5.4}$$

$$\mathrm{oil} = \mathrm{ratn}^{\mathrm{OCRV}} \qquad \text{Equation 5.5}$$

$$\mathrm{ratw} = \mathrm{ratn} = \frac{\mathrm{DTRAPW} - \mathrm{DTRAPWA}}{\mathrm{DTRAPWA} - \mathrm{DTRAPWB}} \qquad \text{Equation 5.6}$$

where the subscripts A and B refer to the relative permeability sets for waterflooding and polymer flooding respectively. DTRAPW is the current polymer concentration, DTRAPWA is the defined polymer concentration for water flooding and DTRAPWB is the defined polymer concentration for polymer flooding. WCRV and OCRV are curvature interpolation parameters that allow additional flexibility in interpolating between sets of curves. The default value for these parameters is 1. From the equations above it is clear that if, for example, WCRV equals to 2, this means that the interpolated krw retains its krwA character more closely over range of interpolation, while if WCRV equals 0.5, this implies that krwB has the dominant influence.

A sensitivity analysis was conducted to WCRV to test its influence to the polymer flood efficiency. Three values of WCRV were tested; 3, 1 and 0.5. The figure below shows the relative permeability that was interpolated in the transition zone, and it is compared to the relative permeabilites sets, which were used for the water flooding (krwA) and the polymer flooding (krwB).

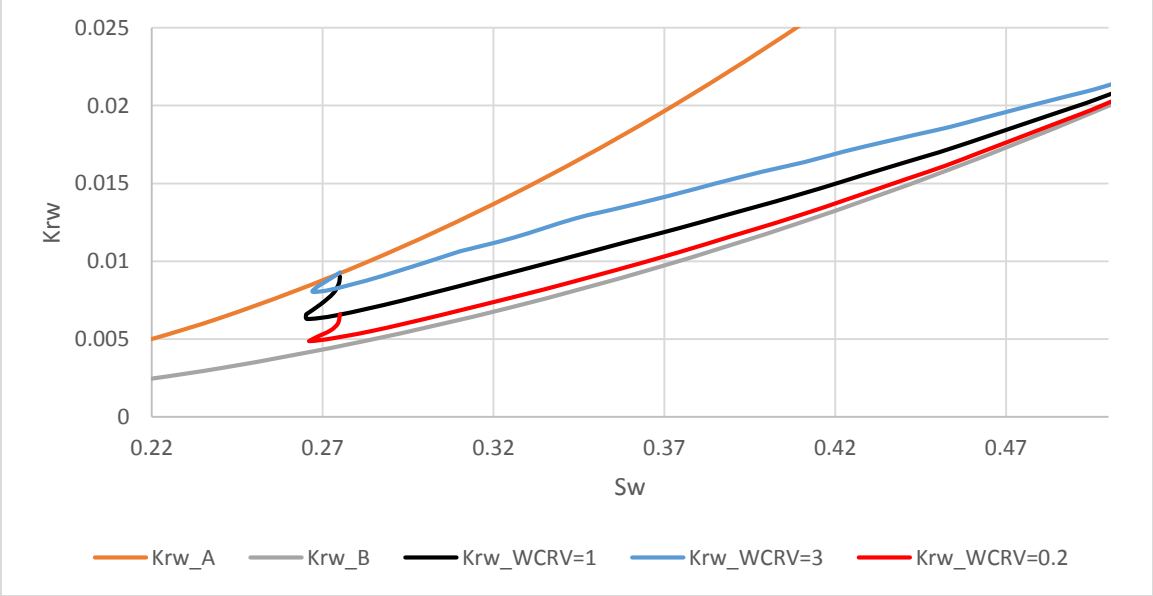

Figure 5.19: Interpolated water relative permeability in the transition zone.

The figure above shows how the interpolated relative permeability can be changed base on the relative permeability sets which are defined in STARS.

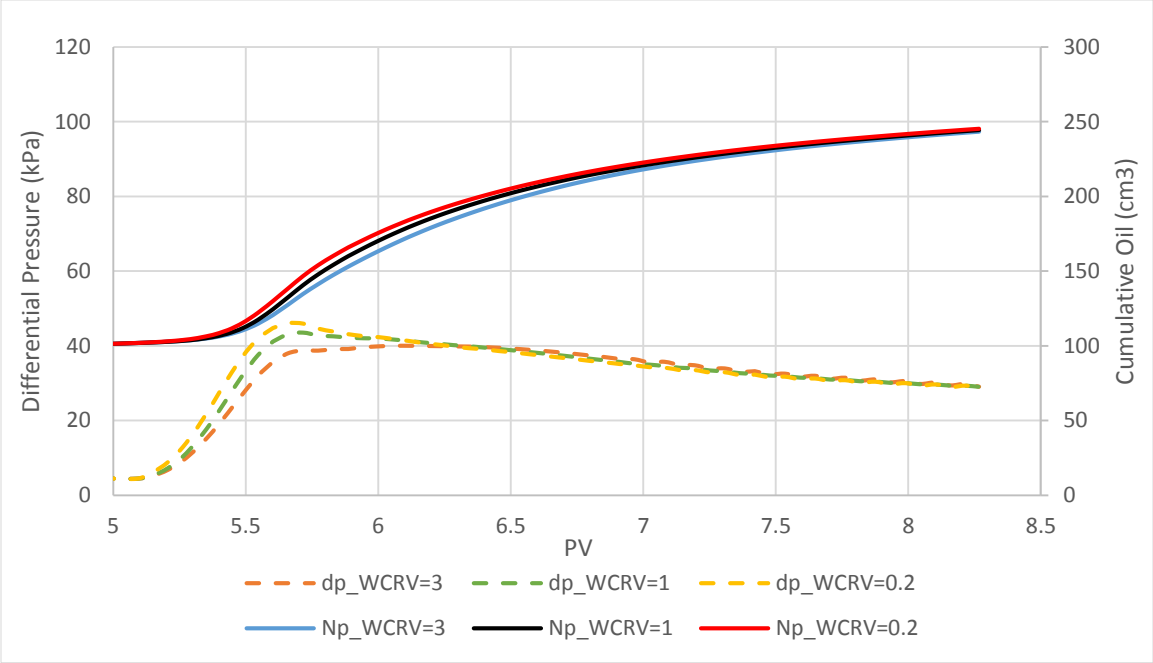

Figure 5.20: Interpolation parameter WCRV sensitivity analysis results on cumulative oil and differential pressure profiles

The flexibility allowed by STARS to change the curvature interpolation parameters can give a significant effect at the beginning of the polymer flooding as it is shown in the figure above. However, the overall oil recovery and the differential pressure at the end of the flood is unaffected, but that change in the beginning of the flood can help to have better history matching.

5.9.Model Restrictions

During the sensitivity analysis, it was found that the differential pressure of Exp3 and Exp4 did not change with the change in the relative permeability curves. However, the cumulative oil profile showed a normal behavior when the relative permeability curves were changed. On the other hand, the other experiments, E7000, E2000, Exp1 and Exp2, have a positive response to all sensitivity analyses.

Waterflooding history matching by alternating relative permeability curves was conducted to Exp3 and Exp4 to observed the change in differential pressure profile. The figures bellows shows the CMOST results of waterflooding history matching for Exp3 and Exp4.

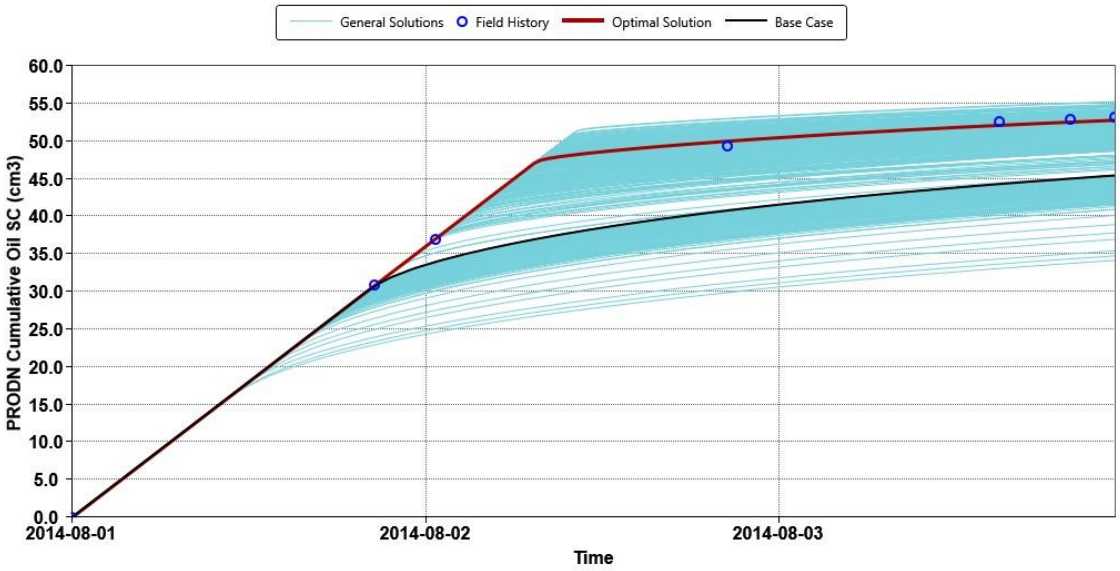

Figure 5.21: Cumulative oil profile of CMOST waterflooding history matching for Exp3

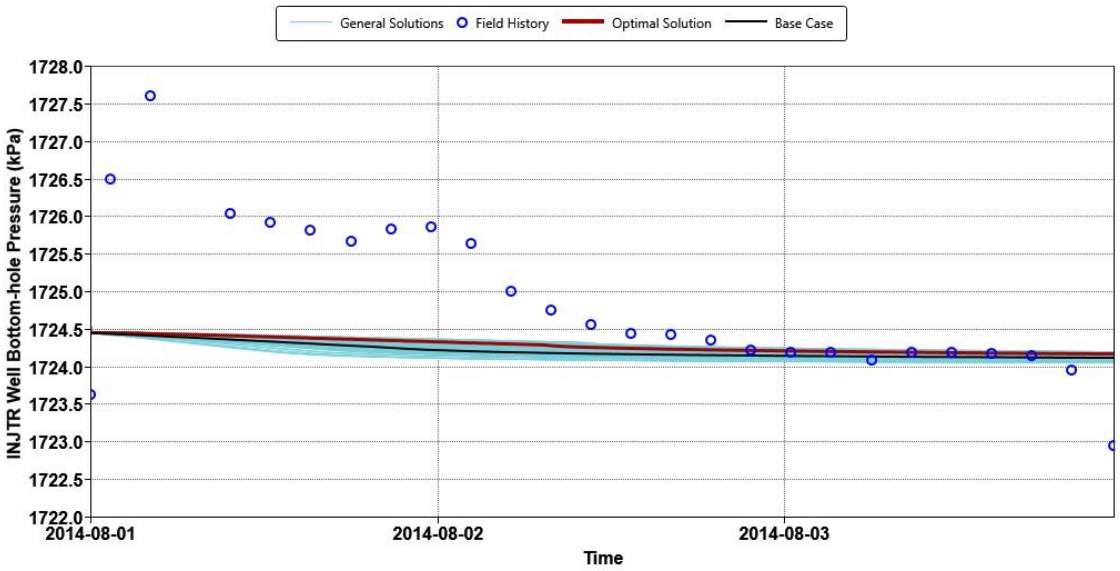

Figure *5.22*: Differential pressure profile of CMOST waterflooding history matching for Exp3

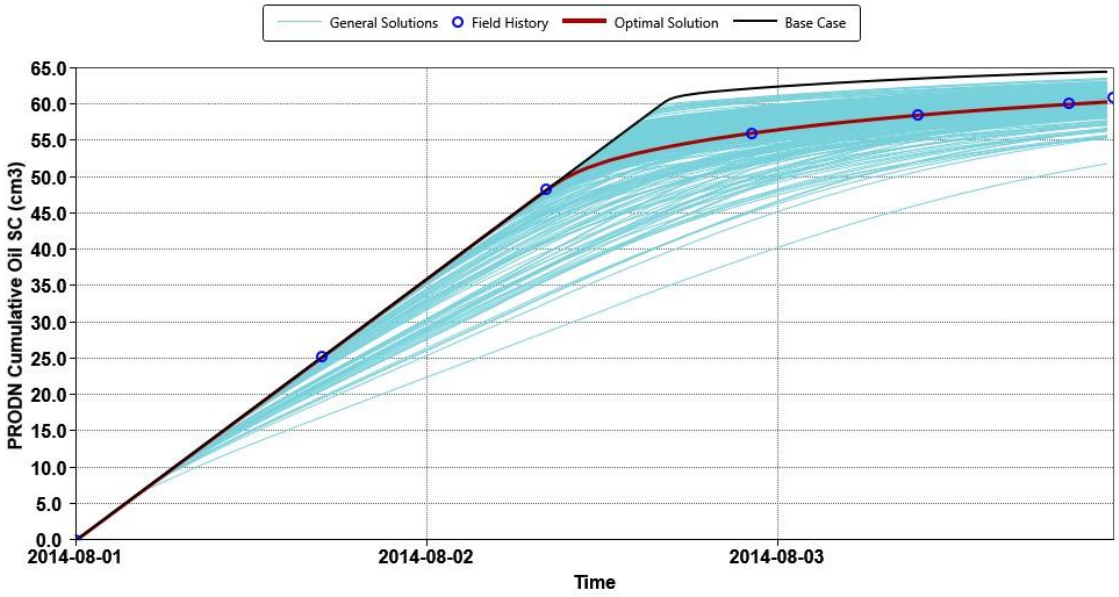

Figure 5.23: Cumulative oil profile of CMOST waterflooding history matching for Exp4

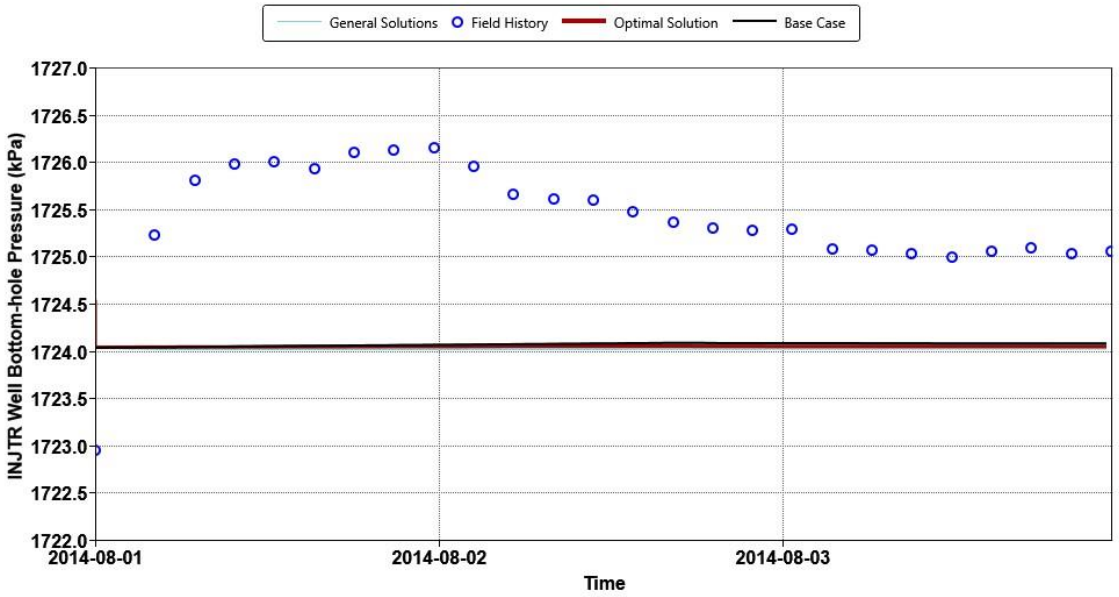

Figure 5.24: differential pressure profile of CMOST waterflooding history matching for Exp4

As it is clear from the figures above, the differential pressure profiles for Exp3 and Exp4 have something wrong. This behavior is not expected since the cumulative oil profiles behave positively as the relative permeability curves changed.

Further sensitivity analyses were conducted to Exp3 and Exp4 to investigate and observe the unknown reasons for this behavior. Firs, the flow rate was alternated with one set of relative permeability curves and observed the differential pressure profile. Second, the relative permeability used in the first step was lowered by factor of 10 and alternated the flow rate. The table below showed the results obtained from this sensitivity analysis.

Table 5.1: Pressure peak values corresponding to different flow rates for all experiments

q_w [ml/min]	dp_7000 [kPa]	dp_2000 [kPa]	dp_Exp1 [kPa]	dp_Exp2 [kPa]	dp_Exp3 [kPa]	dp_Exp4 [kPa]
0.025	54.27	17.3	8	5.7	1.94	1.58
0.05	105.5	31.67	13	10	2.42	1.68
0.1	207.4	60.2	23	18.5	3.38	1.89
0.2	412.4	117.8	43	35.6	5.3	2.3
0.4	819	232	84	70	9.14	3.14
0.8	1623	461	164	138	16.8	4.8

Table 5.2: Pressure peak values corresponding to different flow rates with lowered k_r for all experiments

Kr_{new}= 0.1 Kr_{old}						
q_w [ml/min]	dp_7000 [kPa]	dp_2000 [kPa]	dp_Exp1 [kPa]	dp_Exp2 [kPa]	dp_Exp3 [kPa]	dp_Exp4 [kPa]
0.025	514	146	54	44	6	2.5
0.05	1023	290	104	87	11	3.6
0.1	2023	567	206	172	21	5.6
0.2	4050	1147	408	343	40	9.8
0.4	8020	2285	812	684	78	18.1
0.8	15820	4542	1619	1368	155	35

The tables above shows the pressure peak values for all experiments in this thesis corresponding to different flow rates. The flow rates were increased by the double; therefore, the pressure profile should increase by the double according to Darcy's equation since the relative permeability, viscosity ratio and slab dimension are constant.

In Table 5.2, E7000, E2000, Exp1 and Exp2 showed the expected behavior, the pressure peak values increased by the double as the flow rate increases by the double. However, Exp3 and Exp4 did not show the expected behavior. In Exp3, for the normal relative

permeability curves, the pressure peak value did not change increase by the double for most of the flow rates. It starts to behave normally, after the flow rate of 0.2 *ml/min*. In Exp4, the pressure peak values did not increase by the double for all flow rates.

In Table 5.3 where the relative permeability curves were lowered by factor of 10 and the flow rates were increased by the double, E7000, E2000, Exp1, Exp2 and also Exp3 showed the expected behavior where the pressure peak values increased by the double as the flow rate increases by the double. On the other hand, for Exp4, only in the first two flow rates, the pressure peak values did not showed the expected behavior, but the in the other flow rates, the pressure peak values were increased by the double.

From this discussion, and from the tables above, it can be noticed that the experiments showed the expected pressure behavior when the pressure value is more than 5 *kPa*, when the pressure profile is lowered than 5 *kPa* the unexpected pressure behavior was observed, and when the pressure profile is more than 5 *kPa*, the expected pressure behavior was observed.

It was assumed that it may be something wrong in the data file for Exp3 and Exp4. For this reason, the data file for experiment E7000 was used to simulate Exp3 and Exp4, with the necessary changes in the slab dimensions, and petrophysical and fluids properties. But, There was no different in pressure profile, and the pressure behavior was the same.

The final conclusion that may be given for this unexpected behavior in Exp3 and Exp4 is that STARS has some restrictions with pressure profiles less than 5 *kPa*. Therefore, Exp3 and Exp4 will not be history matching with other experiments in this thesis.

6. Simulation Results and Discussion

History matching for four experiments were conducted for both waterflooding and polymer flooding. A Buckle-Leverett [28] type displacement model was used to history match the four experiments. However, the experiments are considered to be unstable immiscible flooding because of their high adverse mobilities and the Buckle-Leverett model is normally used for the stable displacement flooding. The reason of that is to test whatever is possible to history match the high adverse mobility experiment using Buckle-Leverett displacement model.

In the waterflooding history matching part, the experiments were history matched using CMOST. The only variable that was used in the history match is the relative permeability. Corey correlation for relative permeability was used in CMOST in which only water exponent and the water end point relative permeability were varied. Oil relative permeability curve was kept constant .Cumulative oil production and differential pressure were matched with the experimental data.

In the polymer flooding history matching part, there are more variables that were used to find a good match. LET correlation for relative permeability was used to history match the polymer flooding because it gives more flexibility than Corey correlation, and this flexibility is needed in polymer flooding. The other variables that were used in polymer flooding history matching is polymer adsorption, polymer dispersion, inaccessible pore volume, polymer resistance factor and the interpolated relative permeability parameters.

The main factor that affects and has more influence on the polymer flooding history match the relative permeability curve, because the others variables have some constraints where they cannot excess them. The constraints are usually related to the physical meaning of these variables and the experimental data. Therefore, the relative permeability is the main variable in history matching for both waterflooding and polymer flooding.

6.1. Waterflooding at Various Oil Viscosity Experiments

6.1.1. Water Displacement of 7000 cp Oil

Waterflooding history match was conducted to E7000, which has a 7000 cp oil viscosity using CMOST. CMOST is an automatic history matching tool, that uses STARS models and defined number of variables to use them as variables for obtaining history match. The relative permeability was the variable to history match the cumulative oil production and differential pressure for E7000, and Corey correlation for relative permeability was used by CMOST. The table below shows Corey's parameters defined in CMOST.

Table 6.1: Corey's parameters defined in CMOST.

Corey's Parameters	From	To
krw°	0.1	0.4
nw	0.1	6
kro°	1	
no	2	

The CMOST best match for the cumulative oil production and differential pressure for E7000 is shown in the figure below.

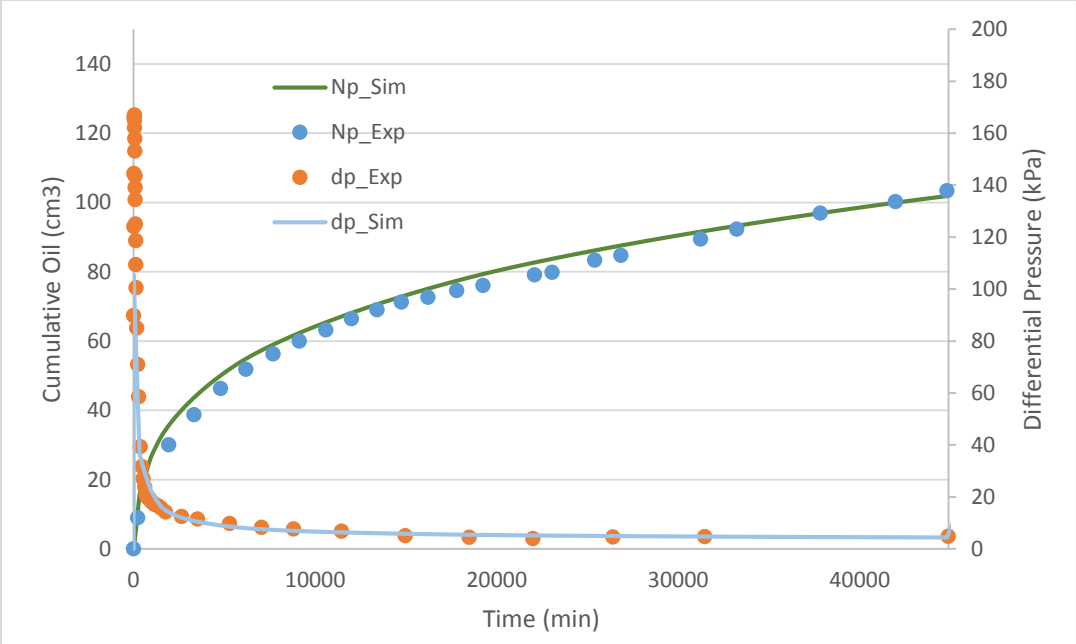

Figure 6.1: Waterflooding history matching of cumulative oil production and differential pressure for E7000

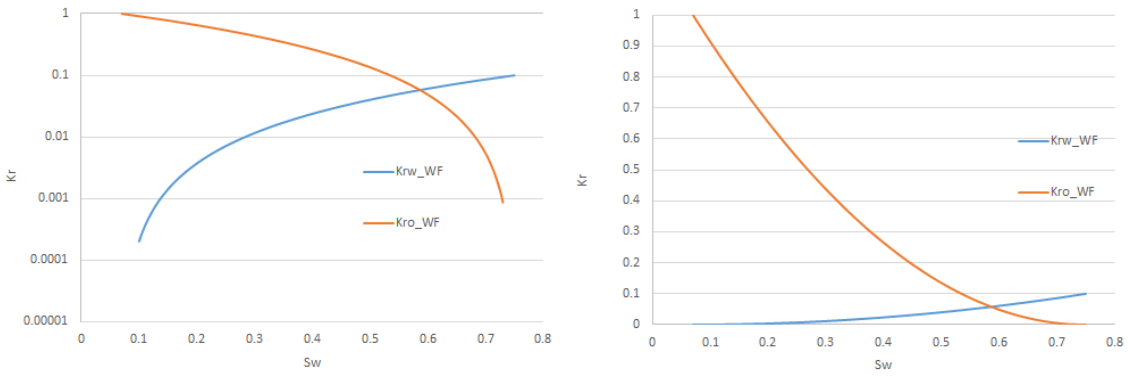

Figure 6.2: Waterflooding history match relative permeability for E7000

Figure 6.1 and 6.2 show the history match for cumulative oil production and differential pressure for E7000 and relative permeability used for the history match, respectively. The match in both cumulative oil production and differential pressure is good. Although, Corey correlation for relative permeability was used to obtain the match, but it did good job to simulated waterflooding in a 7000 cp oil experiment .

From the relative permeability curves, the water end point relative permeability is 0.1 which is low, and the wettability is water wet as it is clear from figure 6.2. However, in reality, the water end point relative permeability is expected to be greater than 0.1, and therefore, the wettability will be less water wet, and furthermore, it could be neutral wet if water end point relative permeability is high enough. The main reason of these expectations is the area restriction when using Buckley-Leverette type of displacement. In the real experiment, during waterflooding, the water injected was flowing through one main channel which is approximately, one-third of the total area as it shown in figure 6.3 below, but in the simulated model, the whole area was used. Therefore, according to Darcy's Low, if the real area is one-third of the simulated area, the real water end point relative permeability will be three times the simulated water end point relative permeability, which is approximately 0.3.

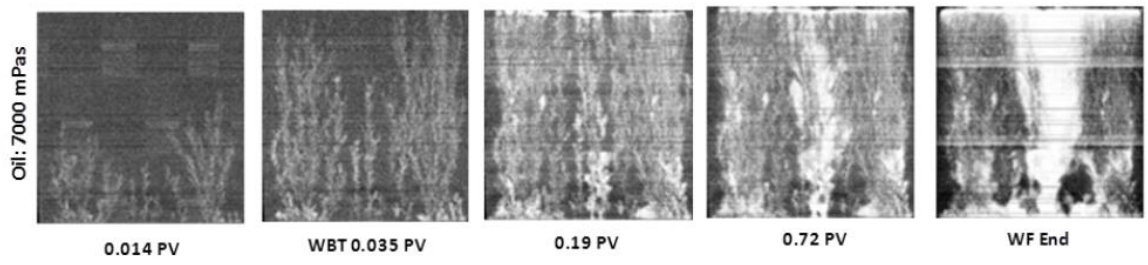

Figure 6.3: Waterflooding of 7000cp oil at various pore volume injected [55]

6.1.2. Water Displacement of 2000 cp Oil

Waterflooding history match was conducted to E2000, which has a 2000 cp oil viscosity using CMOST. The relative permeability was the variable to history match the cumulative oil production and differential pressure for E2000, and Corey correlation for relative permeability was used by CMOST. The same parameters as shown in table 6.1 were used also for this experiment model.

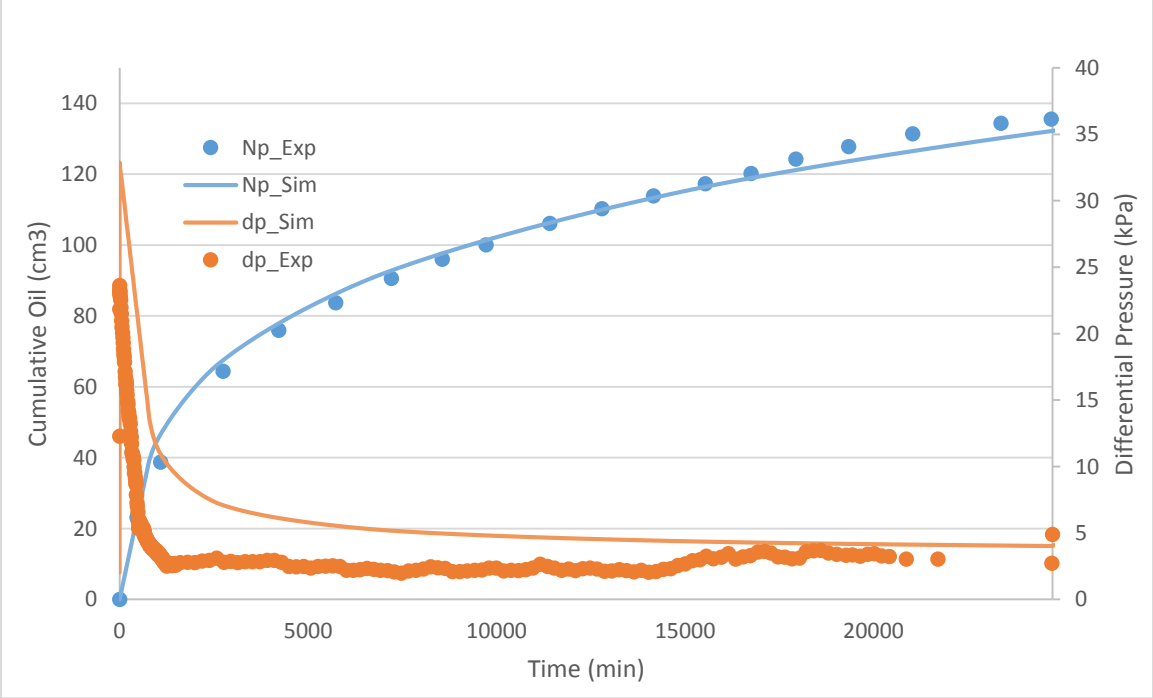

Figure 6.4: Waterflooding history matching of cumulative oil production and differential pressure for E2000

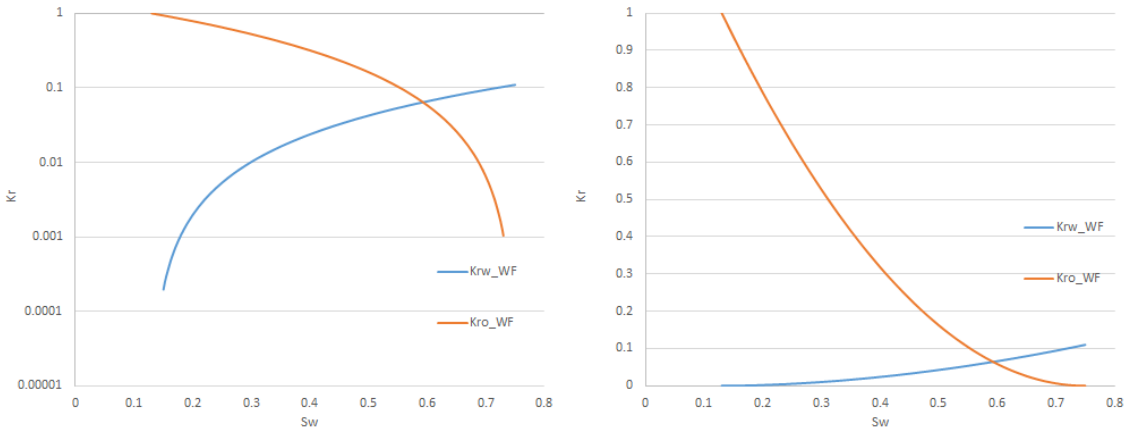

Figure 6.5: Waterflooding history match relative permeability for E2000

Figure 6.4 and 6.5 show the history match for cumulative oil production and differential pressure for E7000 and relative permeability used for the history match, respectively. The match in cumulative oil production is good, but there is mismatches in some part of the differential pressure profile. The strategy used by CMOST is to match the cumulative oil production fist, after that, it tries to match the differential pressure profile as good as possible keeping the cumulative oil production profile well matched. Another restriction causing this mismatches in differential pressure profile is that CMOST uses only Corey correlation for relative permeability which is very simple.

To match the differential pressure profile in E2000 both water and oil mobilities should be increased. According to Darcy's Low, when the total mobility is increased, the differential pressure will decrease. However, the sensitivity between the cumulative oil profile and the differential pressure profile is different. It was found that cumulative oil profile is more sensitive to the change in relative permeability than the differential pressure, Therefore, to match the differential pressure profile, large changes in relative permeability should be conducted which will causes a large mismatch in cumulative oil production because of its high sensitivity. Also, this issue is even more serious when using Corey's correlation because it is very simple and do not allow some changes in certain parts of the relative permeability curve. Therefore, a mismatch in differential pressure profile was observed by CMOST history match.

This mismatch could be avoided if another type of relative permeability is used, or if manual changes in relative permeability was conducted.

The water relative permeability is also low for this experiment model and the water end point relative permeability is slightly more than the previous experiment (E7000). The same reason as discussed previously in E7000 regarding the restriction in area. Also, in this experiment, the injected water was flowing through channels, and the effective flowing area is less than the total area. Therefore, the water relative permeability is expected to be higher than one obtained from history matching, and less water wet than it seems in figure 6.5.

6.1.3. Water Displacement of 616 cp Oil

Waterflooding history match was conducted to Exp1, which has a 616 cp oil viscosity using CMOST. The relative permeability was the variable to history match cumulative oil production and differential pressure for Exp1, and Corey correlation for relative permeability was used by CMOST. The same parameters as shown in table 6.1 were used also for this experiment model.

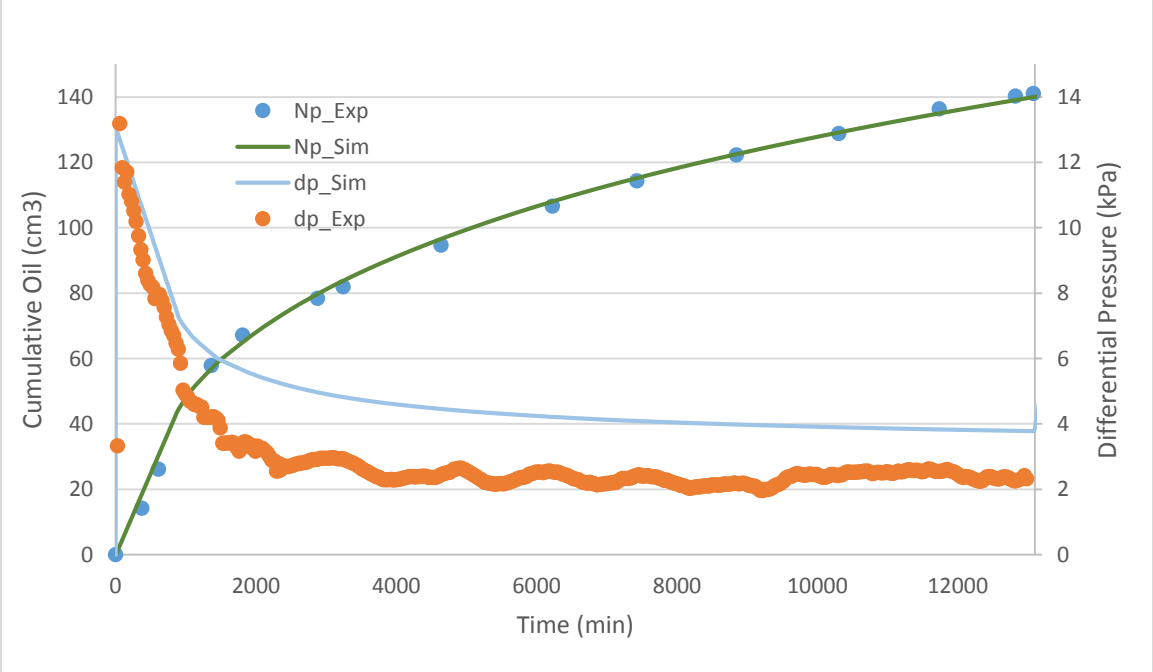

Figure 6.6: Waterflooding history matching of cumulative oil production and differential pressure for Exp1

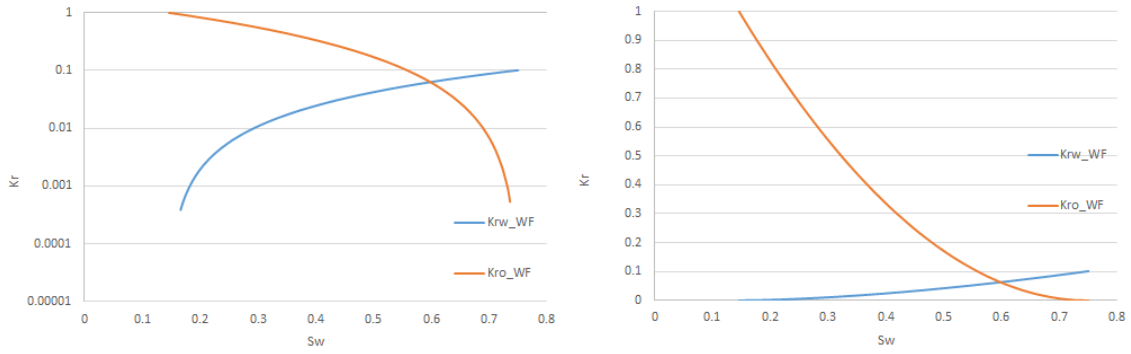

Figure 6.7: Waterflooding history match relative permeability for Exp1

It is clear from figure 6.6 that the history match on the cumulative oil production is very good, however, it is not good for the differential pressure profile. From the relative permeability curves in figure 6.7, the water end point relative permeability is 0.1.

The reason for this poor history match in the differential pressure profile was discussed in the previous sections. The first reason is the strategy used for history matching where, cumulative oil production has the first priority, and then, differential pressure is matched after that. The second reason and the more effective reason is the difference between the effective flowing area in real experiment and the area used be the model which is the total area. In this experiment the difference is even more as it is shown in figure 6.8. therefore, more mismatch is observed in the differential pressure.

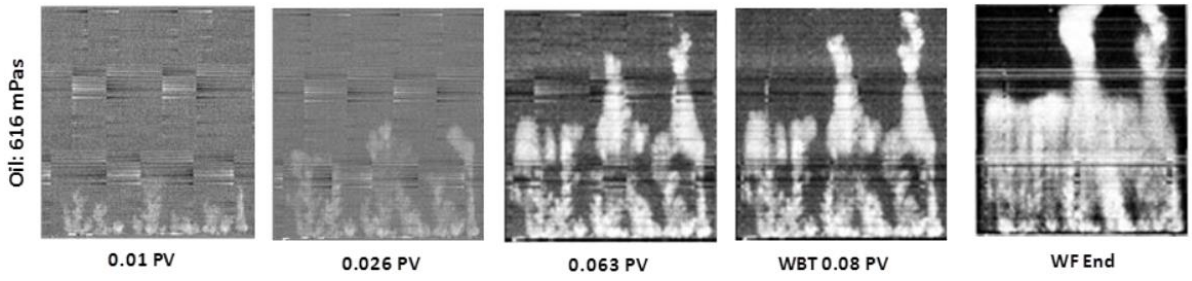

Figure 6.8: Waterflooding of 616 cp oil at various pore volume injected [56]

6.1.4. Water Displacement of 412 cp Oil

Waterflooding history match was conducted to Exp2, which has a 412 cp oil viscosity using CMOST. The relative permeability was the variable to history match the cumulative oil production and differential pressure for Exp2, and Corey correlation for relative permeability was used by CMOST. The same parameters as shown in table 6.1 were used also for this experiment model.

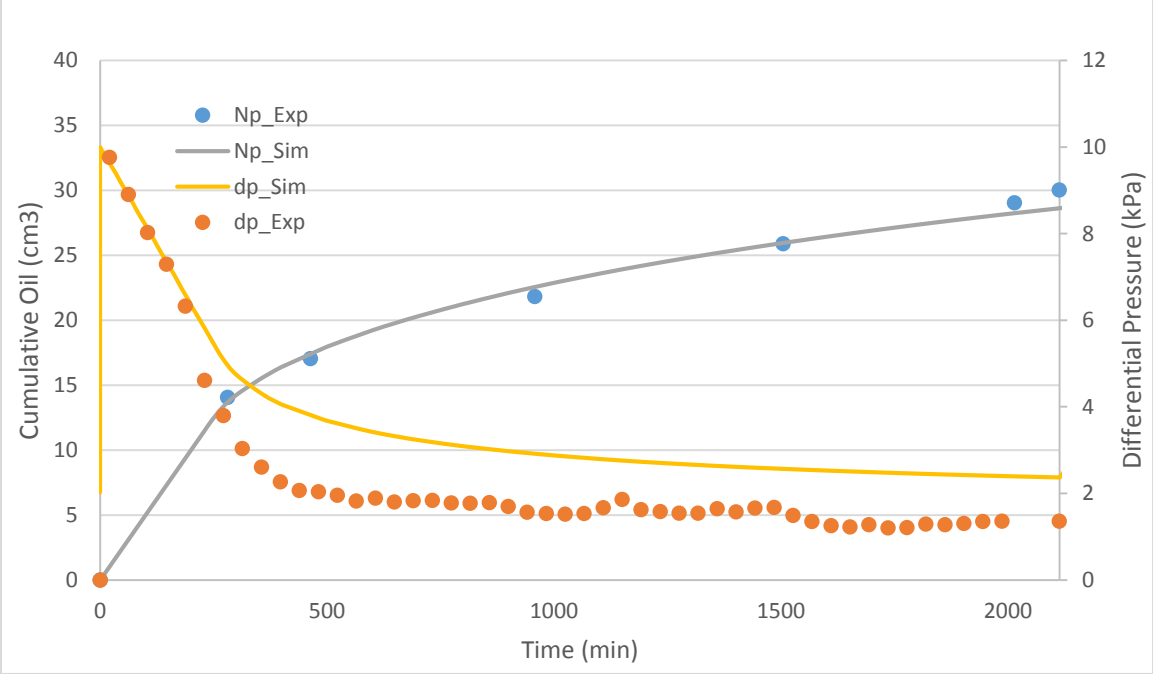

Figure 6.9: Waterflooding history matching of cumulative oil production and differential pressure for Exp1

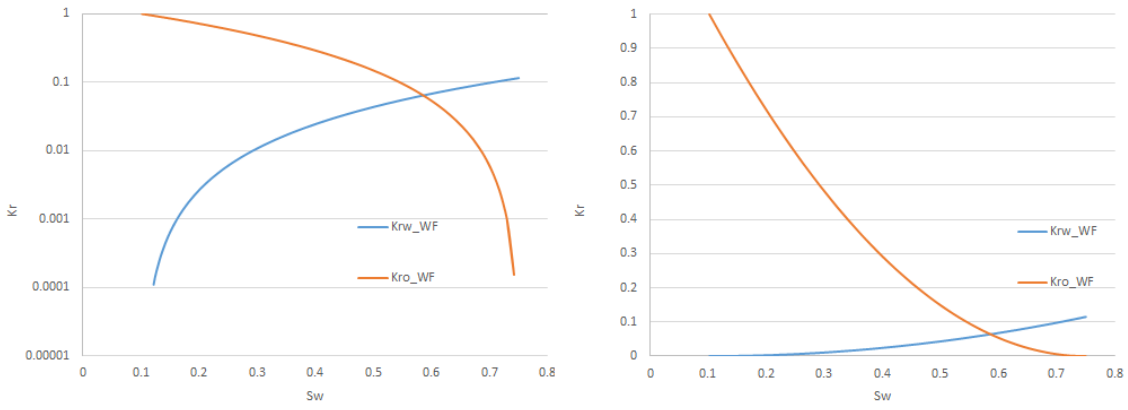

Figure 6.10: Waterflooding history match relative permeability for Exp2

Same observations were also observed for Exp2. There is very good history match in cumulative oil production and less good in the differential pressure profile. However, the water end point relative permeability for this experiment is greater than the others experiment.

However, the mismatch in the differential pressure for Exp2 is also due to the difference between the effective flowing area and the simulated area (total area). The difference is due to the fingering. Figure 6.10 shows the experimental 2D x-Ray images for waterflooding of Exp2.

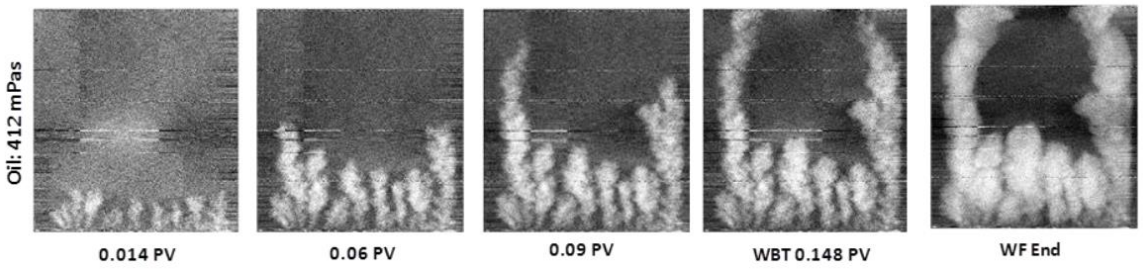

Figure 6.11: Waterflooding of 412 cp oil at various pore volume injected [56]

6.1.5. Waterflooding Results Summary

In this section, waterflooding history match results for all experiments will be viewed and discussed. The relative permeability curves that were used for history matching are shown in figure 6.12. It is clear that both oil and water relative permeabilities for all experiments are almost identical. The difference that appears in the relative permeability is due to initial water saturation variation.

However, there is a small different in water end point relative permeability. Figure 6.13 shows the water end points relative permeability for all experiments. It is clear that k_{rw} is increasing as oil viscosity decreases. However, that increasing is small and there is one point which seems to be out of trend. That point is for Exp1, and as discussed above, it is because of the difference between the effective flowing area and the total area. Furthermore, Exp1 has almost larger difference which leads to smaller k_{rw}.

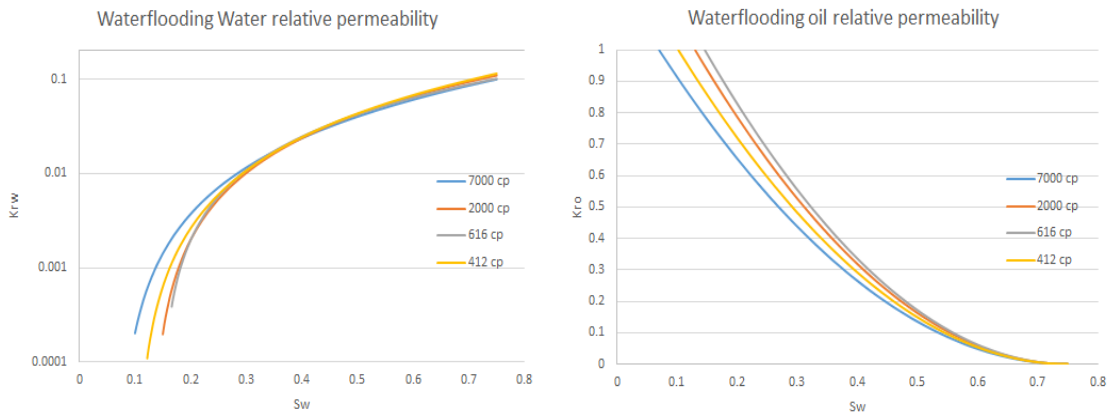

Figure 6.12: Waterflooding relative permeability curves for all experiments

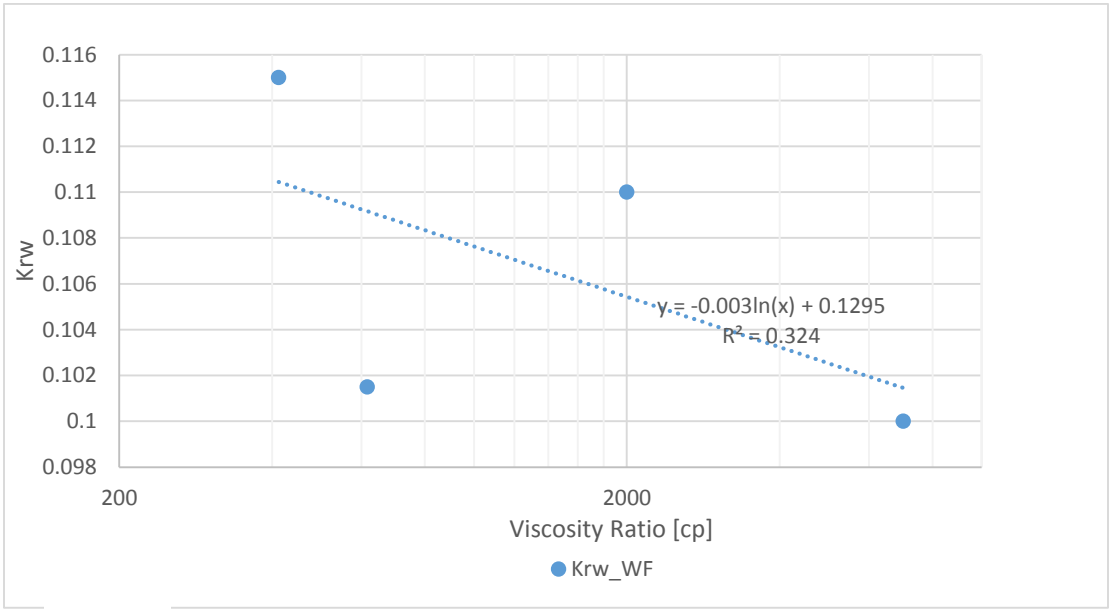

Figure 6.13: Water end points relative permeability of water flood history match for various oil viscosities.

There are several literature researches of effect of heavy oil on oil-water relative permeability. Some of them will be viewed in this section.

Sarma, H.K., Maini B. B., Purves R.W. and Jha K.N. [62] have investigated the effect of oil viscosity on oil/water relative permeability. Their experiment dimension is close to the dimension of the experiments studied in this thesis. However, the flow rate is different. Their results are shown in the figure below.

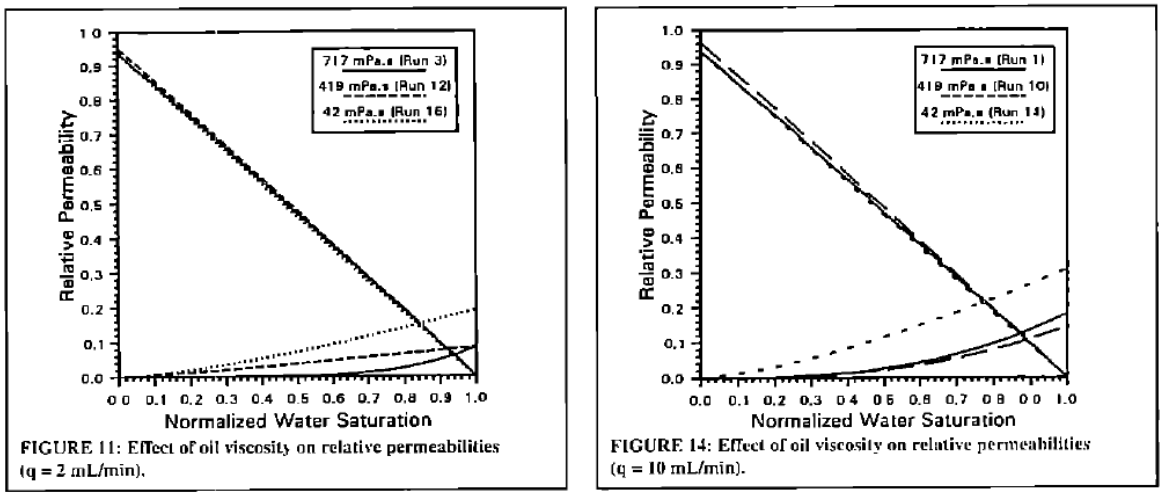

Figure 6.14: Effect of oil viscosity on oil/water relative permeability [62]

Although the flow rate id different from the experiments studied in this thesis, but it is clear that the water end points relative permeability are close to the results obtained from the history matching, especially for Exp1 which has 616 cp oil viscosity.

Another study for the effect of oil viscosity on oil/water relative permeability is conducted by J. Wang, M. Dong and K. Asghari [25]. They have studied the effect of different oil viscosities on a 14 cm length and a 4 cm diameter core. Their results are shown in the figure below.

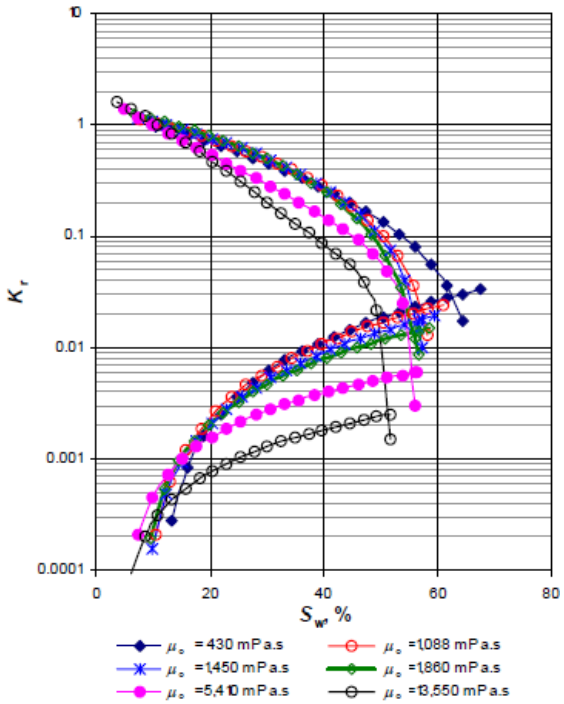

Figure 6.15: Effect of oil viscosity on oil/water relative permeability [25]

They have studies wide range of oil viscosities, and it is clear that water end point relative permeability is increasing as oil viscosity decreases. However, the values of k_{rw} are smaller when compared to k_{rw} obtained from this thesis. The reason is because of the superficial velocity, in Wang et al the superficial velocity is about 4.77 e-4 cm/min while in this study, it is 1.33e-4 cm/min, which means that the flow rate acting on the flowing area is greater than Wang et al experiments. This may explain the difference in water end poin relative permeability. However, there are other factors that affect the results on both experiments.

Another study of the effect of oil viscosity on water/oil relative permeability was conducted by S. Doorwar and K.K. Mohanty [23]. This study was conducted using micro model experiment. The results are shown in the figure below.

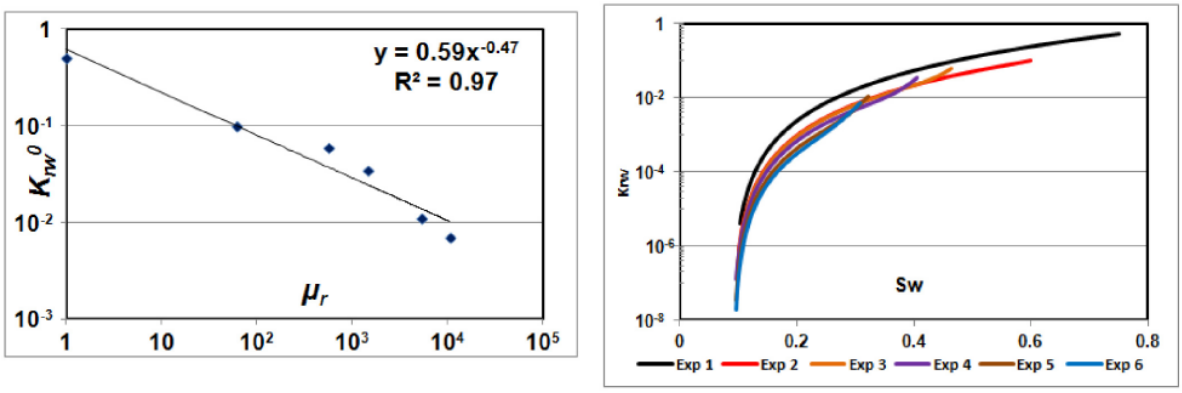

Figure 6.16: Effect of Oil viscosity on oil/water relative permeability. Exp1 has lowest oil viscosity and Exp6 has highest oil viscosity, modified, [23]

In this experiments, also wide range of oil viscosities were tested and the results of water end point relative permeability are close to the values obtained from this thesis. However, the water relative permeability curves seems to also very close to the one obtained from this thesis. The main difference in the results between Doorwar and Mohanty results and the results obtained here is due to the different in experiment dimensions.

6.2. Polymer Flooding at Various Oil Viscosity Experiments

6.2.1. Polymer Displacement of 7000 cp Oil

The cumulative oil production and the differential pressure were history matched for both water flooding and polymer flooding of the E7000 experiment and the figures below show the match and the relative permeability curves that were used.

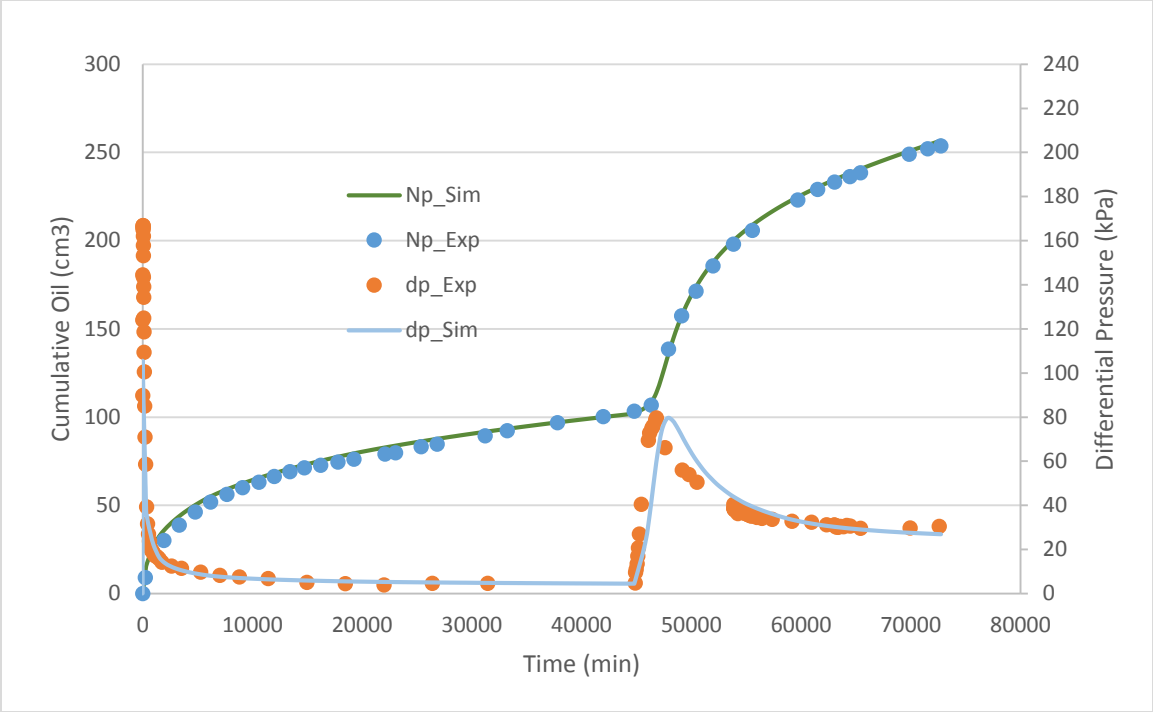

Figure 6.17: E7000 history matching on cumulative oil production and differential pressure profiles

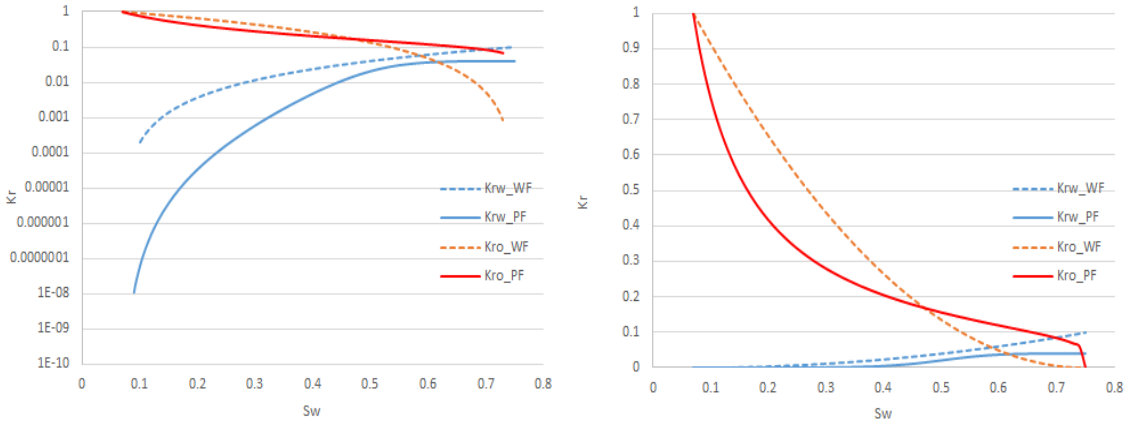

Figure 6.18: E7000 history matching relative permeabilities (logarithmic scale in left and normal scale in right)

As it is clear from the figure above, there is a good history match for both cumulative oil production and differential pressure, for both waterflooding and polymer flooding of the experiment E7000. However, the viscosity ratio in waterflooding is about 7000, there is a good history match by using Corey correlation. The peak of differential pressure was not

reached and the reason of that is may be because the water at the beginning was flowing at restricted area in the slab during the experiment [73].

In the polymer flooding, the flexibility of the LET correlation for relative permeability helped in obtaining a good history match. To describe the polymer flooding history match and check the other parameters that affect the polymer flooding, more graphs will be shown.

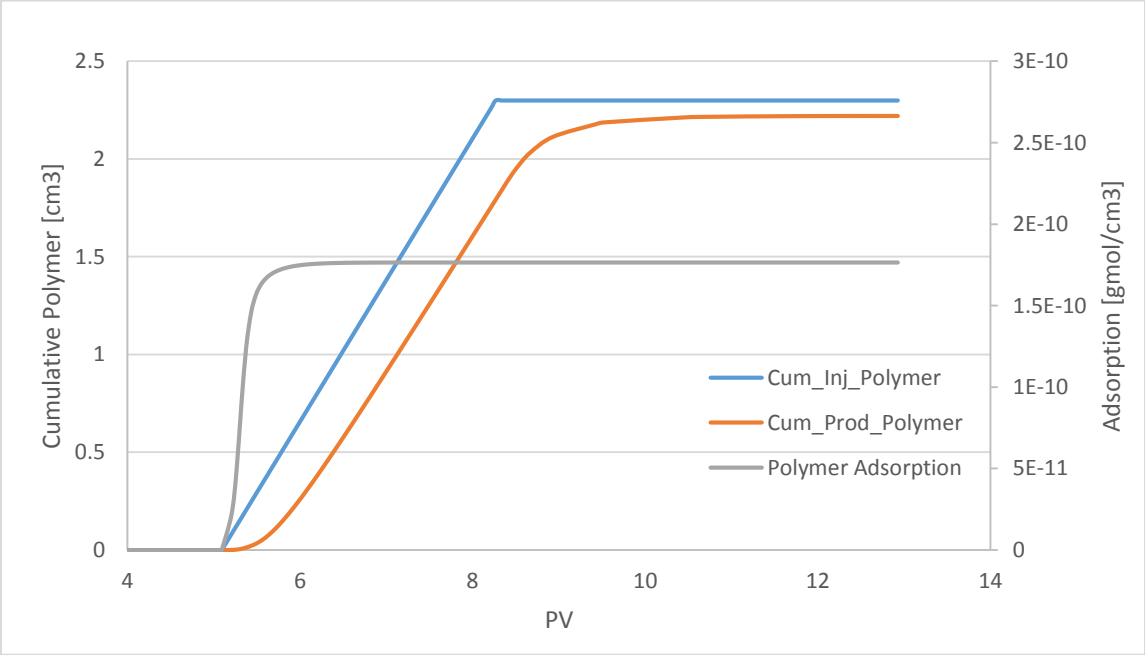

Figure 6.19: E7000 Cumulative polymer injected and produced

The figure above shows the amount of cumulative polymer injected and produced, and also it shows the polymer adsorption used in the simulated model, about 8 pore volume was injected in the actual experiment, but in order to plot this graph, more amount of water should be injected to check the polymer adsorption only. However, the difference between the cumulative polymer injected and the cumulative polymer produced is the polymer adsorption in the rocks. Because of units different, the following conversions will be used:

$$Ads\left(\frac{g}{cm^3}\right) = \frac{Cum_{inj} - Cum_{prod}}{PV} \qquad \textit{Equation 6.1}$$

$$Ads\left(\frac{g}{cm^3}\right) = Ads\left(\frac{gmol}{cm^3}\right) \times M_p\left(\frac{g}{gmol}\right) \qquad \textit{Equation 6.2}$$

Where, Cum_{inj} and Cum_{prod} are the cumulative amount polymer injected and produced respectively. Ads is the polymer adsorption, PV is the pore volume and M_p is the polymer molecular weight.

From the figure above, the difference between the injected amount of polymer and the produced amount is about 0.079 cm^3 , and because the density of polymer used is 1 g/cm^3, the polymer adsorption is 0.079 g. Divide this adsorption by the pore volume which is 440 cm^3 will give 1.8E-4 g/cm^3. To convert the adsorption value given in the figure above, it should be multiplied by polymer molecular weight. 1.8E-10 $gmol/cm^3$ times 1E6 g/gmol will give 1.8E-4 g/cm^3.

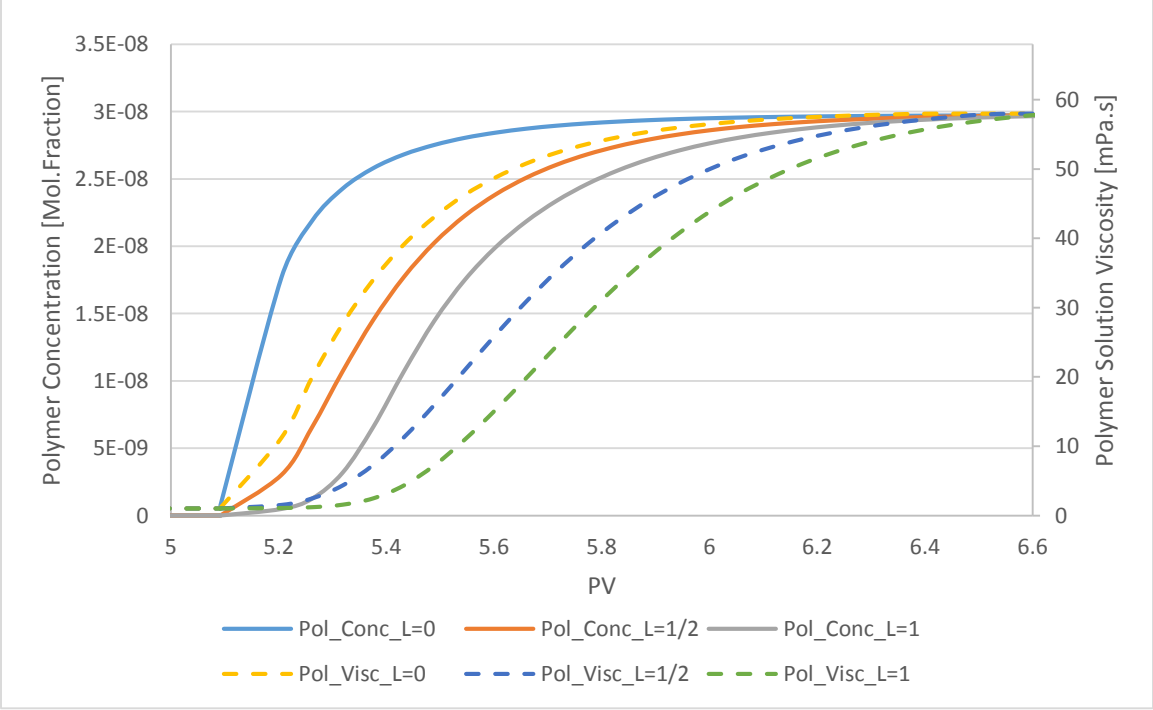

Figure 6.20: E7000 polymer concentration and viscosity profiles

The figure above shows the polymer concentration and viscosity development in the model at different locations. Three locations were tested, at the injection well (L=0), at the middle of the model (L=1/2) and at the production well (L=1). At each location polymer concentration and viscosity were plotted verse the pore volume injected. The polymer viscosity development follows the polymer concentration development at each location.

It can be noticed that the polymer concentration profiles at the injection well and at the production well are close to each other. This is because of low polymer adsorption that was used to match the experimental data. In order to have a quick polymer response, the polymer adsorption was minimized. Also, the relative permeability interpolation parameters (WCRV and OCRV) were used to have this quick response.

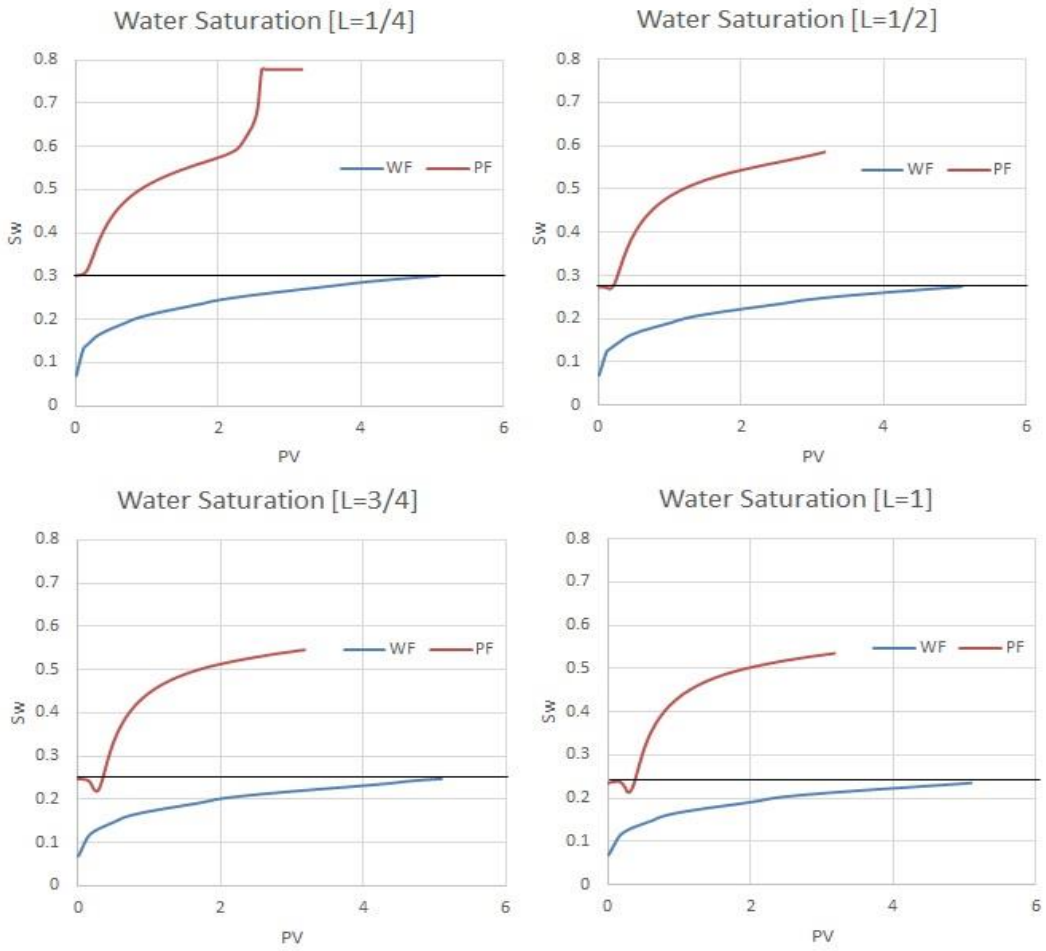

Figure 6.21: E7000 water saturation profiles at different locations

The figure above shows the internal water saturation profile for both waterflooding and polymer flooding at different locations in the model. Four locations were tested, at L=1/4, L=1/2, L=3/4 and at L=1. In the waterflooding part, it is clear that as the location is closer to the production well (L=1), the water saturation at the end of waterflooding is lower.

In this experimental model, it is noticeable that the slope of water saturation in the polymer flooding part is greater than the waterflooding part. It is the same observation as in the cumulative oil production profile where, the oil recovery in the polymer flooding increases at higher rate than in the waterflooding part.

In the polymer flooding part, the same observation as in the waterflooding is true, as the water saturation at the end of the polymer flooding is lower as the location is closer to the production well. However, There is unexpected behavior of water saturation at L=1/4, there is a quick increase in water saturation, but that behavior is disappeared at the other location. It may be because that location is very close to the injection well.

Also, from the figure above, it is clear that the oil bank saturation is increasing as the location is closer to the production well. However, the oil bank saturation development is less than the other experiments as it will be shown later.

Another way to view water saturation changes in the model with different pore volume injected is to plot the water saturation gradient, which gives a good view of water saturation changes as function of the dimensionless length.

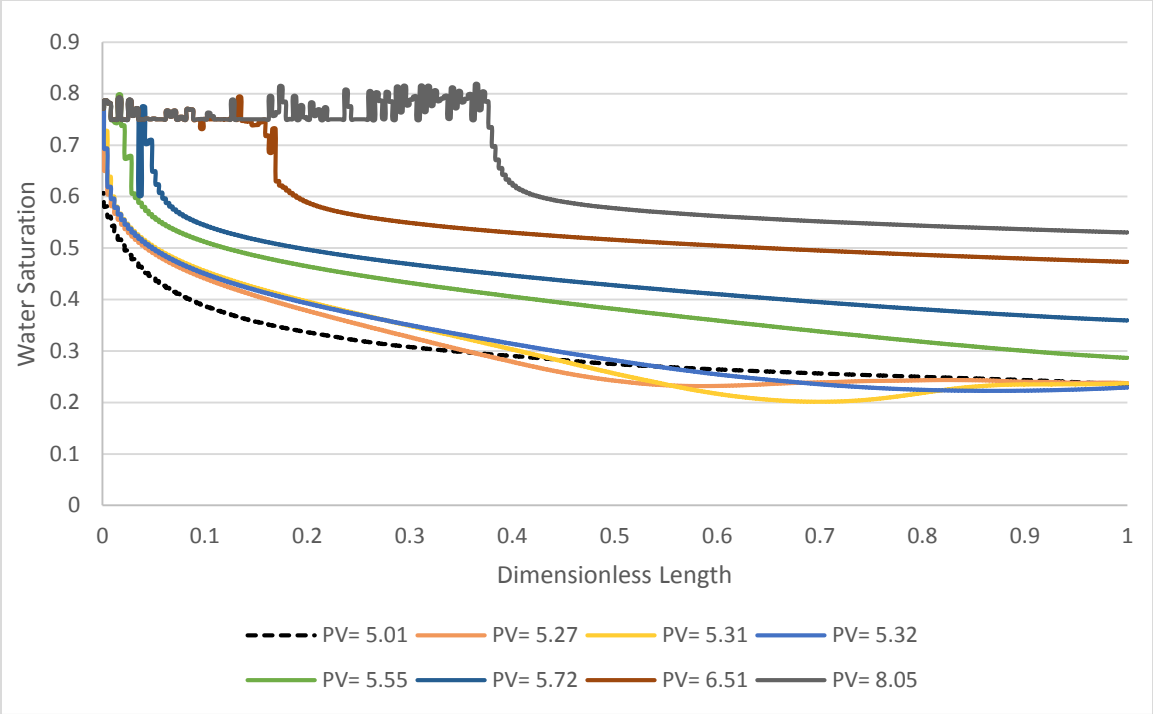

Figure 6.22: Water saturation gradient for of water and polymer flooding of 7000 cp oil viscosity experiment

In figure above it is clear that the model is trying to mimic the real experiment water saturation gradient. Although Buckley Leverette type of displacement was used to model the experiments, but as results of history match and the parameter used to obtain that match, the water saturation front is not steep as it is in the ideal Buckley-Leverette water saturation front. The main parameter that affects water saturation front is polymer dispersion, and for this experiment it was 0.005 cm2/day.

Also oil bank saturation can be observed from the figure above, and it is increasing as dimensionless time is increasing.

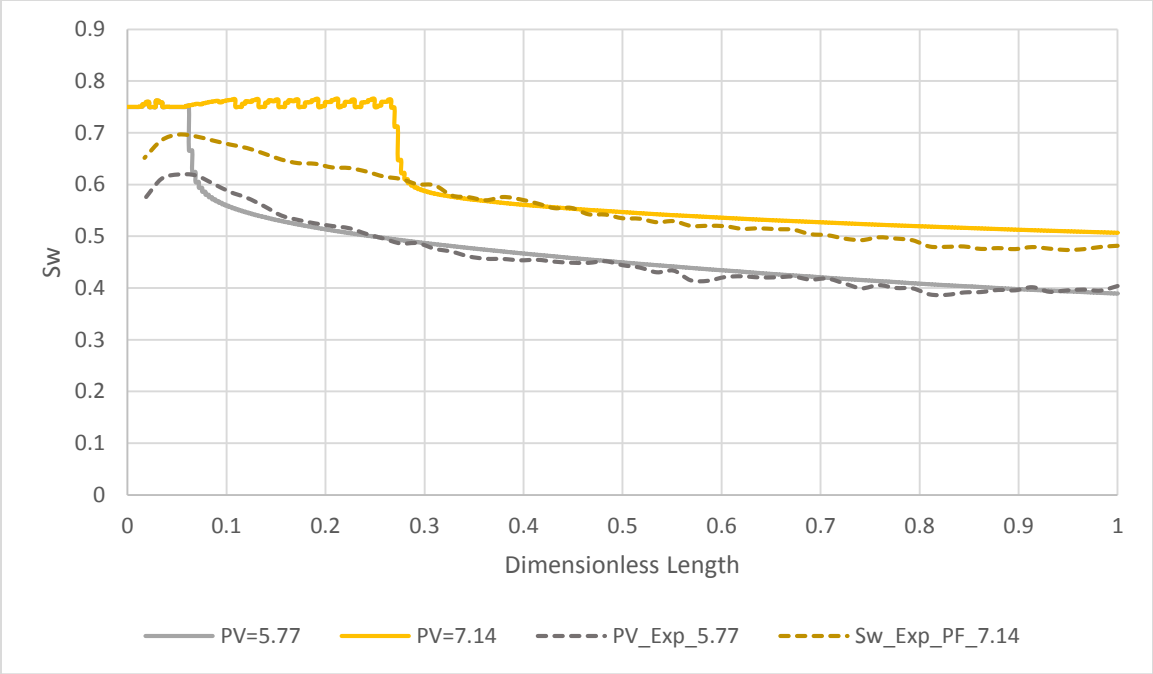

Figure 6.23: comparison of water saturation gradient between the real experiment and the simulated model

The figure above shows the water saturation gradient of the simulated model and the real experiment obtained from the x-ray images of E7000. Water saturation gradient was average form the x-ray image to have one value of it at each length. However, internal water saturation is surly different.

6.2.2. Polymer Displacement of 2000 cp Oil

The cumulative oil production and the differential pressure were history matched for both water flooding and polymer flooding of the E7000 experimental model and the figures below show the match and the relative permeability curves that were used.

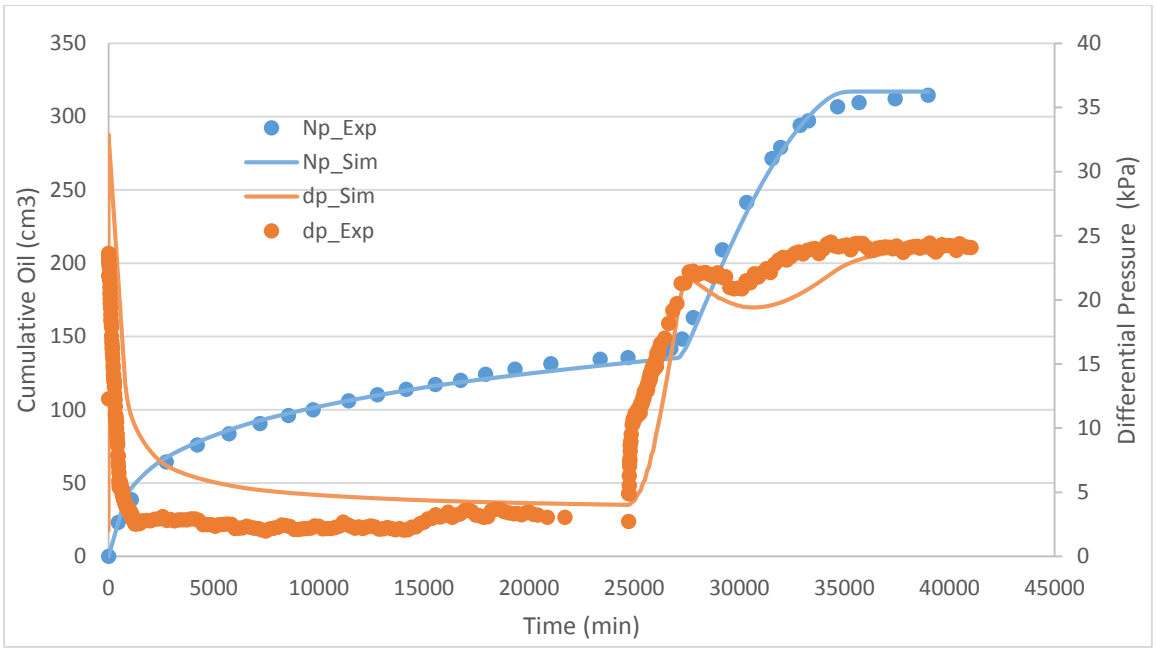

Figure 6.24: E2000 history match on cumulative oil production and differential pressure profiles

It is clear from the figure above, there is a good history match for both cumulative oil production and differential pressure, for both waterflooding and polymer flooding of the experiment E2000. However, in the waterflooding part, the same reason as in E7000, the pressure beak was not reached in this simulation model. Also, the pressure at the end of waterflooding was not matched very good. This is because that in CMOST the water end point relative permeability range was set to be between 0.1 and 0.4, and to match the pressure data it was required to have lower than 0.1 for K_{rw}.

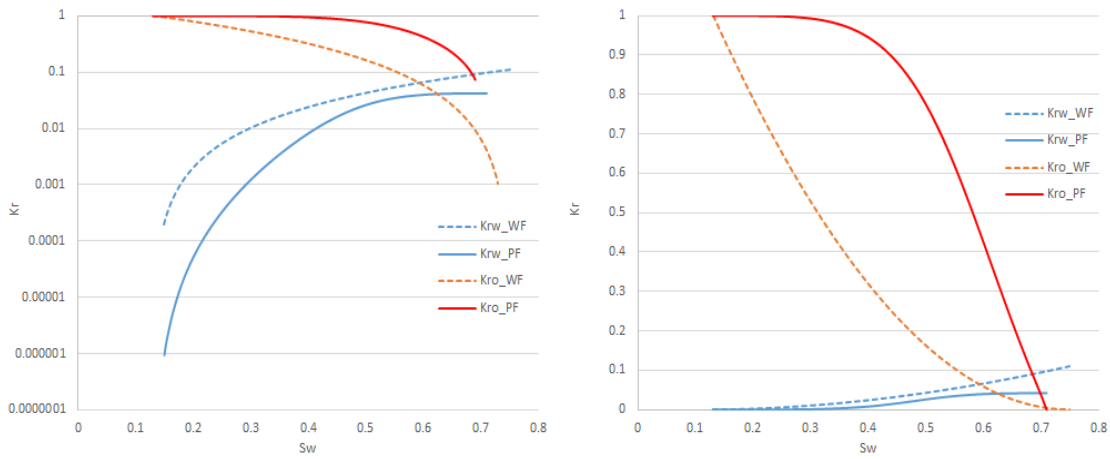

Figure 6.25: E2000 history matching relative permeabilities (logarithmic scale in left and normal scale in right)

The figure above shows the relative permeability E2000 for both waterflooding and polymer flooding. In order to match the cumulative oil production in the polymer flooding part, the oil relative permeability curve was increased as it shown in the figure above. This oil relative permeability seems to be abnormal. However, Skuage [74] has shown mathematically, that for unstable miscible flooding, the oil relative permeability can reach value of 10. Therefore, it is considered to be normal to have high oil relative permeability for unstable immiscible flooding.

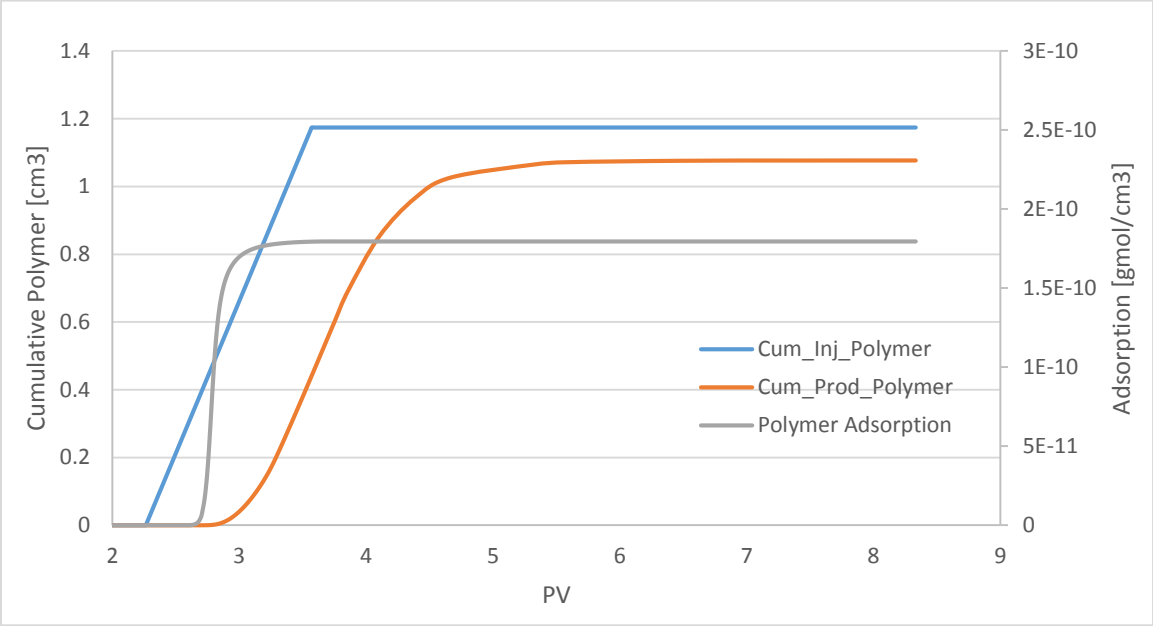

Figure 6.26: E2000 Cumulative polymer injected and produced

The figure above shows the amount of cumulative polymer injected and produced, and also it shows the polymer adsorption in this experiment, about 3.5 pore volume was injected in the actual experiment, but in order to plot this graph, more amount of water should be injected to check the polymer adsorption only. Using the same conversion equation as before (Equation 6.1 and Equation 6.2), the polymer adsorption was compared to the different in cumulative polymer injected and produced and it was found that the polymer adsorption is exactly equal to the different in cumulative polymer injected and produced.

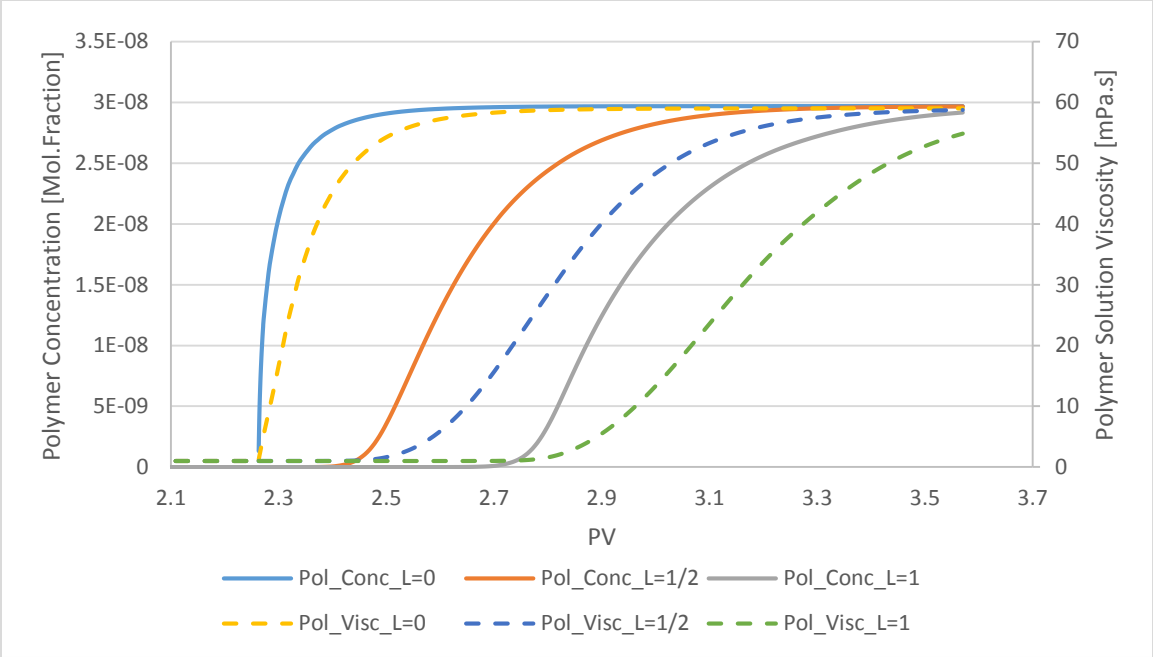

Figure 6.27: E2000 polymer concentration and viscosity profiles.

The figure above shows the polymer concentration and viscosity development in the model at different locations. Three locations were tested, at the injection well (L=0), at the middle of the model (L=1/2) and at the production well (L=1). At each location, polymer concentration and viscosity were plotted verse the pore volume injected. The polymer viscosity development follows the polymer concentration development at each location.

In this experiment the polymer concentration profiles in different locations are clear. The viscosity in the production did not reach its target value because there was not enough pore volume injected, but it was almost near the target value. Also, it can be noticed that the viscosity starts building up when the polymer concentration starts building up. At the injection well the polymer concentration and viscosity increased faster than when they are at different locations.

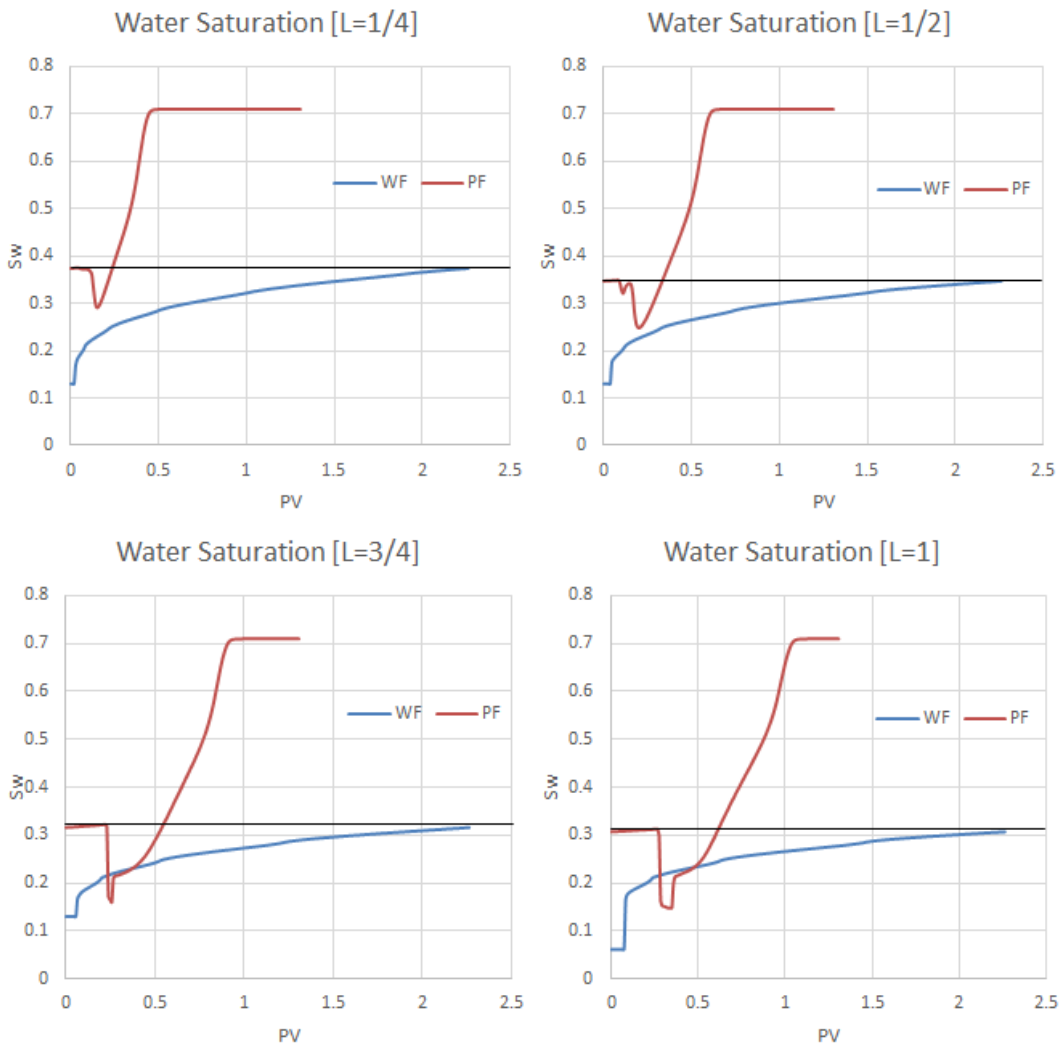

Figure 6.28: E2000 water saturation profiles

The figure above shows the internal water saturation profile for both waterflooding and polymer flooding at different locations in the model. Four locations were tested, at L=1/4, L=1/2, L=3/4 and at L=1. In the waterflooding part, it is clear that as the location is closer to the production well (L=1), the water saturation at the end of waterflooding is lower, and this is true for polymer flooding part. In this model the residual oil saturation was reached in all different locations. This can be noticed also in the cumulative oil profile where at the end of the polymer flooding, there was almost no oil production the profile was constant.

In this experimental model, it is noticeable that the slope of water saturation in the polymer flooding part is greater than the water flooding part. It is the same observation as in the

cumulative oil production profile where, the oil recovery in the polymer flooding increases at higher rate than in the waterflooding part.

Also, the oil bank saturation can be noticed much better in this model than the E7000 model. The oil bank saturation increases as the location is closer to the production well (L=1)

Another way to view water saturation changes in the model with different pore volume injected is to plot the water saturation gradient, which gives a good view of water saturation changes as function of the dimensionless length.

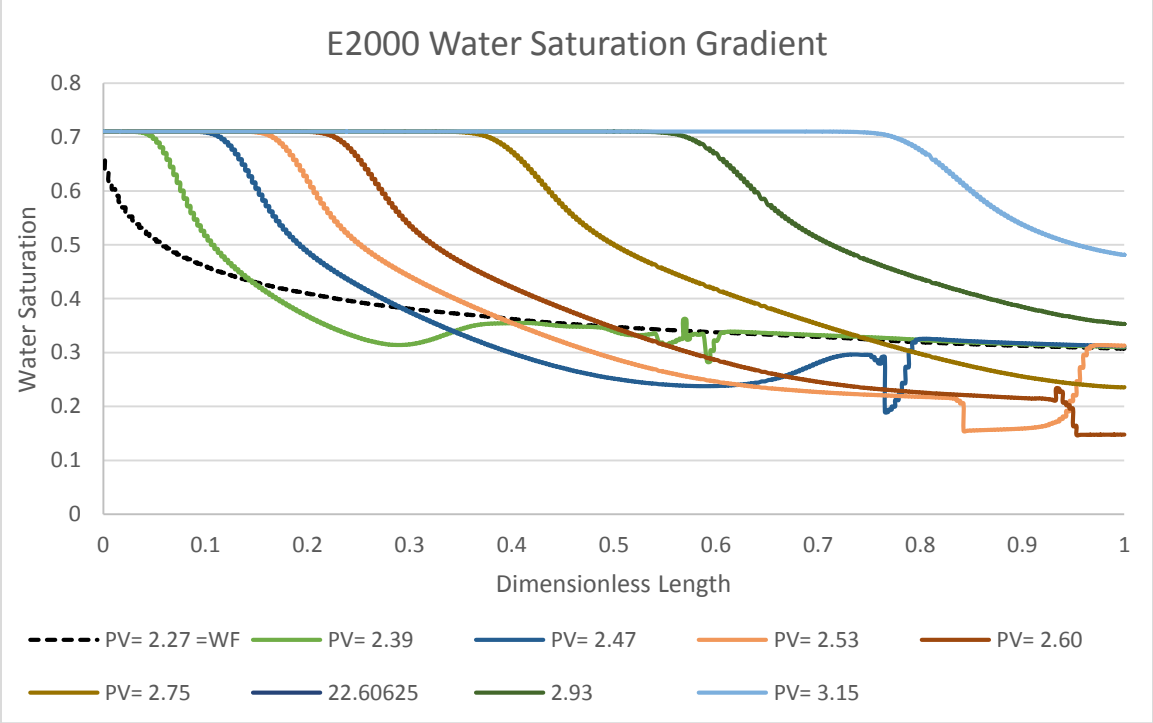

Figure 6.29: Water saturation gradient for of water and polymer flooding of 2000 cp oil viscosity experiment

In figure above it is clear that the model is trying to mimic the real experiment water saturation gradient. Although Buckley Leverette type of displacement was used to model the experiments, but as results of history match and the parameter used to obtain that match, the water saturation front is not steep as it is in the ideal Buckley-Leverette water saturation

front. The main parameter that affects water saturation front is polymer dispersion, and for this experiment it was 0.001 cm2/day.

In this experiment the ideal Buckley-Leverette water saturation front is observed. This is because the polymer dispersion for this experiment is less than the previous one, therefore, the water saturation front is more steep.

Also oil bank saturation can be observed from the figure above, and it is increasing as dimensionless time is increasing.

6.2.3. Polymer Displacement of 616 cp Oil

The cumulative oil production and the differential pressure were history matched for both waterflooding and polymer flooding of the Exp1 experimental model and the figures below show the match and the relative permeability curves that were used.

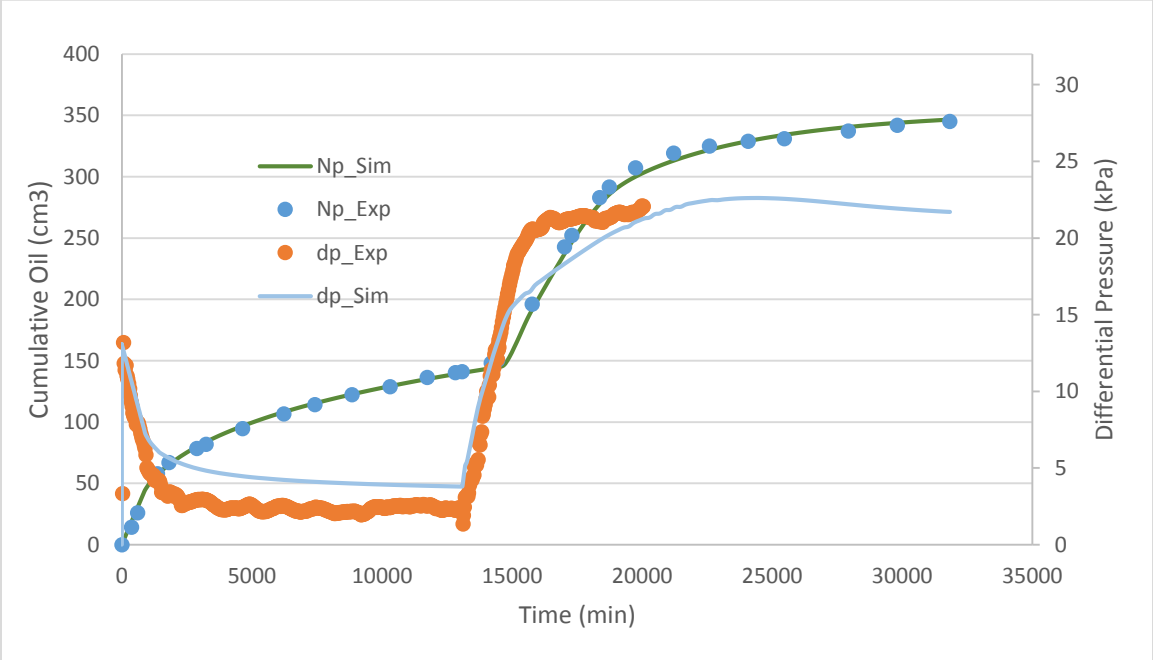

Figure 6.30: Exp1 history match on cumulative oil production and differential pressure profiles

The figure above shows the polymer concentration and viscosity development in the model at different locations. Three locations were tested, at the injection well (L=0), at the middle

of the model (L=1/2) and at the production well (L=1). At each location, polymer concentration and viscosity were plotted verse the pore volume injected. The polymer viscosity development follows the polymer concentration development at each location.

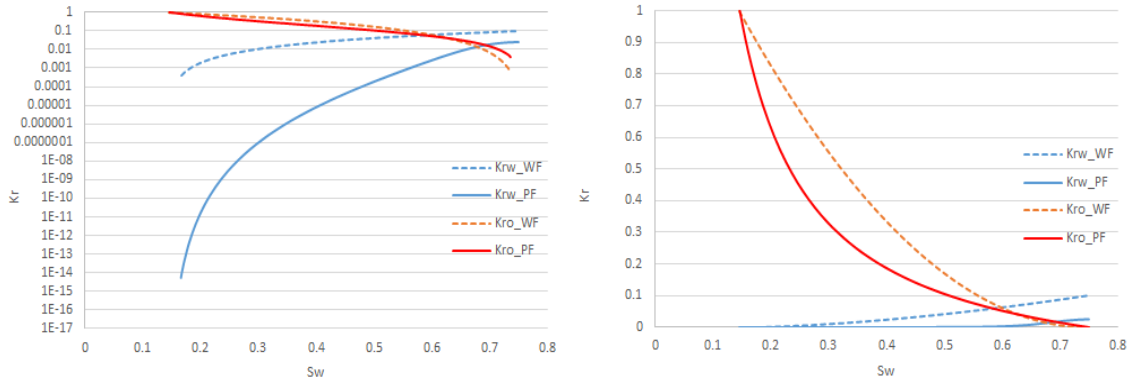

Figure 6.31: Exp1 history matching relative permeabilities (logarithmic scale in left and normal scale in right).

The figures above show the history matching in the cumulative oil production and the differential pressure, and the relative permeabilities that were used in the history matching for both waterflooding and polymer flooding. There is a good history match in the cumulative oil production. In fact, the waterflooding history match using Corey correlation for relative permeability is considered very good for unstable flooding with high adverse mobility ratio. However, the differential pressure at the end of the waterflooding was not matched, but the difference between the experiment and the model is 2 kPa (0.02 mbar). However, the peak of the differential pressure was matched.

In the polymer flooding part, there is a goof history match for both cumulative oil production and the differential pressure. However, there was a small mismatch in the differential pressure profile, and this is may be because of the viscous fingering pattern formed.

More graphs related to Exp1 model will be shown that are related to the polymer flooding to check and explain the polymer flooding parameters used in the model. Polymer adsorption, dispersion, viscosity and the internal water saturation will be shown below.

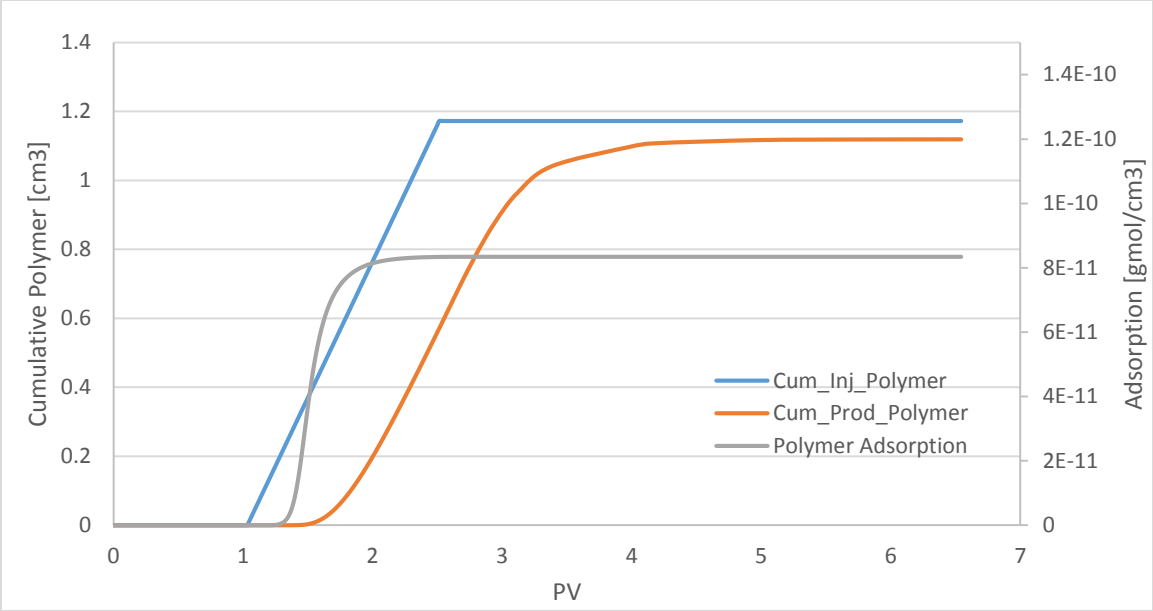

Figure 6.32: Exp1 cumulative polymer injected and produced

The figure above shows the amount of cumulative polymer injected and produced, and also it shows the polymer adsorption in this experiment. About 2.5 pore volume was injected in the actual experiment, but in order to plot this graph, more amount of water should be injected to check the polymer adsorption only. Using the same conversion equation as before (Equation 6.1 and Equation 6.2), the polymer adsorption was compared to the different in cumulative polymer injected and produced, and it was found that the polymer adsorption is exactly equal to the different in cumulative polymer injected and produced.

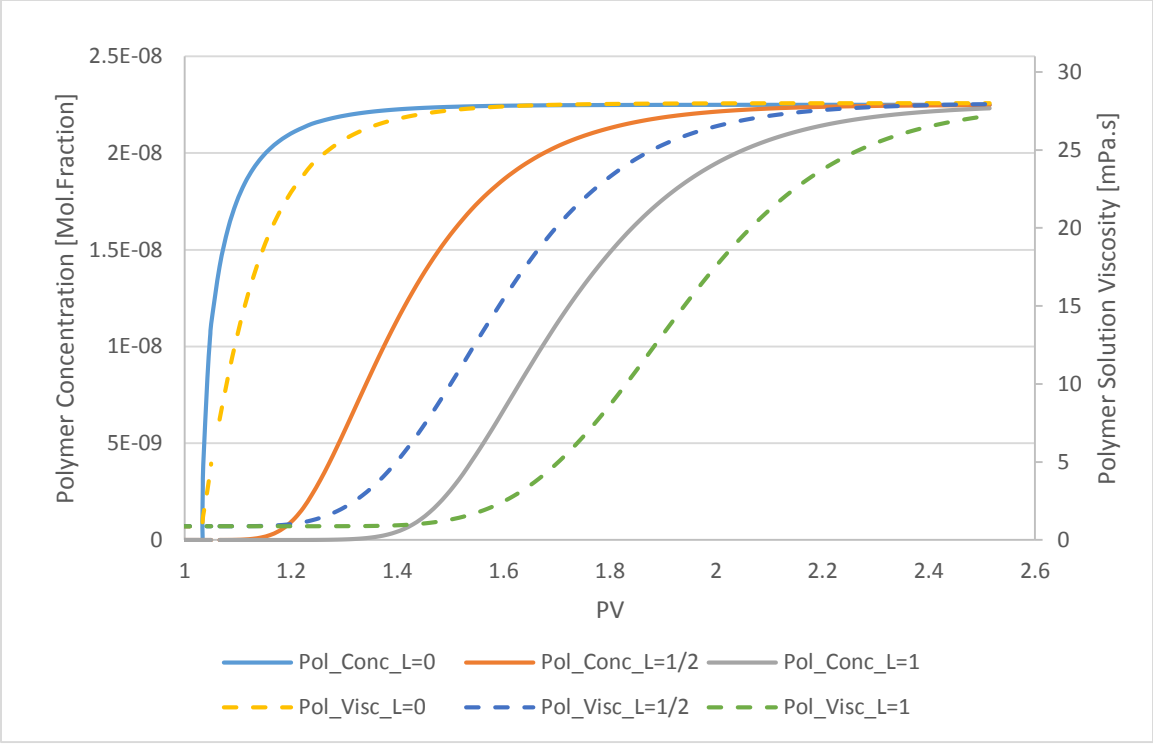

Figure 6.33: Exp1 polymer concentration and viscosity profiles

The figure above shows the polymer concentration and viscosity development in the model at different locations. Three locations were tested, at the injection well (L=0), at the middle of the model (L=1/2) and at the production well (L=1). At each location, polymer concentration and viscosity were plotted verse the pore volume injected. The polymer viscosity development follows the polymer concentration development at each location.

In this experiment, both the polymer concentration and viscosity reached the target values in all locations. It is clear that the polymer viscosity profiles at each location follow the polymer concentration profiles and also the rate of development with the pore volume injected is the same.

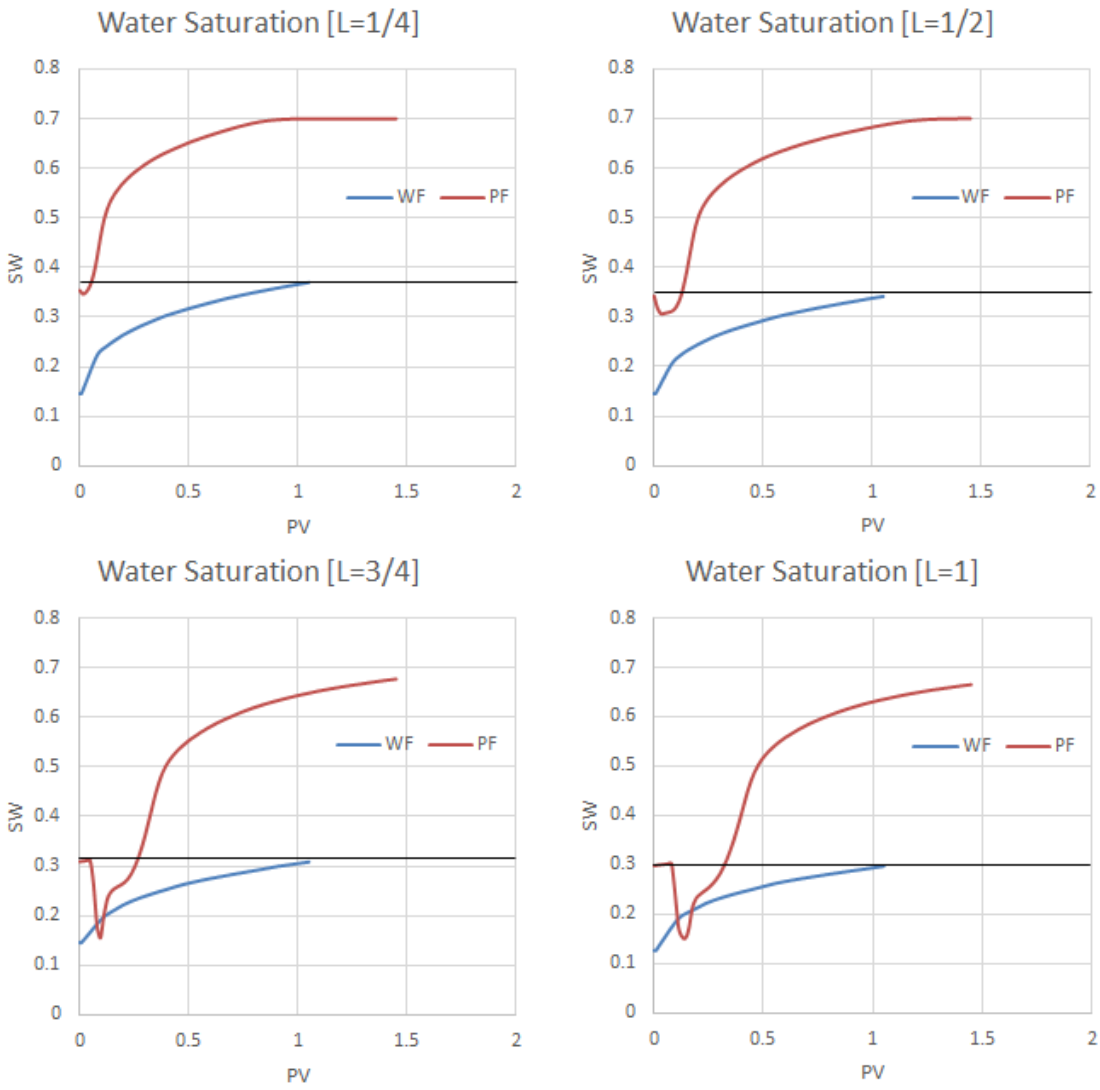

Figure 6.34: Exp1 internal water saturation profiles

The figure above shows the internal water saturation profile for both waterflooding and polymer flooding at different locations in the model. Four locations were tested, at L=1/4, L=1/2, L=3/4 and at L=1. In the waterflooding part, it is clear that as the location is closer to the production well (L=1), the water saturation at the end of waterflooding is lower, and this is true also for polymer flooding part. The residual oil saturation was reached at L=1/4 and L=1/2, which means that half of the model reached the residual oil saturation and the other half did not.

Same observation was noticed as the previous experiments regarding the slope of water saturation in the polymer flooding part in which water saturation in polymer flooding part increasing faster than the water saturation in polymer flooding part. Also, the oil bank saturation increases as the location is closer to the production well (L=1)

Another way to view water saturation changes in the model with different pore volume injected is to plot the water saturation gradient, which gives a good view of water saturation changes as function of the dimensionless length.

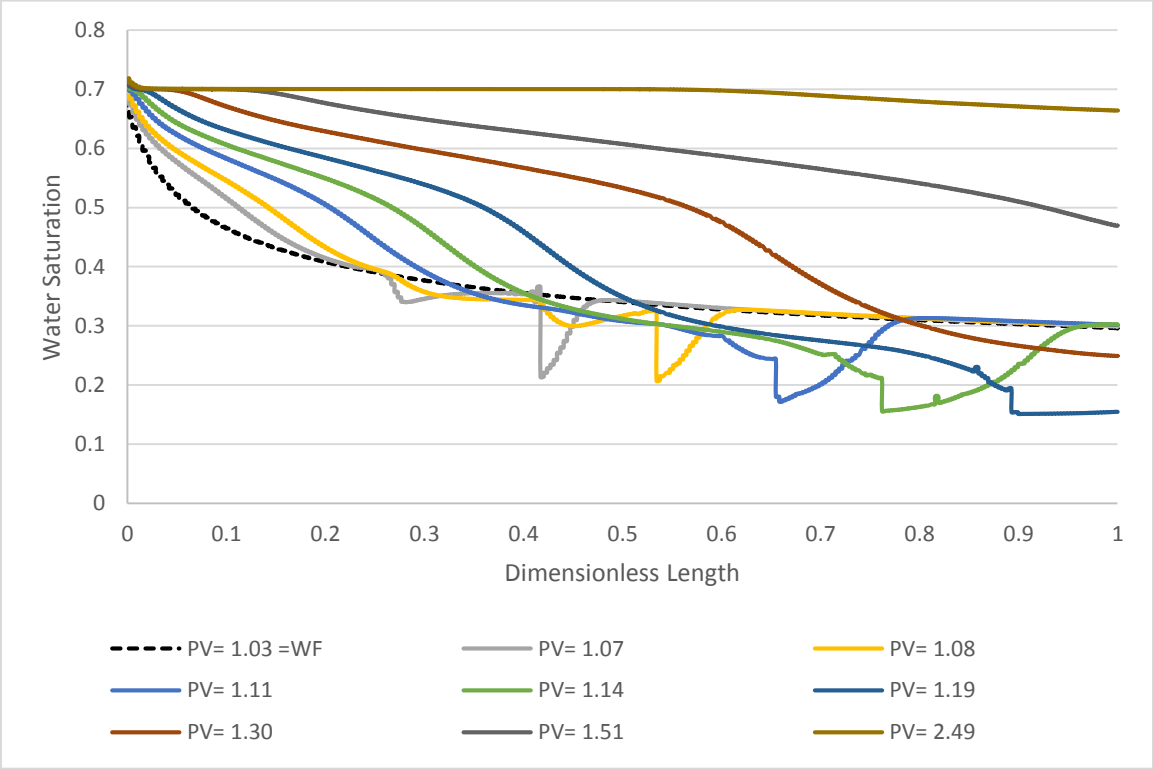

Figure 6.35: Water saturation gradient for of water and polymer flooding of 616 cp oil viscosity experiment

In figure above it is clear that the model is trying to mimic the real experiment water saturation gradient. Although Buckley Leverette type of displacement was used to model the experiments, but as results of history match and the parameter used to obtain that match, the water saturation front is not steep as it is in the ideal Buckley-Leverette water saturation front. The main parameter that affects water saturation front is polymer dispersion, and for this experiment it was 0.001 cm2/day.

In this experiment the ideal Buckley-Leverette water saturation front is not observed, although, the polymer dispersion is the same as in the E2000 experiment. This may be because Exp1 polymer concentration less than Exp1, and also Exp1 PV is greater than E2000 experiment.

Also oil bank saturation can be observed from the figure above, and it is increasing as dimensionless time is increasing.

6.2.4. Polymer Displacement of 412 cp Oil

The cumulative oil production and the differential pressure were history matched for both water flooding and polymer flooding of the Exp1 experimental model and the figures below show the match and the relative permeability curves that were used.

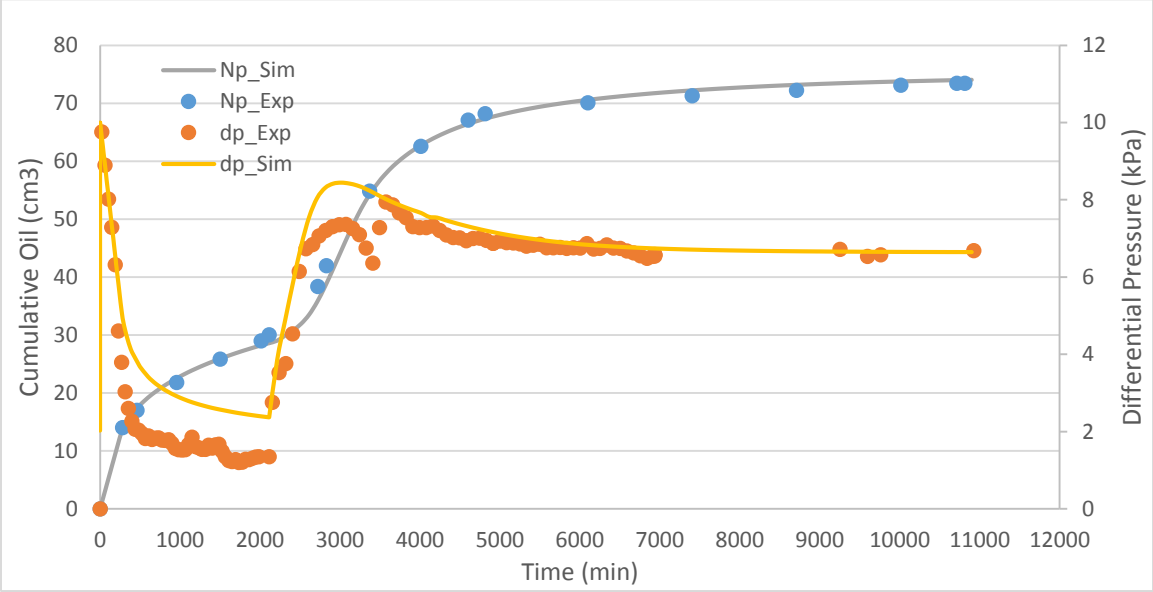

Figure 6.36: Exp2 history match on cumulative oil production and differential pressure profiles

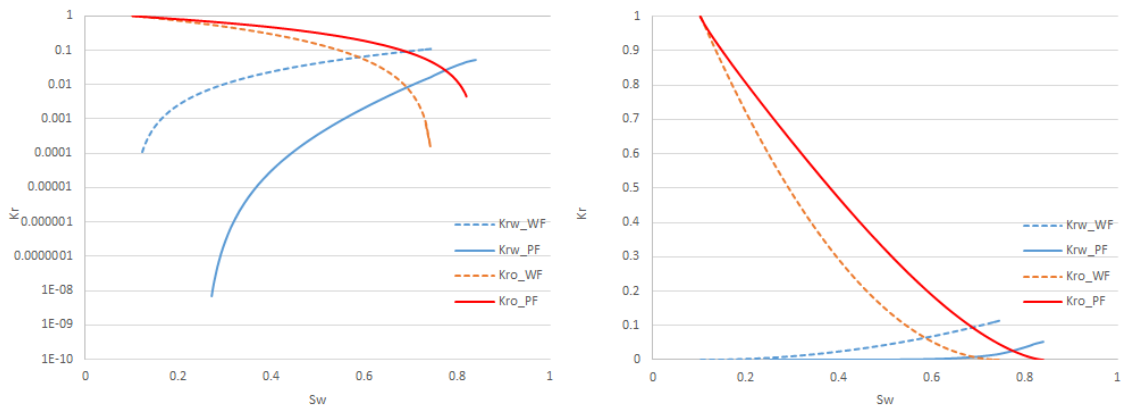

Figure 6.37: Exp2 history matching relative permeabilities (logarithmic scale in left and normal scale in right)

It is clear from figure 6.16 that there is a good history match in the cumulative oil production for both water flooding and polymer flooding. However, there is a mismatch in the differential pressure profile at the end of waterflooding and the different between the actual experiment data and the model is about 1 kPa. However, the peak of the differential pressure profile was matched.

In the polymer flooding part, both cumulative oil production and differential pressure profile were matched very good. There is a mismatch at the peak of differential pressure profile, but it is clear that there was an error during the experiment. This is a valid assumption since the scale of the pressure is very small, and it is clear that the differential pressure profile follow the model pressure line.

In this experiment, it is clear that the residual oil saturation was reached because the cumulative oil profile is almost constant at the end of polymer flooding.

More graphs related to Exp1 model will be shown that are related to the polymer flooding to check and explain the polymer flooding parameters used in the model. Polymer adsorption, dispersion, viscosity and the internal water saturation will be shown below.

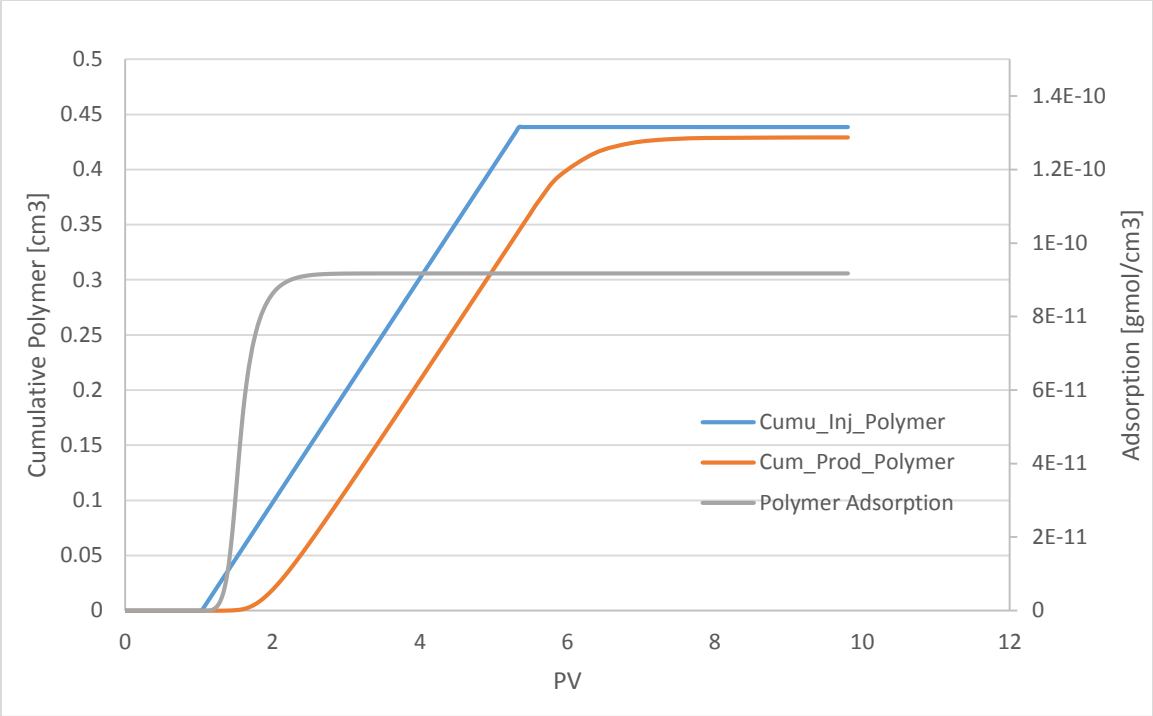

Figure 6.38: Exp2 cumulative polymer injected and produced

The figure above shows the amount of cumulative polymer injected and produced, and also it shows the polymer adsorption in this experiment. About 5.3 pore volume was injected in the actual experiment, but in order to plot this graph, more amount of water should be injected to check the polymer adsorption only. Using the same conversion equation as before (Equation 6.1 and Equation 6.2), the polymer adsorption was compared to the different in cumulative polymer injected and produced, and it was found that the polymer adsorption is exactly equal to the different in cumulative polymer injected and produced.

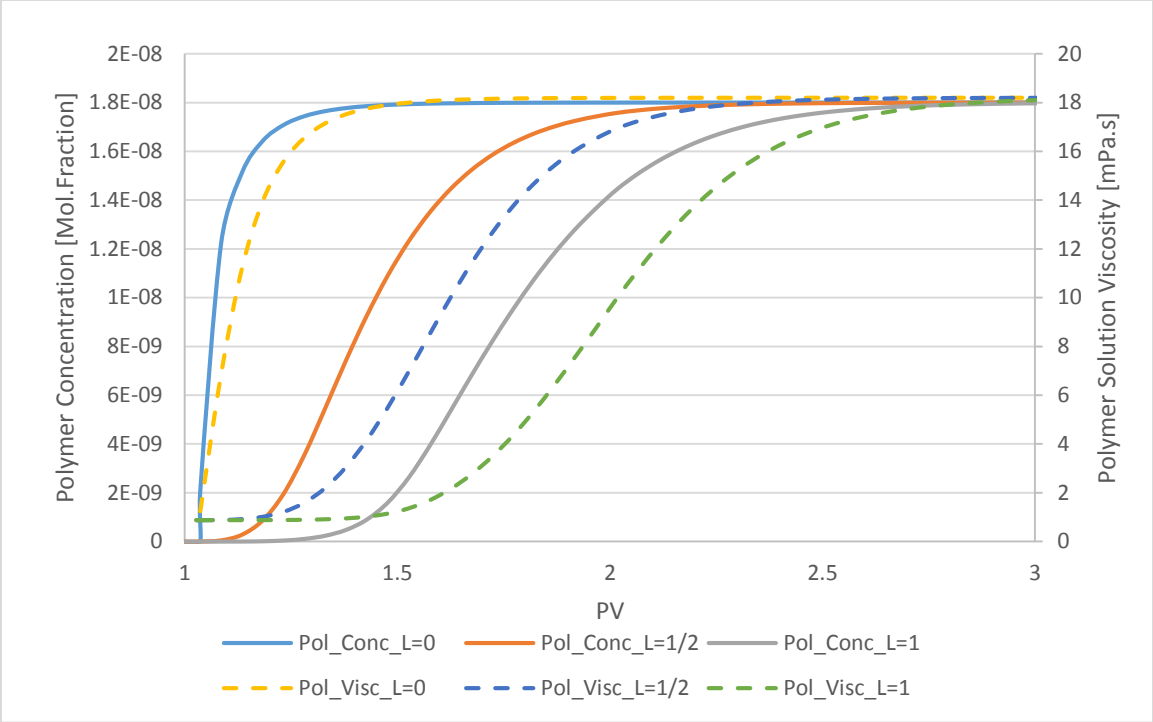

Figure 6.39: Exp2 polymer concentration and viscosity profiles.

The figure above shows the polymer concentration and viscosity development in the model at different locations. Three locations were tested, at the injection well (L=0), at the middle of the model (L=1/2) and at the production well (L=1). At each location, polymer concentration and viscosity were plotted verse the pore volume injected. The polymer viscosity development follows the polymer concentration development at each location.

In this experiment, the polymer concentration and viscosity profiles reached the target at almost 3 pore volume injected, and in this experiment about 5.3 pore volume was injected. The different between the polymer concentration profiles at the injection and production wells is not big. It was required for the polymer about 0.5 pore volume injected to reach the production well.

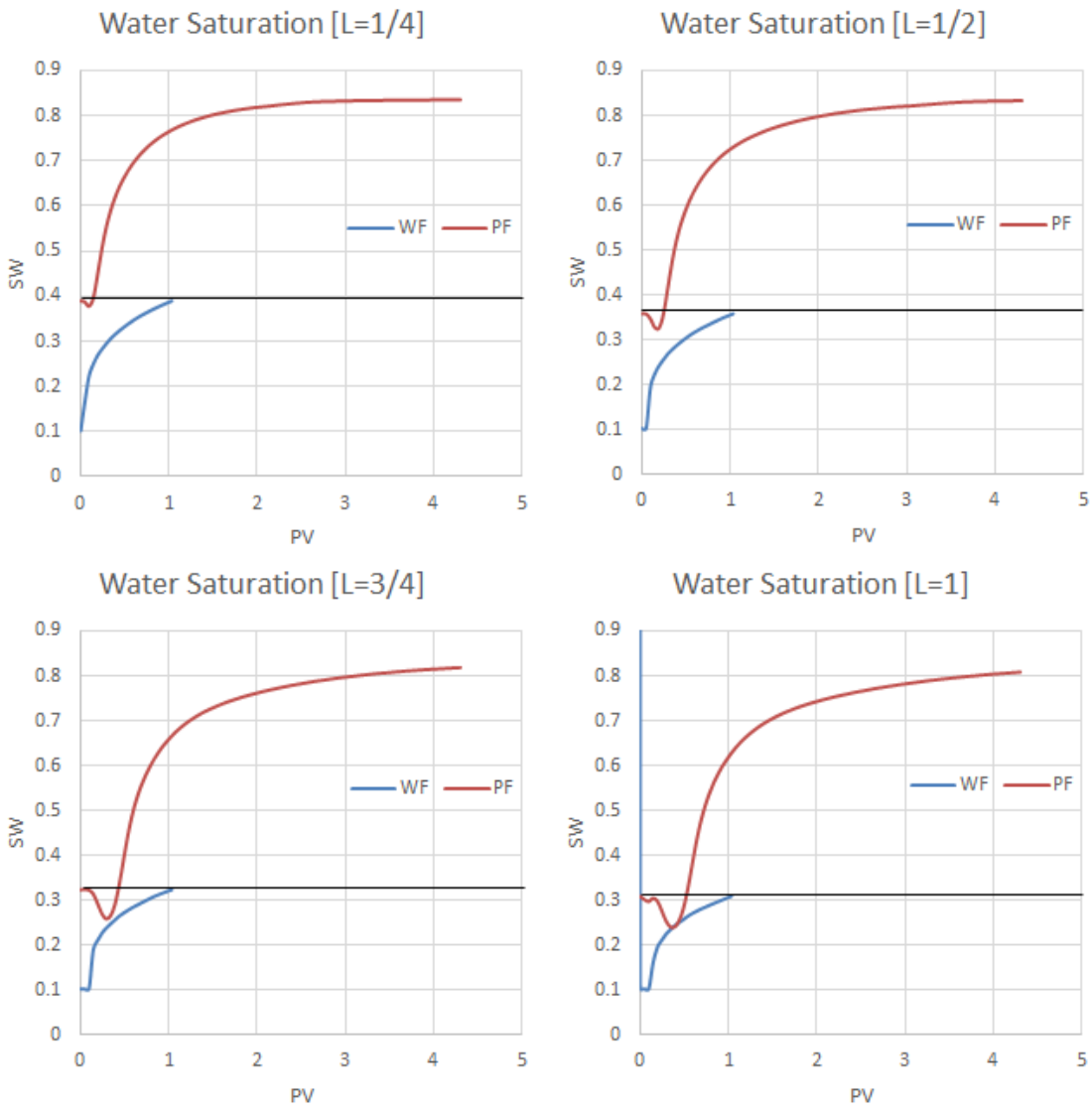

Figure 6.40: Exp2 internal water saturation profiles

The figure above shows the internal water saturation profile for both waterflooding and polymer flooding at different locations in the model. Four locations were tested, at L=1/4, L=1/2, L=3/4 and at L=1. In the waterflooding part, it is clear that as the location is closer to the production well (L=1), the water saturation at the end of waterflooding is lower, and this is also true for polymer flooding part. It is noticeable that the oil bank saturation is increasing as the location is closer to the production well.

Another way to view water saturation changes in the model with different pore volume injected is to plot the water saturation gradient, which gives a good view of water saturation changes as function of the dimensionless length.

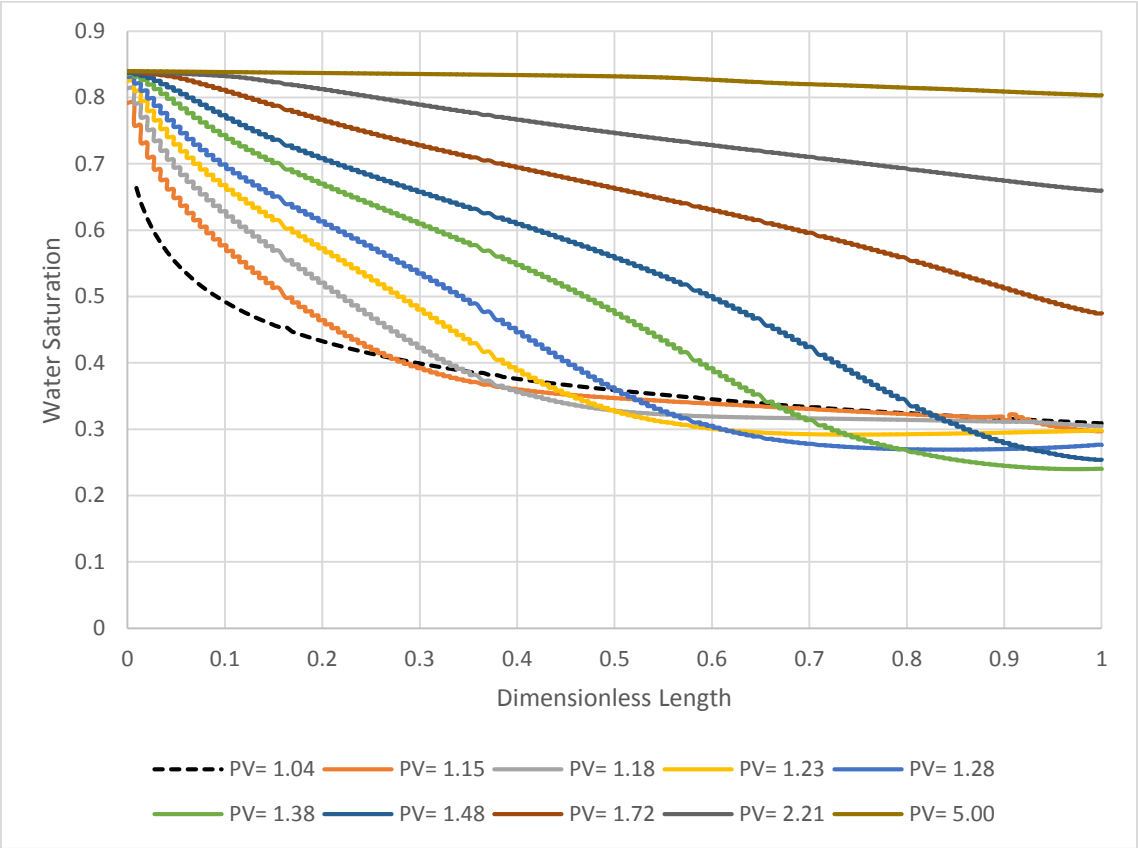

Figure 6.41: Water saturation gradient for of water and polymer flooding of 7000 cp oil viscosity experiment

In figure above it is clear that the model is trying to mimic the real experiment water saturation gradient. Although Buckley Leverette type of displacement was used to model the experiments, but as results of history match and the parameter used to obtain that match, the water saturation front is not steep as it is in the ideal Buckley-Leverette water saturation front. The main parameter that affects water saturation front is polymer dispersion, and for this experiment it was 0.001 cm2/day.

In this experiment the ideal Buckley-Leverette water saturation front is not observed. This is mainly because of the physical dispersion. Although the it is same as in E2000, but

physical dispersion is a dimension dependent. Exp2 PV is less than other experiments PVs. Therefore, it is greater for Exp2 when compared to other experiments.

Also oil bank saturation can be observed from the figure above, and it is increasing as dimensionless time is increasing.

6.3.Results Summary

In the previous sections, the history match for each experiment model was discussed individually. In this section, the summary of all experiments results will be discussed. The relative permeability for waterflooding and polymer flooding of all experiments will be shown. Also, the end point water saturation trend for waterflooding and polymer flooding will be shown.

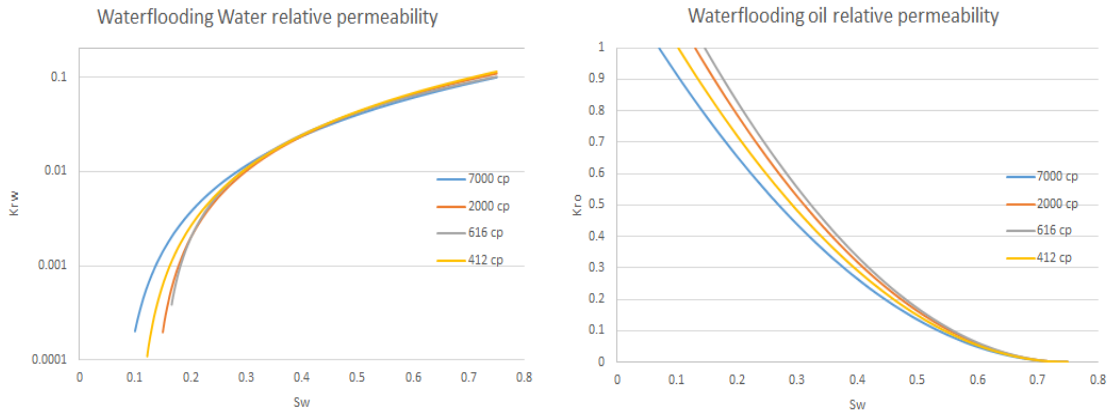

Figure 6.42: Waterflooding relative permeability curves for all experiments

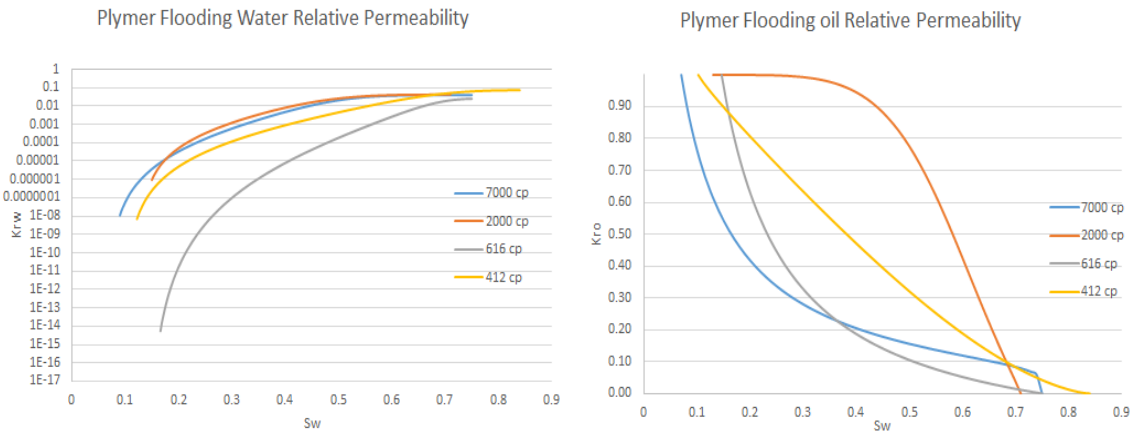

Figure 6.43: Polymer flooding relative permeability curves for all experiments

The figures above show the relative permeability curves of polymer flooding. In the polymer flooding, the water relative permeability curves are close to each other for E7000, E2000 and Exp2. However, the water relative permeability of Exp1 is lower compared to the other experiments, and this is may be because of viscous fingering of Exp1. As it shown in Appendix 2, There are two main channels in Exp1 that water and polymer were flowing through, and these channels are responsible for the pressure build up. In the model, there are no channels, and in order to match the differential pressure profile, both water end point relative permeability and water relative permeability curves should be lowered. On the other hand, the oil relative permeability curves are not identical as in the waterflooding. Each curve was varied to match the cumulative oil production and differential pressure profiles.

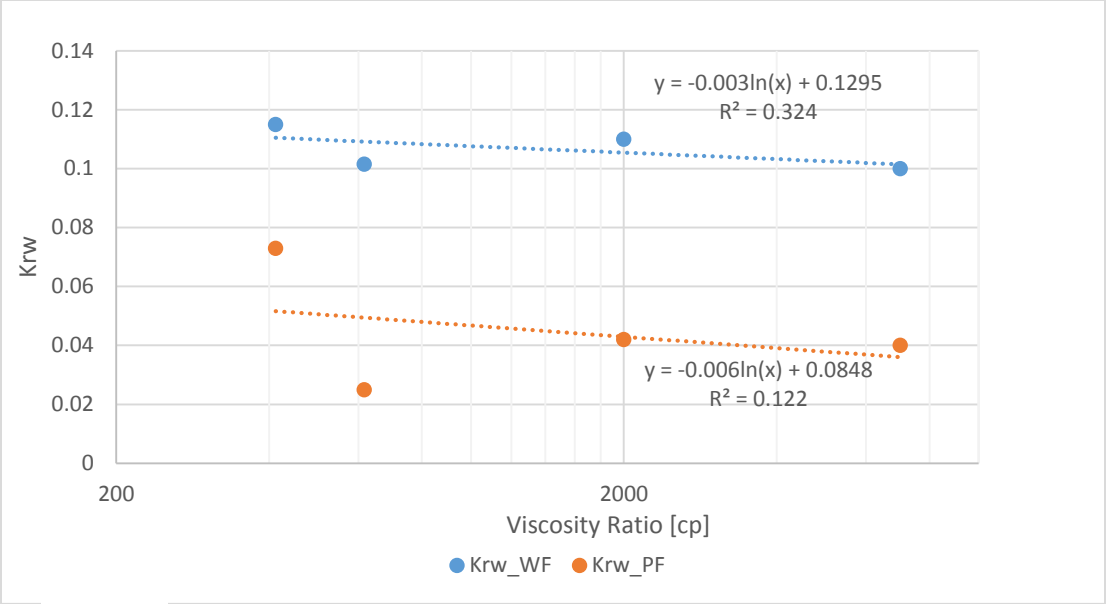

Figure 6.44: Water end points relative permeabilities trend for waterflooding and polymer flooding

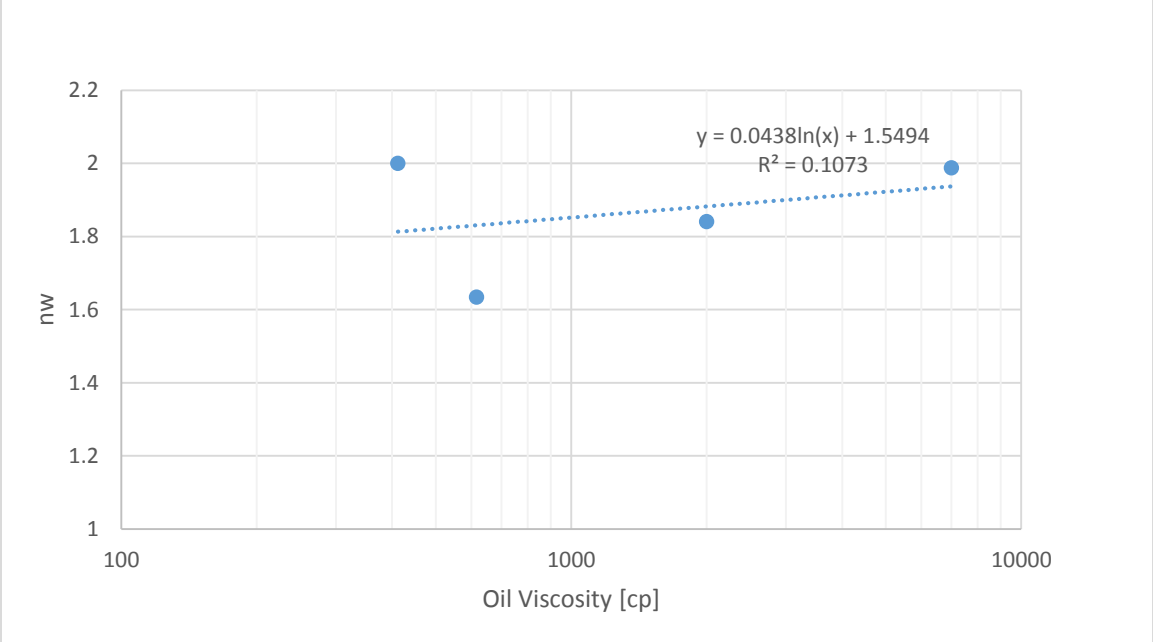

Figure 6.45: waterflooding Corey water exponent trend for all experiments

Figure 6.23 shows the water end point relative permeability for waterflooding and polymer flooding. There is a good trend of krw in the both waterflooding and polymer flooding. However, krw for Exp1 is out of the trend because of the viscous fingering as mentioned before.

Figure 6.24 shows the water exponent of Corey correlation for waterflooding relative permeability. There is very good trend for E2000. E2000 and Exp1. However, Exp2 water exponent seems to be out of trend.

Table 6.2: Polymer flooding history matching parameters

Polymer Parameter	E7000	E2000	Exp1	Exp2
Polymer Concentration [ppm]	1650	1650	1250	1000
Polymer Viscosity [cp]	58	58	28	18
Polymer Adsorption [µg/g]	21	22.3	10	9.7
Polymer Dispersion [cm2/day]	0.005	0.001	0.001	0.001
Inaccessible Pore Volume	0.9	1	1	1
Resistance Factor	1	1	1	1
WCRV	0.01	0.01	0.01	0.08
OCRV	0.01	1	1	0.1

The polymer flooding parameters that were used in the history matching are listed in the table above. In E7000 and E2000 which have higher polymer concentration compared to the other experiments, the polymer adsorption is also higher than the other experiments. The difference between E7000 and E2000 in polymer dispersion and IPV obtained from the simulated model is due to the difference in pore volume and mainly in oil viscosity. Therefore, it was required to changes more parameter in E7000 to match the cumulative oil production and differential pressure.

The adsorption values are in the range between 10 to 20 µg/g. However, these values are considered to be normal. F.Wassmuth et al [63] reported HPAM polymer adsorption of 10 µg/g and F. Delaplace et al [64] reported 12 µg/g in one simulated layer in field scale and F. Wassmuth et al reported another values which are 40 µg/g and 50 µg/g .

Polymer dispersion, inaccessible pore volume and the resistance factor were almost the same for all experiments. Only E7000 has slightly different values.

The relative permeability interpolation parameters have significant effects to the history match. They allowed to have a quicker response for both cumulative oil production and the differential pressure.

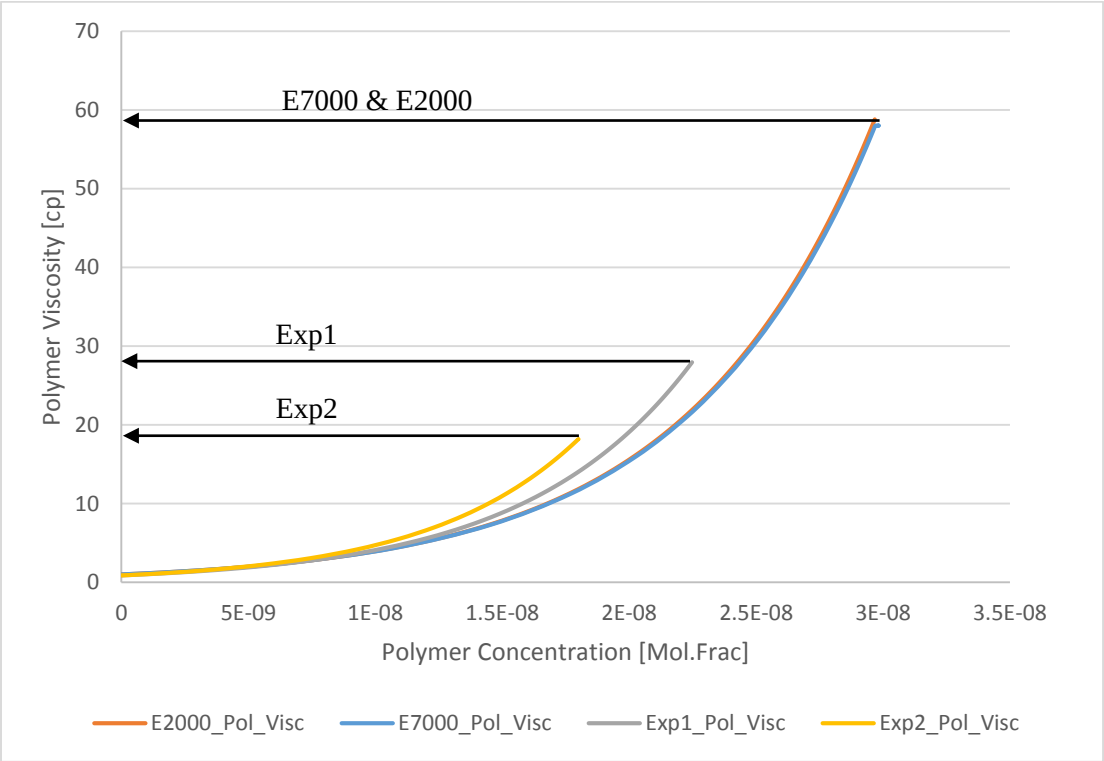

Figure 6.46: Polymer viscosity/concentration profiles for all experiments

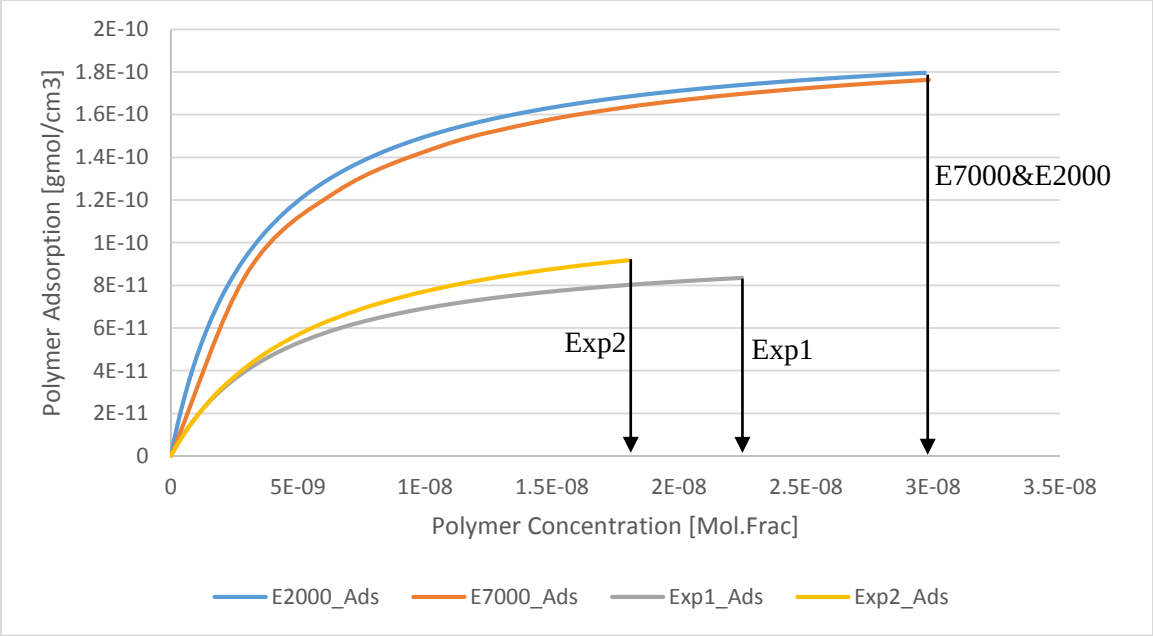

Figure 6.47: Polymer adsorption/concentration profiles for all experiments

Figure 6.34 and figure 6.35 show the polymer viscosity and adsorption versus polymer concentration for all experiments. They show the viscosity development as the polymer concentration increasing. As mentioned before E7000 and E2000 have an identical concentration, therefore, their viscosity/concentration profiles are also identical as it is clear in figure 6.25. Exp1 and Exp2 follow different profile depending on their polymer concentrations.

Polymer adsorption was defined using the Langmuir-type isotherm. Two parameters and the polymer concentration were used to define the polymer adsorption for each experiment. Equation 3.5 shows the Langmuir-type isotherm equation. As it is clear in figure 6.26 almost all experiments reached the maximum adsorption.

Several studies regarding history matching and finding good relative permeabilities for unstable immiscible flooding are published. Skauge and Salmo [61] have conducted a history match for E7000 and they have history matched the oil production, differential pressure for both waterflooding and polymer flooding and the in-situ oil saturation distribution after waterflooding. They have found very good history match and showed that

using water relative permeability to predict the polymer flooding performance is not efficient, and the prediction is mismatched the experimental results.

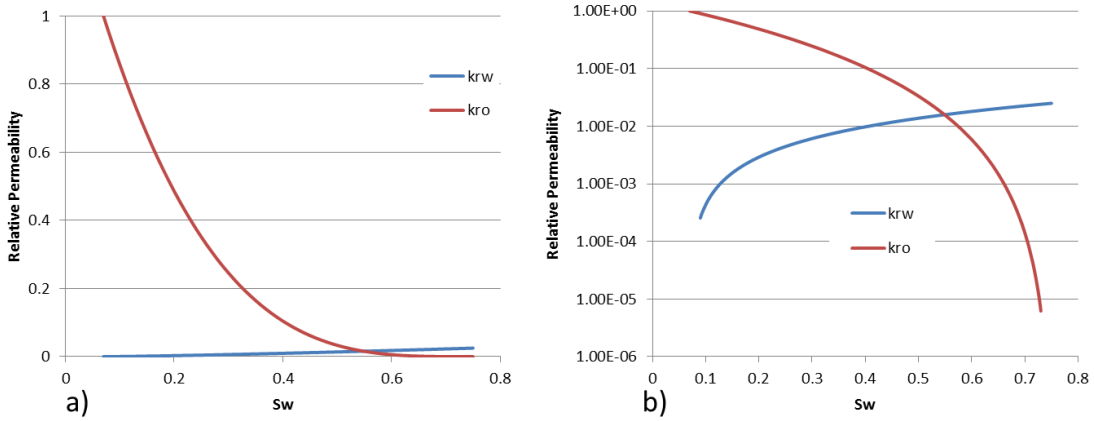

Figure 6.48: Relative permeability for waterflooding history matching [61]

The relative permeability for waterflooding from Salmo and Skauge [1] looks very similar to the relative permeability of waterflooding from this thesis.

Bondino [56] has conducted a history match to E7000 and he matched the oil production, differential pressure for both waterflooding and polymer flooding, and the crossflow from the unswept area into the water channels during the polymer flooding. One set of relative permeability was used for both waterflooding and polymer flooding with some manual modifications. Also, bulk and in-situ rheological measurements were used in the history matching.

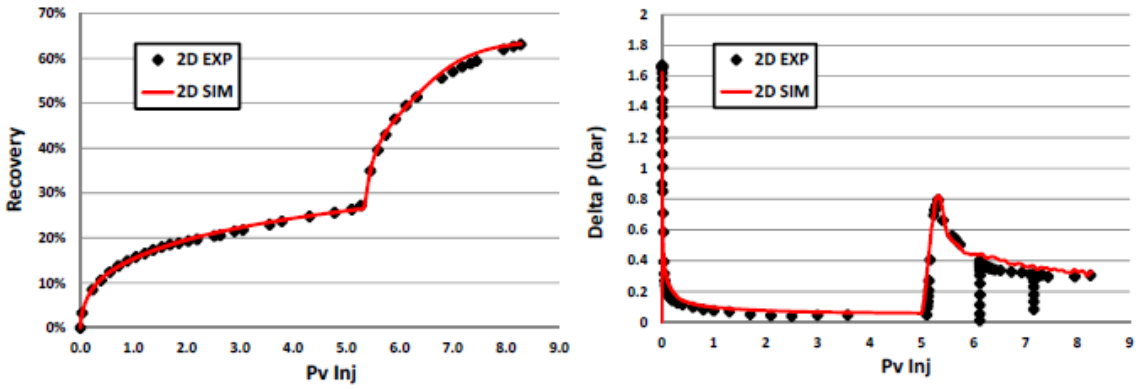

Figure 6.49: Bondino oil production and differential pressure history matching [56]

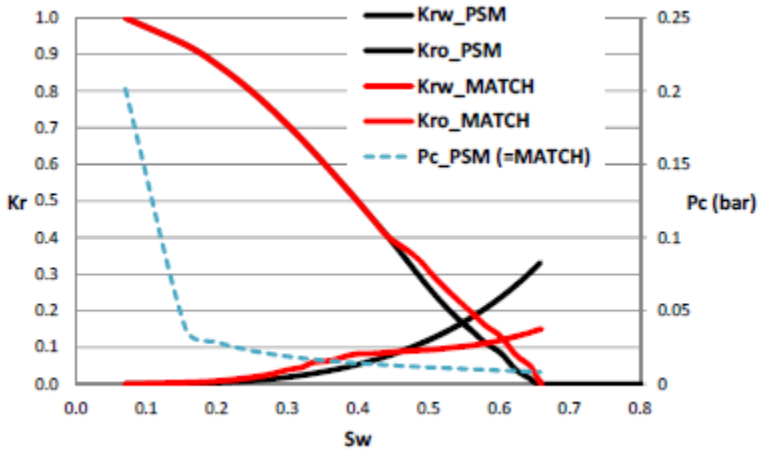

Figure 6.50: Bondino relative permeability used in the history match [56]

Although, Salmo and Skauge [1] and Bondino [53] conducted a history match for one of the experimenters that was simulate in this thesis. The difference between their results and the results obtained from this thesis is normal because they history matced the expeiments with additional experimental results. However, the waterflooding history match can be compared since there is no difference in the history matched experimental results.

Another study for polymer flooding history matching by P. Delaplace et al [64], which a history matching of a case study for a heavy oil field in Canada. The water end point relative permeability used in the history match is shown in the table and figure below.

Table 6.3: Water end points relative permeabilities for different three layers [64]

	Swi	Sorw	Krowm	Krwmax	Sorg	Sgrm	Krogi	Krgm
Bar Complex Top	0.3	0.2	1	0.1	0.05	0.005	0.96	0.02
Bar Complex Good Pay	0.3	0.2	1	0.1	0.05	0.005	0.96	0.02
Bar Margin	0.55	0.2	1	0.15	0.05	0.005	0.96	0.02

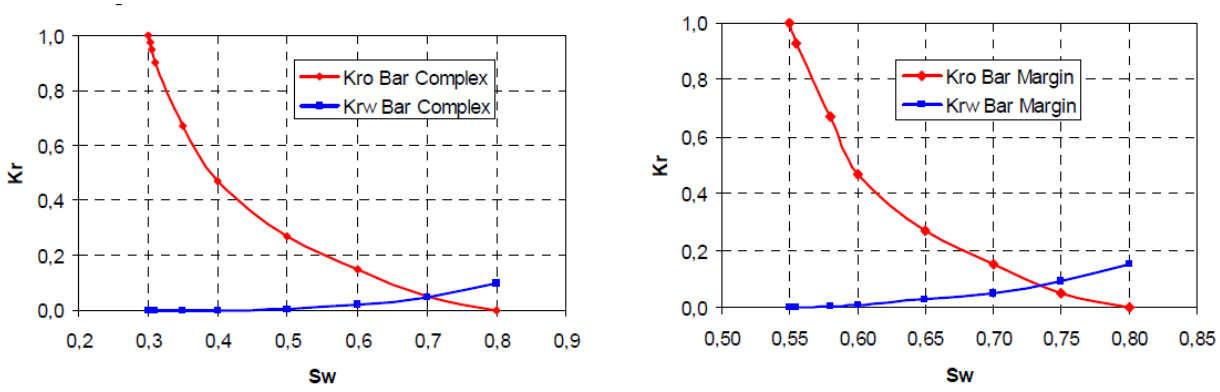

Figure 6.51: Relative permeability curves of history match for a field in Canada [64]

The oil viscosity of the field is 1650 cp and different polymer concentrations slugs were injected, 500 ppm, 1000 ppm, 1500,ppm and 2000 ppm. However, the water end points relative permeability is 0.1 in average for all layers. This is not much far from k_{rw} obtained from this thesis taking into consideration the number of different parameters and factors affecting the results.

Another study of estimating relative permeability from polymer flooding was conducted by C. Fabbri et al [65]. Their experiemnts conducted on a 30 cm core for a 5500 cp oil using 2000 ppm polymer concentration. The relative permeability for their history match is shown in the figure below.

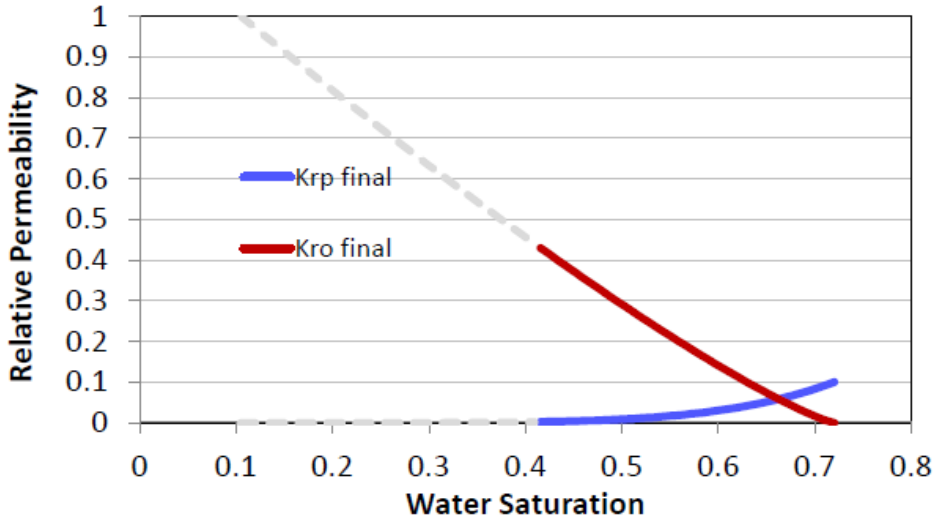

Figure 6.52: Relative permeability of a history match for 5500 cp oil [65]

Also in this experiment history match, the water end point relative permeability is 0.1, which considered to be low.

7. Conclusion

The objective of this thesis was to obtain a history match for six experiments which have high viscosity ratios. The history match should be conducted for unstable waterflooding and polymer flooding, and obtain relative permeability curves for both waterflooding and polymer flooding. The experiential results that should be history matched are cumulative oil production and differential pressure.

A sensitivity analysis was conducted to the models before history matching stared. Numerical dispersion and physical dispersion were tested at the beginning to remove any numerical dispersion effect. After that, all polymer parameters that were used in the models were tested. Polymer viscosity, polymer concentration, polymer molecular weight, polymer adsorption, reversible and irreversible adsorption, inaccessible pore volume and the relative permeability were tested to investigate their degree of sensitivity in the history match.

There were some program restrictions in which two experiments could not be simulated using STARS. The restrictions were regarding the differential pressure profile, which showed unreal responses to the sensitivity analysis.

In the first part of this thesis, a history match was obtained for waterflooding using CMOST. Corey correlation for relative permeability was used to history match the cumulative oil production and the differential pressure. The history match was very good for all experiments in cumulative oil profile and less good in the differential pressure profile. There were mismatches at the end of waterflooding for E2000, Exp1 and Exp2. The differences between the experimental results and the simulated models were 2 kPa for E2000 and Exp1, and 1 kPa for Exp2.

In the second part of this thesis, a history match was obtained for polymer flooding. LET correlation for relative permeability was used to history match the cumulative oil production and the differential pressure. Also, other polymer parameters were used such as polymer adsorption, dispersion, inaccessible pore volume and resistance factor. A very

good history match was obtained for all experiments. The polymer adsorption was in the range of 10 µg/g to 20 µg/g, depending on the polymer concentration of the experiment, and the polymer dispersion values were 0.001 for E2000, Exp1 and Exp2, and 0.005 for E7000. Resistance factor was 1 for all experiments and the inaccessible pore volume was also 1 for all experiments except E7000 which was 0.9.

It was found that the relative permeability was the main factor that affects the history match in both waterflooding and polymer flooding. Although, the polymer parameters had significant effects, but there had some constraints and they cannot be used freely, and therefore, only the relative permeability had the most significant role in obtaining the history match. Water end point relative permeability trend was determined for both waterflooding and polymer flooding.

8. Further Work

There are several suggestions regarding the investigations and studies of simulation models that test and simulate the unstable immiscible waterflooding and polymer flood at adverse mobility ratio.

Obviously, the first recommendation is to simulate and history match the two experiments that were not simulated because of STARS restrictions. Exp3 and Exp4 are important to this thesis since they have lowered adverse mobility compared to the other experiments, and that will surly help in obtaining the trend of all experiments.

Since all experiments were scanned by X-ray and the internal water saturation can be determined using the X-ray images, it is recommended to obtain a history match for all experiments using cumulative oil production, differential pressure and the internal water saturation, and compare the results with the results from this thesis.

Also, it is recommended to carry out further experiments which have viscosity ratio between 600 and 2000 since the trend obtained using the current experiments has a relatively big gab. It is believed that experiments of viscosity ratio between 600 and 2000 will have significant help to understand the trend and the investigations of the adverse mobility immiscible flooding.

More sensitivity analyses that describe the relationship between oil/polymer viscosity ratio and the recovery factor are recommended. It is important to find the optimum oil/polymer viscosity ratio to the oil recovery. Also, it is recommended to investigate the relationship between the volume of polymer used and the volume of oil produced and find the optimum polymer volume to the volume of oil produced.

9. References

[1] OPEC, "Monthly Oil Market Report, Oil demand outlook for 2015," 2015.

[2] BP, "Statistical Review of World Energy 2014, 2013 in review," June 2014. [Online]. Available: bp.com/statisticalreview.

[3] IEA, "International Energy Agency," 2015. [Online]. Available: http://www.iea.org/aboutus/faqs/oil.

[4] EIA, "United States Energy Information Administration, Short-Term Energy Outlook," May 2015. [Online]. Available: http://www.eia.gov/forecasts/steo/images/Fig6.png.

[5] K. S. Sorbie, Polymer-Improved Oil Recovery, Boca Raton, Florida: Blackie and Son Ltd, 1991.

[6] L. W. Lake, Enhanced oil recovery, Englewood Cliffs, NJ: Prentice Hall, 1989.

[7] H. Rashedi, F. Yazdian and S. Naghizadeh, Microbial Enhanced Oil Recovery, L. Romero-Zerón, Ed., InTech, 2012, pp. 73-75.

[8] J. Sevin and B. Capron, "Seizing the EOR Opportunity," Schlumberger Business Consulting.

[9] T. Ahmed, Reservoir Engineering, 2nd ed., London: Butterworth-Heinemann, 2001.

[10] M. Skarestad and A. Skauge, Reservoarteknikk II, Bergen: University of Bergen, 2007.

[11] A. B. Zolotuchin and J.-R. Ursin, Introduction to petroleum reservoir engineering, Kristiansand: Hoyskoleforl, 2000.

[12] R. C. Selley and S. Sonnenberg, Elements of Petroleum Geology, 3rd ed., Elsevier Inc., 2015.

[13] R. E. Collins, Flow of Fluids Through Porous Materials, Tulsa: The Petroleum Pub, 1976.

[14] M. C. Leverett, "Flow of Oil-water Mixtures through Unconsolidated Sands," *Trans AIME,* vol. 132, no. 1, pp. 149-171, 1939.

[15] C. R. Sandberg, L. S. Gournay and R. Sippel, "The Effect of Fluid-Flow Rate and Viscosity on Laboratory Determinations of Oil-Water Relative Permeability," *AIME Trans,* vol. 213, pp. 36-43, 1958.

[16] A. S. Odeh, "Effect of Viscosity Ratio on Relative Permeability," *AIME Trans,* vol. 216, pp. 346-352, 1959.

[17] T. A. Edmondson, "Effect of Tempreture on Waterflooding," *Journal of Canadian Petroleum,* vol. 4, no. 4, pp. 236-242, 1965.

[18] S. W. Poston, S. Ysral and A. K. M. S. Hossain, "The Effect of Temperature on Irreducible Water Saturation and Relative Permeability of Unconsolidated Sands," *Society of Petroleum Engineers Journal,* vol. 10, no. 02, pp. 171-180, 1970.

[19] A. H. Sufi, H. J. Ramey and W. E. Brigham, "Temprerature Effects on Relative Permeabilities of Oil-Water Systems," in *57th Annul Technical Conference and Exhibition,* New Orleans, Louisiana USA, 26-29 September, 1982.

[20] M. A. Miller and H. J. Ramey, "1985," *Effect of Temperature on Oil/Water Relative Permeabilities of Unconsolidated and Consolidated Sands,* vol. 25, no. 06, pp. 945-953, Journal of Petroleum Technology.

[21] H. Y. Lo and N. Mungan, "Effect of Temperature on Water-Oil Relative Permeabilities in Oil-Wet and Water-Wet Systems," in *Fall Meeting of the Society of Petroleum Engineers of AIME,* Las Vegas, Nevada, USA, September-3, 1071.

[22] M. Kumar and T. A. Inouye, "Low-Temperature Analogs of High-Temperature Water/Oil Relative Permeabilities," in *SPE Annual Technical Conference and Exhibition* , New Orleans, USA, 25-28 September, 1994.

[23] S. Doorwar and K. K. Mohanty, "Extension of the Dielectric Breakdown Model for Simulation of Viscous Fingering at Finite Viscosity Ratios," *Phys Rev E,* vol. 90, no. 1, 2014.

[24] S. Akin, L. M. Castanier and W. E. Brigham, "Effect of Temperature on Heavy-Oil/Water Relative Permeabilities," in *SPE Annual Technical Conference and Exhibition,* New Orleans, Lousisana, USA, 27-30 September, 1998.

[25] J. Wang, M. Dong and K. Asghari, "Effect of Oil Viscosity on Heavy Oil-Water Relative Permeability Curves," in *SPE/DOE Symposium on Improved Oil Recovery*, Tulsa, Oklahome, USA, 22-26 April, 2006.

[26] N. Mosavat, O. Zarivnyy and F. Torabi, "Developing New Corey-Based Water/Oil Relative Permeability Correlations for Heavy Oil Systems," in *SPE Heavy Oil Conference-Canada*, Calgary , Alberta , Canada, 11-13 June, 2013.

[27] S. K. Masalmeh, "Determination of Waterflooding Residual Oil Saturation for Mixed to Oil-Wet Carbonate Reservoir and its Impact," in *SPE Reservoir Characterisation and Simulation Conference and Exhibition*, Abu Dhabi, UAE, 16-18 September, 2013.

[28] L. P. Dake, Fundamentals of Reservoir Engineering, Amsterdam: ELSEVIER SCIENCE B.V., 1978.

[29] S. E. Buckley and M. C. Leverett, "Mechanism of Fluid Displacement in Sands," *Society of Petroleum Engineers*, vol. 146, no. 01, pp. 107-116, 1942.

[30] M. Dawson, D. P. Yale and A. P. Kushnick, "Experimental and Computational Investigations of Viscous Fingering at High Mobility Contrasts," in *SPE Annual Technical Conference and Exhibition*, San Antonio, Texas, USA, 8-10 October, 2012.

[31] B. Habermann, "The Efficiency of Miscible Displacement as a Function of Mobility Ratio," in *35th Annual Fall Meeting of SPE*, Denver, 2-5 October, 1960.

[32] P. G. Saffman and G. Taylor, "The Penetration of a Fluid into a Porous Medium or Hele-Shaw Cell Containing a More Viscous Liquid," *Proceedings of the Royal Society of London. Series A, Mathematical and Physical Sciences*, vol. 245, no. 1242, pp. 312-329, 1958.

[33] I. Bondino, E. Santanach-Carreras, D. Levitt, S. Jouenne and M. Bourrel, "Polymer Flooding of Heavy Oil Under Adverse Mobility Conditions," in *SPE Enhanced Oil Recovery Conference*, Kuala Lumpur, Malaysia, 2-4 July, 2013.

[34] Stalkup and F. Jr, "Miscible Displacement," American Institute of Mining, Metallurgical, and Petroleum Engineers Inc, United States of America, 1983.

[35] R. L. Chuoke, P. Vanmeurs and C. Vanderpoel, "The Instability of Slow, Immiscible, Viscous Liquid-Liquid Displacements in Permeable Media," *Trans AIME,* vol. 216, pp. 188-194, 1959.

[36] H. Outmans, "Nonlinear Theory for Frontal Stability and Viscous Fingering in Porous Media," *Society of Petroleum Engineers Journal,* vol. 2, no. 02, pp. 165-176, 1962.

[37] A. Scheidegger, "Growth of Instabilities on Displacement Fronts in Porous Media.," *Physics of Fluids,* vol. 3, p. 94, 1960.

[38] R. L. Perrine, "The Development of Stability Theory for Miscible Liquid-Liquid Displacement," *Society of Petroleum Engineers Journal,* vol. 1, no. 01, pp. 17-25, 1961.

[39] J. W. Gardner and J. G. J. Ypma, "An Investigation of Phase Behavior – Macroscopic Bypassing Interaction in CO2 Flooding," in *SPE Enhanced Oil Recovery Symposium,* Tulsa, April 4-7, 1982.

[40] T. K. Perkins, O. C. Johnston and R. N. Hoffman, "Mechanics of Viscous Fingering in Miscible Systems," *Society of Petroleum Engineers Journal,* vol. 5, no. 03, pp. 301 - 317, 1965.

[41] R. Moorhouse, M. D. Walkinshaw and S. Arnott, "Extracellular Microbial Polysaccharides," *American Chemical Society Symposium,* vol. 45, p. 90, 1977.

[42] P. J. a. M. C. W. Whitcombe, "Rheology of Xanthan Gum," *Journal of Rheology,* vol. 22, no. 5, pp. 493-505, 1978.

[43] G. Chauveteau, "Rodlike Polymer Solution Flow Through Fine Pores: Influence of Pore Size on Rheological Behavior," *Journal of Rheology,* vol. 26, pp. 111-142, 1982.

[44] R. S. Seright and B. J. Henrici, " Xanthan Stability at Elevated Temperatures," in *SPE/DOE Fifth Symposium on EOR*, Tulsa, Oklahoma, 20-23 April, 1986.

[45] J. C. Philips, J. W. Miller, W. C. Wernau, B. E. Tate and M. H. Auerbach, "A High-Pyruvate Xanthan for EOR," *Society of Petroleum Engineers Journal,* vol. 25, no. 04, pp. 594-602, 1985.

[46] K. Walters, Rheometry, London: Chapman and Hall, 1975.

[47] W. R. Schowalter, Mechanics of Non-Newtonian Fluids., New York: Pergamon Press, 1978.

[48] R. B. Bird, R. C. Armstrong and O. Hassager, Dynamics of Polymeric Liquids, 2nd ed., vol. 1, Chichester: John Wiley & Sons, Inc, 1987.

[49] R. Dawson and R. B. Lantz, "Inaccessible Pore Volume in Polymer Flooding," *Society of Petroleum Engineers Journal*, vol. 12, no. 05, pp. 448-452, 1972.

[50] G. P. Willhite and J. G. Dominguez, Improued Oil Recouery by Surfactant and Polymer Flooding, D. O. Shah and R. S. Shecter, Eds., New York.: Academic Press Inc, (1977).

[51] R. S. Seright, "The Effects of Mechanical Degradation and Viscoelastic Behavior on Injectivity of Polyacrylamide Solutions," *Society of Petroleum Engineers Journal*, vol. 23, no. 03, pp. 475 - 485, 1983.

[52] R. S. Seright, R. P. Adamski, J. C. Roffall and W. W. Liauh, " Rheology and mechanical degradation of EOR polymers," in *SPE/British Society of Rheology Conference on Rheology in Crude Oil Production*, Imperial College, London, UK, 13-15 April, 1983.

[53] R. R. Jennings, J. H. Rogers and T. J. West, "Factors Influencing Mobility Control By Polymer Solutions," *Journal of Petroleum Technology*, vol. 23, no. 03, pp. 391-401, 1971.

[54] A. Skauge, P. A. Ormehaug, B. F. Vik, C. Fabbri, I. Bondino and G. Hamon, "Polymer Flood Design for Displacement of Heavy Oil Analysed by 2D-imaging," in *17th European Symposium on Improved Oil Recovery*, St. Petersburg, Russia, 16-18 April, 2013.

[55] A. Skauge, P. A. Ormehaug, T. Gurholt, B. Vik, I. Bondino and G. Hamon, "2-D Visualisation of Unstable Waterflood and Polymer Flood for Displacement of Heavy Oil," in *SPE Improved Oil Recovery Symposium*, Tulsa, Oklahoma, USA, 14-18 April, 2012.

[56] T. Skauge, B. F. Vik, P. A. Ormehaug, B. K. Jatten, V. Kippe, I. Skjevrak, D. C. Standnes, K. Uleberg and A. Skauge, "Polymer Flood at Adverse Mobility Ratio in 2D Flow by X-ray Visualization," in *SPE EOR Conference at Oil and Gas West Asia*, Muscat, Oman, 31 March–2 April , 2014.

[57] I. Bondino, R. Nguyen, G. Hamon, P. A. Ormehaug, A. Skauge and S. Jouenne, "Tertiary polymer flooding in extra heavy oil: an investigation using 1D and 2D experiments, core scale simulation and pore scale network models," in *International Symposium of the Society of Core Analysts*, Austin, Texas, USA 18-21 September, 2011.

[58] CMG, "CMG STARS User Guide," Computer Modelling Group Ltd., 2013.

[59] CMG, "CMG CMOST User Guide," Computer Modelling Group Ltd., 2013.

[60] A. T. Corey, "The Interrelation Between Gas and Oil relative Permeabilities," in *18th Technical Conference on Petroleum Production*, Pennsylvania, 1954.

[61] F. Lomeland, E. Ebeltoft and W. H. Thomas, "A New Versatile Relative Permeability Correlation," in *International Symposium of the Society of Core Analysts*, Toronto, Canada, 21-25 August, 2005.

[62] H. Sarma, B. B. Maini, R. W. Purves and K. N. Jha, "On the Use of Buckley-Leverett Analysis to Characterize Unstable Immiscible Displacements," in *CIM 1992 Annual Technical Conference*, Caracas, Venezuela, March 8-11, 1992.

[63] F. Wassmuth, K. Green and J. Bai, "Associative Polymers Outperform Regular Polymers Displacing Heavy Oil in Heterogeneous Systems," in *SPE Heavy Oil Conference* , Calgary, Alberta, Canada, 12-14 June, 2012.

[64] P. Delaplace, E. Delamaide, F. Roggero and G. Renard, "History Matching of a Successful Polymer Flood Pilot in the Pelican Lake Heavy Oil Field (Canada)," in *SPE Annual Technical Conference and Exhibition* , New Orleans, Louisiana, USA, 30 September–2 October, 2013.

[65] A. Skauge and I. Salmo, "Relative Permeability Functions for Tertiary Polymer Flooding," in *18th European Symposium on Improved Oil Recovery*, Dresden, Germany, 14-16 April , 2015.

[66] C. Fabbri, C. Romero, F. Aubertin, M. Nguyen, S. Hourcq and G. Hamon, "Secondary Polymer Flooding in Extra-Heavy Oil: Gaining Information on Polymer-Oil Relative Permeabilities," in *SPE Enhanced Oil Recovey Conference* , Kuala Lumpur, Malaysia, 2-4 July, 2013.

Appendix A: STARS Data File and Parameters

STARS data file that was used for history matching of E7000 experiment is attached below. Because all experiments were conducted using the same set up, E7000 data file can be used for all experiments with the necessary changes as shown in table 4.1.

```
**************************************E7000 STARS Data File**********************************
INUNIT LAB
WSRF WELL 1
WSRF GRID TIME
WSRF SECTOR TIME
*OUTPRN *GRID  *SW  *SO  *W *X *Y *Z *SG *PRES  ** WATER AND OIL
SATURATIONS AND PRESSURE              *VISW     *ADSORP  ** WATER VISC AND
ADSORPTION              *MASFR    *ADSPCMP *VISO *KRW *KRO *LOGIFT
*LOGCAPN
*OUTSRF *GRID  *SW  *SO  *W   *X *Y *Z *SG *PRES    *PERMI  *PERMK
           *MASS *ADSORP   *VISW *VISO *KRW *KRO *LOGIFT *LOGCAPN
*WATMOB *OILMOB *IFT
           *ADSPCMP          ** Special Adsorption Component (Mass Frac)
OUTPRN *WELL  *ALL
OUTSRF *GRID  *ALL
OUTSRF  WELL COMPONENT ALL
OUTSRF SPECIAL MASSFRAC 'INJTR' 'POLYMER'
OUTSRF SPECIAL DELP  'INJTR' 'PRODN'
OUTSRF SPECIAL MOLEFRAC  'INJTR' 'POLYMER'
OUTSRF SPECIAL MASSFRAC 'INJTR' 'POLYMER'
OUTSRF SPECIAL MOLEFRAC  'PRODN' 'POLYMER'
OUTSRF SPECIAL MASSFRAC 'PRODN' 'POLYMER'
OUTSRF SPECIAL VOLFRAC 'PRODN' 'POLYMER'
OUTSRF SPECIAL VOLFRAC 'INJTR' 'POLYMER'


OUTSRF SPECIAL DELPBLK 5,1,302 5,1,1
OUTSRF SPECIAL DELPBLK 2,1,302 2,1,1
OUTSRF SPECIAL DELPBLK 9,1,302 9,1,1
** Pressure in block uba1 minus pressure in block uba2.

**OUTSRF *SPECIAL MOLEFRAC  'INJTR' 'POLYMER'
**OUTSRF *SPECIAL MOLEFRAC  'PRODN' 'POLYMER'
WPRN GRID 0
OUTPRN GRID NONE
OUTPRN RES NONE
**$ *************************************************************************
**$ Definition of fundamental cartesian grid
**$ *************************************************************************

**  ==============  GRID AND RESERVOIR DEFINITION  =================
```

```
GRID CART 10 1 302
KDIR DOWN
DI CON 3
DJ CON 2.05
DK 10*0.01 3000*0.1 10*0.01


**$  0 = null block, 1 = active block
NULL CON           1

POR
 10*0.999 3000*0.24 10*0.999

PERMI
 10*160470 3000*2800 10*160470
PERMJ EQUALSI
PERMK EQUALSI
**  0 = pinched block, 1 = active block
PINCHOUTARRAY CON           1

END-GRID
ROCKTYPE 1
************************************
prpor 2533
cpor 2.96e-8

** ================== COMPONENT PROPERTIES ============== **

**$ Model and number of components
MODEL 3 3 3 2
COMPNAME 'H2O' 'POLYMER' 'DEAD_OIL'
CMM
            0     1000    0.456
PCRIT
            0       0         0
TCRIT
            0       0         0


PRSR 101
TEMR 26

PSURF 101
TSURF 25

MASSDEN
0.001  0.001  0.001
AVISC
1        58        7000

VSMIXCOMP 'POLYMER'
```

```
VSMIXENDP  0        2.97e-8

** ==================  ROCK-FLUID DATA  ================== **
ROCKFLUID
RPT 1 WATWET

*INTCOMP 'POLYMER' *WATER
**  ------------------------------------------------
KRINTRP 1
WCRV 0.05    **Curvature change parameter for water relative permeability.
OCRV 0.05    **Curvature change parameter for water relative permeability.
DTRAPW  0

SWT
 SMOOTHEND LINEAR
**       Sw          krw       krow
0.07     0                     1
0.1125 0.00040384    0.878906
0.155   0.00160198    0.765625
0.1975 0.00358696    0.660156
0.24     0.00635484    0.5625
0.2825 0.00990289    0.472656
0.325   0.014229      0.390625
0.3675 0.0193314     0.316406
0.41     0.0252088     0.25
0.4525 0.0318598     0.191406
0.495   0.0392834     0.140625
0.5375 0.0474786     0.0976563
0.58     0.0564445     0.0625
0.6225 0.0661803     0.0351562
0.665   0.0766853     0.015625
0.7075 0.0879587     0.00390625
0.75     0.1       0


KRINTRP 2
DTRAPW 2.97e-8

SWT
**       Sw          krw       krow
0.07     0                     1
0.08     6.51937E-10   0.906415627
0.09     1.09123E-08   0.828421299
0.1      5.78328E-08   0.762414204
0.11     1.91482E-07   0.705822045
0.12     4.90098E-07   0.656759167
0.13     1.06622E-06   0.61381177
0.14     2.07401E-06   0.575898994
0.15     3.71788E-06   0.542180355
0.16     6.2629E-06    0.511992431
0.17     1.0047E-05    0.484804562
```

0.18	1.54956E-05	0.460187211
0.19	2.31387E-05	0.437788968
0.2	3.36318E-05	0.417319546
0.21	4.77795E-05	0.398537042
0.22	6.65647E-05	0.381238248
0.23	9.11819E-05	0.365251207
0.24	0.000123077	0.350429415
0.25	0.000163993	0.336647275
0.26	0.000216025	0.323796485
0.27	0.000281681	0.311783151
0.28	0.000363952	0.300525464
0.29	0.000466395	0.289951799
0.3	0.000593218	0.279999175
0.31	0.000749382	0.270611976
0.32	0.000940695	0.261740896
0.33	0.001173921	0.253342056
0.34	0.001456868	0.245376268
0.35	0.001798468	0.23780841
0.36	0.002208811	0.230606901
0.37	0.002699125	0.223743251
0.38	0.003281666	0.217191676
0.39	0.003969473	0.21092877
0.4	0.004775959	0.204933221
0.41	0.005714286	0.19918556
0.42	0.006796484	0.19366795
0.43	0.00803232	0.188363994
0.44	0.009427932	0.183258569
0.45	0.010984321	0.178337681
0.46	0.012695873	0.17358833
0.47	0.014549158	0.168998391
0.48	0.016522278	0.164556509
0.49	0.018585056	0.160251997
0.5	0.020700244	0.156074741
0.51	0.02282574	0.152015115
0.52	0.024917614	0.148063894
0.53	0.026933492	0.144212167
0.54	0.028835781	0.140451249
0.55	0.030594224	0.136772591
0.56	0.032187444	0.133167678
0.57	0.033603379	0.129627916
0.58	0.03483871	0.126144501
0.59	0.035897565	0.122708256
0.6	0.036789829	0.119309442
0.61	0.037529355	0.115937494
0.62	0.038132319	0.112580699
0.63	0.038615837	0.109225735
0.64	0.038996912	0.105857037
0.65	0.039291697	0.102455883
0.66	0.039515033	0.098999009
0.67	0.039680207	0.095456458
0.68	0.039798871	0.091788037

```
0.69    0.039881072  0.087937156
0.7     0.039935355  0.083819238
0.71    0.039968896  0.079297658
0.72    0.039987661  0.074126207
0.73    0.03999656   0.067778255
0.74    0.039999595  0.058690363
0.75    0.04    0


ADSCOMP 'POLYMER' WATER
ADSLANG
0.05 0 2.5e8

ADMAXT 2e-10
ADRT 2e-10
PORFT 0.90
RRFT 1

**  ----------------------------------------------------------------
DISPI_WAT 'POLYMER' CON        0.005  **(cm2/day)
DISPJ_WAT 'POLYMER' EQUALSI
DISPK_WAT 'POLYMER' EQUALSI

** ================= INITIAL CONDITIONS ====== ============== **
INITIAL
VERTICAL OFF

INITREGION 1

PRES CON      101
TEMP CON      26

SW ALL
10*1 3000*0.07 10*0.07

MFRAC_OIL 'DEAD_OIL' CON      1
MFRAC_WAT 'POLYMER' CON       0
MFRAC_WAT 'H2O' CON           1



** ================= NUMERICAL CONTROL ====================== **
NUMERICAL
ISOTHERMAL
DTMIN 1e-15
** ================  RECURRENT DATA  ====================== **
RUN

Date 2014 08 1
DTWELL 0.01
**$
```

```
WELL  'INJTR'
INJECTOR UNWEIGHT 'INJTR'
**
INCOMP  WATER  1  0  0


OPERATE  MAX  STW  0.05  CONT
**         rad  geofac  wfrac  skin
GEOMETRY  K  1.0  1.0     1.0     0.0
PERF  TUBE-END  'INJTR'
** UBA       ff   Status  Connection
   1 1 302   1.0  OPEN    FLOW-FROM  'SURFACE'  REFLAYER
   2 1 302   1.0  OPEN    FLOW-FROM  1
   3 1 302   1.0  OPEN    FLOW-FROM  2
   4 1 302   1.0  OPEN    FLOW-FROM  3
   5 1 302   1.0  OPEN    FLOW-FROM  4
   6 1 302   1.0  OPEN    FLOW-FROM  5
   7 1 302   1.0  OPEN    FLOW-FROM  6
   8 1 302   1.0  OPEN    FLOW-FROM  7
   9 1 302   1.0  OPEN    FLOW-FROM  8
   10 1 302  1.0  OPEN    FLOW-FROM  9
************************************************

WELL  'PRODN'
PRODUCER 'PRODN'
OPERATE  MIN  BHP 101 CONT
         ** 1722.525

**         rad  geofac  wfrac  skin
GEOMETRY  K  1.0  1.0  1.0  0.0
PERF  TUBE-END  'PRODN'
** UBA      ff   Status  Connection
   1 1 1   1.0  OPEN    FLOW-TO  'SURFACE'  REFLAYER
   2 1 1   1.0  OPEN    FLOW-TO  1
   3 1 1   1.0  OPEN    FLOW-TO  2
   4 1 1   1.0  OPEN    FLOW-TO  3
   5 1 1   1.0  OPEN    FLOW-TO  4
   6 1 1   1.0  OPEN    FLOW-TO  5
   7 1 1   1.0  OPEN    FLOW-TO  6
   8 1 1   1.0  OPEN    FLOW-TO  7
   9 1 1   1.0  OPEN    FLOW-TO  8
   10 1 1  1.0  OPEN    FLOW-TO  9
************************************************

TIME   1
TIME   10
TIME   100
TIME   1000
TIME   1500
TIME   2000
```

TIME 2500
TIME 3000
TIME 3500
TIME 4000
TIME 4500
TIME 5000
TIME 5500
TIME 6000
TIME 6500
TIME 7000
TIME 7500
TIME 8000
TIME 8500
TIME 9000
TIME 9500
TIME 10000
TIME 10500
TIME 11000
TIME 11500
TIME 12000
TIME 12500
TIME 15000
TIME 15500
TIME 20000
TIME 20500
TIME 21000
TIME 21500
TIME 22000
TIME 23000
TIME 23500
TIME 24500
TIME 25000
TIME 26000
TIME 26500
TIME 27000
TIME 27500
TIME 30000
TIME 30500
TIME 31000
TIME 31500
TIME 32000
TIME 34500
TIME 35000
TIME 35500
TIME 36000
TIME 36500
TIME 37000
TIME 37500
TIME 38000
TIME 38500
TIME 39000

```
TIME   39500
TIME   40000
TIME   40500
TIME   41000
TIME   41500
TIME   42000
TIME   42500
TIME   43000
TIME   43500
TIME   44000
TIME   44808

WELL  'INJTR'
INJECTOR UNWEIGHT 'INJTR'
INCOMP  WATER  0.9999999703 2.97e-8 0

TIME   44810
TIME   44910
TIME   45010
TIME   45110
TIME   45210
TIME   45310
TIME   45410
TIME   45510
TIME   45610
TIME   45710
TIME   45810
TIME   45910
TIME   46010
TIME   46110
TIME   46210
TIME   46310
TIME   46410
TIME   46510
TIME   46610
TIME   46710
TIME   46810
TIME   46910
TIME   47010
TIME   47110
TIME   47210
TIME   47310
TIME   47410
TIME   47510
TIME   47610
TIME   47710
TIME   47810
TIME   47910
TIME   48010
TIME   48110
TIME   48210
```

TIME 48310
TIME 48410
TIME 48510
TIME 48610
TIME 48710
TIME 48810
TIME 48910
TIME 49010
TIME 49110
TIME 49210
TIME 49310
TIME 49410
TIME 49510
TIME 49610
TIME 49710
TIME 49810
TIME 49910
TIME 50010
TIME 50110
TIME 50210
TIME 50310
TIME 50410
TIME 50510
TIME 50610
TIME 50710
TIME 50810
TIME 50910
TIME 51010
TIME 51110
TIME 51210
TIME 51310
TIME 51410
TIME 51510
TIME 51610
TIME 51710
TIME 51810
TIME 51910
TIME 52010
TIME 52110
TIME 52210
TIME 52310
TIME 52410
TIME 52510
TIME 52610
TIME 52710
TIME 52810
TIME 52910
TIME 53010
TIME 53110
TIME 53210
TIME 53310

TIME 53410
TIME 53510
TIME 53610
TIME 53710
TIME 53810
TIME 53910
TIME 54010
TIME 54110
TIME 54210
TIME 54310
TIME 54410
TIME 54510
TIME 54610
TIME 54710
TIME 54810
TIME 54910
TIME 55010
TIME 55110
TIME 55210
TIME 55310
TIME 55410
TIME 55510
TIME 55610
TIME 55710
TIME 55810
TIME 55910
TIME 56010
TIME 56110
TIME 56210
TIME 56310
TIME 56410
TIME 56510
TIME 56610
TIME 56710
TIME 56810
TIME 56910
TIME 57010
TIME 57110
TIME 57210
TIME 57310
TIME 57410
TIME 57510
TIME 57610
TIME 57710
TIME 57810
TIME 57910
TIME 58010
TIME 58110
TIME 58210
TIME 58310
TIME 58410

TIME 58510
TIME 58610
TIME 58710
TIME 58810
TIME 58910
TIME 59010
TIME 59110
TIME 59210
TIME 59310
TIME 59410
TIME 59510
TIME 59610
TIME 59710
TIME 59810
TIME 59910
TIME 60010
TIME 60110
TIME 60210
TIME 60310
TIME 60410
TIME 60510
TIME 60610
TIME 60710
TIME 60810
TIME 60910
TIME 61010
TIME 61110
TIME 61210
TIME 61310
TIME 61410
TIME 61510
TIME 61610
TIME 61710
TIME 61810
TIME 61910
TIME 62010
TIME 62110
TIME 62210
TIME 62310
TIME 62410
TIME 62510
TIME 62610
TIME 62710
TIME 62810
TIME 62910
TIME 63010
TIME 63110
TIME 63210
TIME 63310
TIME 63410
TIME 63510

TIME 63610
TIME 63710
TIME 63810
TIME 63910
TIME 64010
TIME 64110
TIME 64210
TIME 64310
TIME 64410
TIME 64510
TIME 64610
TIME 64710
TIME 64810
TIME 64910
TIME 65010
TIME 65110
TIME 65210
TIME 65310
TIME 65410
TIME 65510
TIME 65610
TIME 65710
TIME 65810
TIME 65910
TIME 66010
TIME 66110
TIME 66210
TIME 66310
TIME 66410
TIME 66510
TIME 66610
TIME 66710
TIME 66810
TIME 66910
TIME 67010
TIME 67110
TIME 67210
TIME 67310
TIME 67410
TIME 67510
TIME 67610
TIME 67710
TIME 67810
TIME 67910
TIME 68010
TIME 68110
TIME 68210
TIME 68310
TIME 68410
TIME 68510
TIME 68610

```
TIME   68710
TIME   68810
TIME   68910
TIME   69010
TIME   69110
TIME   69210
TIME   69310
TIME   69410
TIME   69510
TIME   69610
TIME   69710
TIME   69810
TIME   69910
TIME   70010
TIME   70110
TIME   70210
TIME   70310
TIME   70410
TIME   70510
TIME   70610
TIME   70710
TIME   70810
TIME   70910
TIME   71010
TIME   71110
TIME   71210
TIME   71310
TIME   71410
TIME   71510
TIME   71610
TIME   71710
TIME   71810
TIME   71910
TIME   72010
TIME   72110
TIME   72210
TIME   72310
TIME   72410
TIME   72510
TIME   72610
TIME   72710
TIME    72754.80

STOP
 ** This water injection was used to check the polymer adsorption irreversibility.
 WELL  'INJTR'
INJECTOR UNWEIGHT 'INJTR'
INCOMP  WATER  1 0 0


TIME    73754
```

TIME 83754
TIME 93754
TIME 103754
TIME 113754

STOP
****

STARS Data File

A typical STARS data file is divided into nine groups [49]:

- Input/Output Control
- Reservoir Description
- Other Reservoir Properties
- Component Properties
- Rock-fluid Data
- Initial Conditions
- Numerical Methods Control
- Geomechanical Model
- Well and Recurrent Data

Each keyword should follow its group and normally, it cannot be within another group [49].

The simplest model for waterflooding experiment that has two wells; injection and production wells will be described briefly in the next paragraphs.

First in the Input/Output group, the parameter that control the input and output for the model should be specified such as file name, units, output results and restart control.

In the reservoir description section, the experiment grids should be created and the experiment properties should be assigned for each grid such as porosity and permeability.

In the Component Properties section, first the number of components used in the experiment should be specified. Then, molecular weight, critical pressure, critical temperature, mass density and viscosity should be defined for each component. Also, both pressure and temperature for both surface and reservoir should be assigned fin the model.

In the Rock-Fluid Data section, relative permeability table should be defined. Initial pressure, temperature, water saturation and components concentrations should be specified in the Initial Conditions section.

Finally, injection and production wells are defined in the Well and Recurrent Data suction. Also, the experiment life time is specified in this section.

STARS Polymer Flooding Parameters

In the STARS simulator section, a waterflooding experiment model was described and the required information to build a simple waterflooding model was mentioned. In this section, polymer flooding parameters that are required to build a simple polymer flooding model will be explained. The required keywords are:

- MODEL : in this keyword, the number of components in the model is specified. For example:

  MODEL 3 3 3 2

  Starting from the left, first number is the total number of components in the model (fluids and rocks). The second number is the total number of the fluid (water, oil and gas) components. The third number is the total number of components in water and oil phases only, and the fourth number is the total numbers of components in water phase only.
- COMPONENT : The components names should be defined in this key word. The order of the component is important. First, the components in the water phase are defined, then the ones in oil phase, then the ones in gas phase and finally the rock type components are defined.
- CMM, MASSDEN, PCRIT, TCRIT, AVISC: as mentioned before, molecular weight, mass density, critical pressure, critical temperature and viscosity should also be specified for the polymer.
- VSMIXCOMP, VSMIXENDP and VSMIXFUNC: the purpose of these keywords is to specified the nonlinear mixing rule for liquid viscosities. For example:

  VSMIXCOMP 'POLYMER' **(Phase name)

VSMIXENDP 0 2.97e-7 **(polymer concentration)

VSMIXFUNC f1 …f11 **(eleven entries defined nonlinear mixing rule function)

- SHEARTAB: this keyword defines the shear rate table for polymer shear effect.
- INTCOMP: this keyword specifies the interpolation component. For polymer option, it is used to defined the polymer relative permeability table with help with others keyword.
- KRINTRP: this keyword specifies the interpolation set number. For each set there is a different relative permeability table.
- DTRAPW: this keyword always come with KRINTRP, and for the polymer option, it specifies the set that should be used by defining the polymer concentration in this it. For example, if there are two relative permeabilities defined in the model for waterflooding and polymer flooding, DTRAPW determines which set to use. If the value of DTRAPW is zero, the waterflooding relative permeability set will be used, and if DTRAPW is the polymer concentration value, the polymer flooding relative permeability set will be used.
- ADSCOMP: this keyword specified the polymer adsorption option.
- ADSTABLE or ADSLANG : These two keyword specify the polymer adsorption curve that is used in the model. ADSTABLE is a table polymer concentration and polymer adsorption. The relationship between polymer concentration and adsorption is linear. ADSLANG uses the Langmuir isothermal coefficients to specify the polymer adsorption, and as it is clear from figure 6, the relationship between polymer concentration and adsorption is not linear.
- ADMAXT: is the maximum adsorption capacity.
- ADRT: is the residual adsorption level. If ADRT is zero, the adsorption is considered completely reversible, and if ADRT is equal to ADMAXT, the adsorption is considered to be completely irreversible. If ADRT is between zero and ADMAXT, the adsorption is considered partially reversible.
- PORFT: is the keyword responsible for inaccessible pore volume option in STARS. PORFT determines the fraction of accessible pore volume in the model. If PORFT is 1, that means that all the pore volume is accessible and if it is 0.9, that means 10% of the pore volume is inaccessible.

- RRFT: is the residual resistance factor for polymer adsorption.
- DISPI_WAT, DISPJ_WAT, DISPK_WAT: these keywords specify the physical dispersion of the polymer used in the model.
- Finally polymer concentration should be specified in the injection well. For example, in water, polymer and oil system:

  WELL 'INJTR'

  INJECTOR UNWEIGHT 'INJTR'

  INCOMP WATER 0.999999703 2.97e-7 0

  From the left, first number is water concentration, second number is polymer concentration and third number is oil concentration. The polymer concentration value that is specified in this injection well will determined the interpolation set number. Therefore, this value should be the same as the value in the keyword DTRAPW.

Appendix B: 2D X-Ray Images

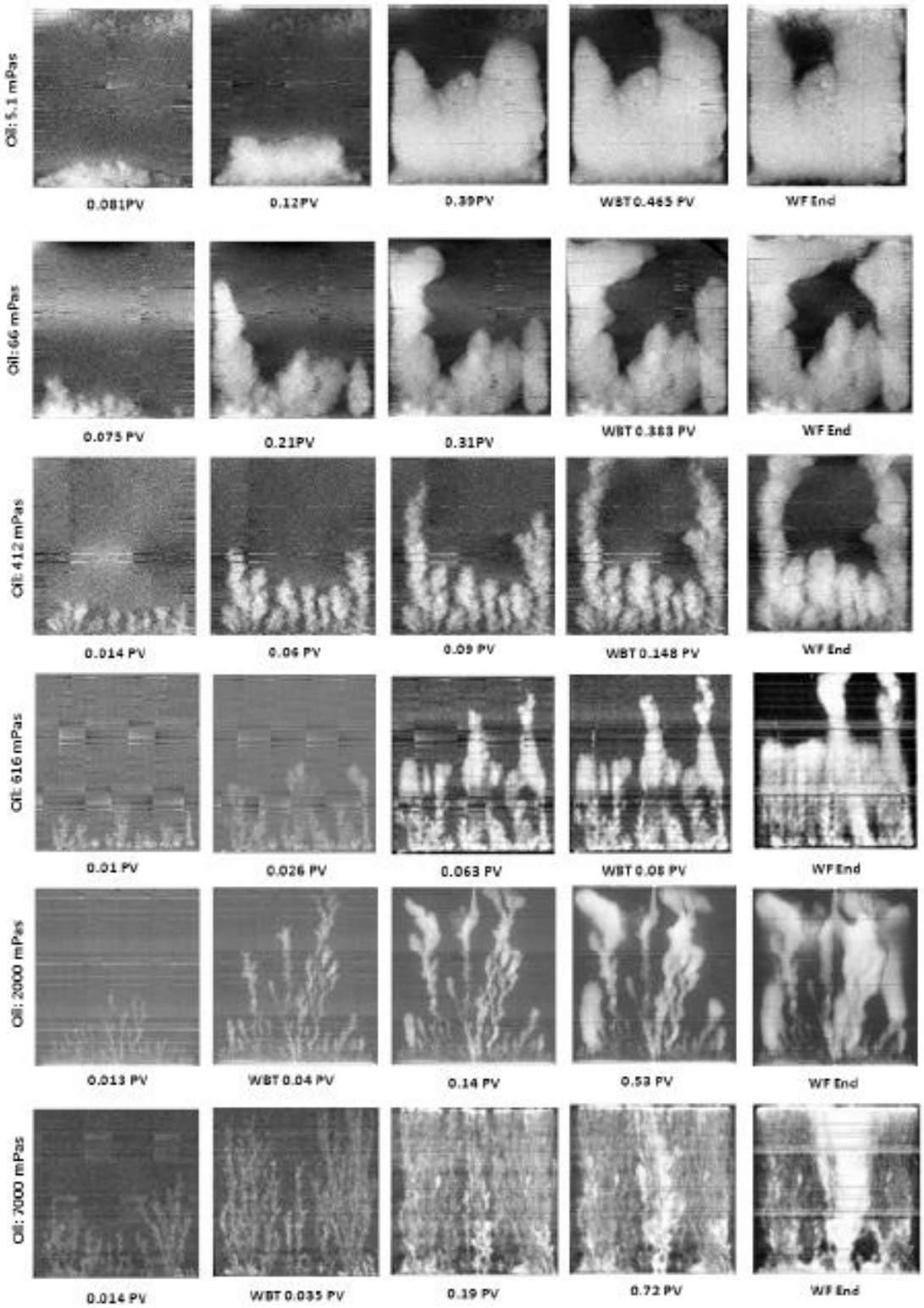

Figure 0.1: 2D x-ray images of water flood for 6 different oil-water viscosity ratios captured at different PV of injected water. White color indicates areas with higher water saturation. The water breakthrough (WBT) for the different water floods is also indicated. As the images are contrast enhanced to better illustrate the observed finger pattern, the grayscale does not represent true water saturation [56]

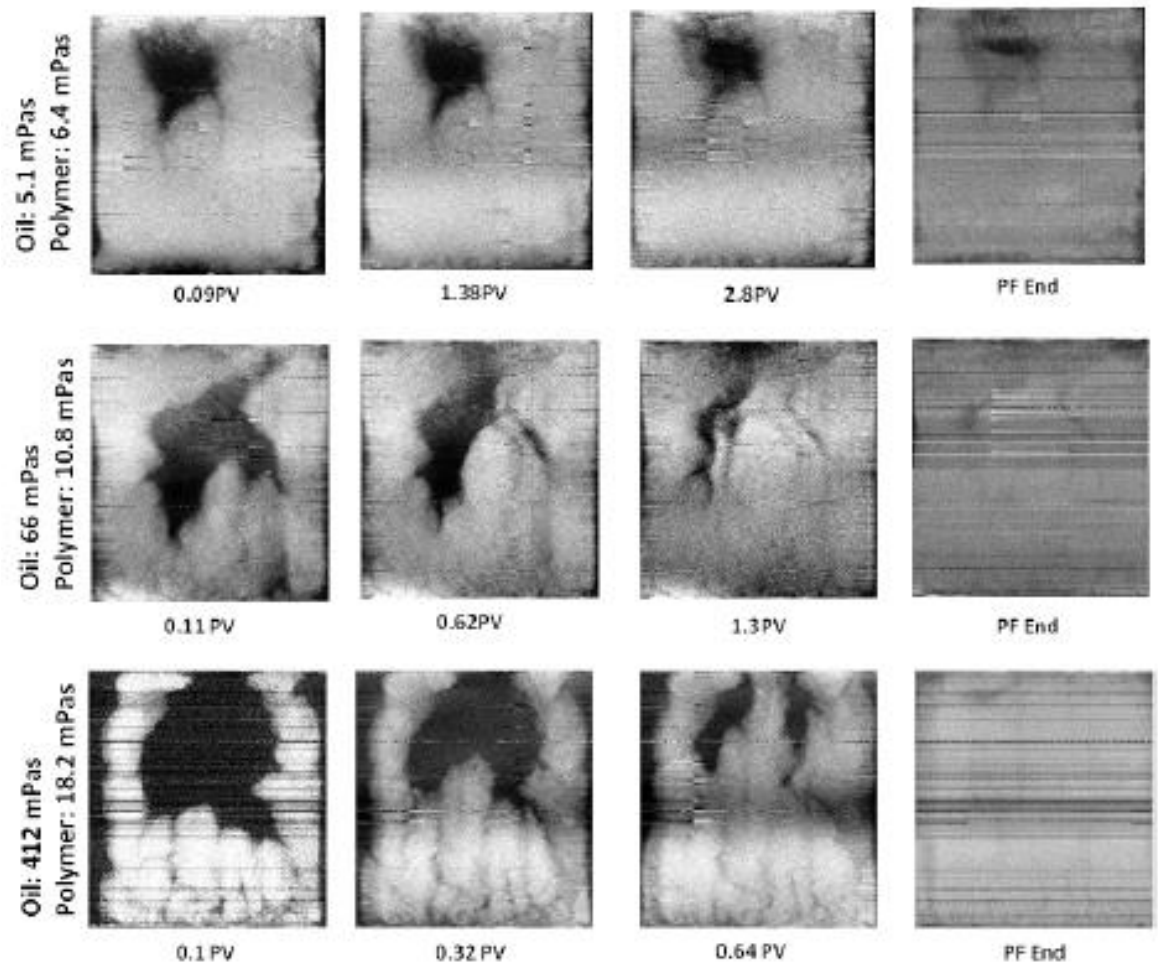

Figure 0.2: 2D x-ray images of polymer flood for different oil-water viscosity ratios captured at different PV of injected polymer. White color indicates areas with higher water saturation [56]

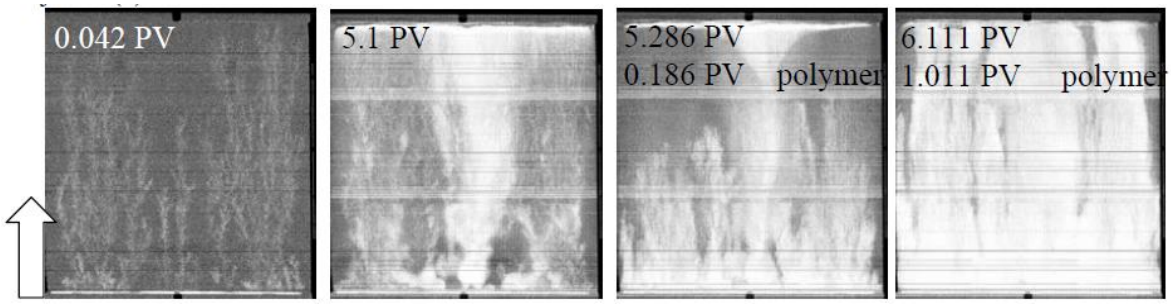

Figure 0.3: 2D x-ray images of polymer flood for 7000 oil-water viscosity ratio captured at different PV of injected polymer. White color indicates areas with higher water saturation [57]